INTEGRATED LIMIT EQUILIBRIUM METHOD FOR SLOPE STABILITY ANALYSIS

A THESIS SUBMITTED TO
THE GRADUATE SCHOOL OF NATURAL AND APPLIED SCIENCES
OF
MIDDLE EAST TECHNICAL UNIVERSITY

BY

YAĞIZER YALÇIN

IN PARTIAL FULFILLMENT OF THE REQUIREMENTS
FOR
THE DEGREE OF MASTER OF SCIENCE
IN
CIVIL ENGINEERING

SEPTEMBER 2018

Approval of the thesis:

INTEGRATED LIMIT EQUILIBRIUM METHOD FOR SLOPE STABILITY ANALYSIS

submitted by **YAĞIZER YALÇIN** in partial fulfillment of the requirements for the degree of **Master of Science in Civil Engineering Department, Middle East Technical University** by,

Prof. Dr. Halil Kalıpçılar
Dean, Graduate School of **Natural and Applied Sciences** _____________________

Prof. Dr. İsmail Özgür Yaman
Head of Department, **Civil Engineering** _____________________

Asst. Prof. Dr. Onur Pekcan
Supervisor, **Civil Engineering Dept., METU** _____________________

Examining Committee Members:

Prof. Dr. Erdal Çokça
Civil Engineering Dept., METU _____________________

Asst. Prof. Dr. Onur Pekcan
Civil Engineering Dept., METU _____________________

Prof. Dr. Oğuzhan Hasançebi
Civil Engineering Dept., METU _____________________

Prof. Dr. Seyhan Fırat
Civil Engineering Dept., Gazi University _____________________

Assoc. Prof. Dr. Zeynep Gülerce
Civil Engineering Dept., METU _____________________

Date: 07.09.2018

I hereby declare that all information in this document has been obtained and presented in accordance with academic rules and ethical conduct. I also declare that, as required by these rules and conduct, I have fully cited and referenced all material and results that are not original to this work.

Name, Last name: Yağızer, Yalçın

Signature :

ABSTRACT

INTEGRATED LIMIT EQUILIBRIUM METHOD FOR SLOPE STABILITY ANALYSIS

Yalçın, Yağızer

M.S., Department of Civil Engineering

Supervisor: Asst. Prof. Dr. Onur Pekcan

September 2018, 144 pages

Limit equilibrium is a well-established concept with successful implementations to slope stability analysis problems. Based on different underlying assumptions, there are numerous limit equilibrium methods (LEMs), yet all of them interpret the system reliability to that of the critical slip surface, which requires iterative optimization procedures to locate. Therefore, a complete analysis framework involves modules to (i) generate/represent, (ii) analyze and (iii) optimize slip surfaces, all of which influence the reliability and time complexity of the solutions. Within this context, many studies were conducted in the past two decades, mostly focusing on improved optimization procedures. However, little effort is available on the development of enhanced surface generation algorithms and analysis strategies. In that regard, the present study introduces Integrated Limit Equilibrium Method (ILEM), wherein novel procedures are incorporated to generate and analyze slip surfaces. Facilitating the optimization process, ILEM generates trial slip surfaces with scaled quadratic splines, which require a minimal number of geometric variables for accurate surface representation. In addition, quadratic functions render it possible to develop a unified formulation of common LEMs with differential equations. The governing equations are derived and closed-form solutions are obtained through analytical integration, eliminating the need for and the error imposed by slice approximation of conventional

LEMs. Moreover, high-order numerical integration methods are proven to yield impartial accuracy with reasonable computational effort. The reliability and refined efficiency of ILEM are validated through comparative benchmark testing. With significant improvement over available approaches, ILEM is proposed as an improved limit equilibrium technique for slope stability analysis.

Keywords: Slope Stability Analysis, Integrated Limit Equilibrium Method, General Slip Surface, Engineering Optimization

ÖZ

ŞEV STABİLİTESİ ANALİZİ İÇİN İNTEGRAL TABANLI LİMİT DENGE YÖNTEMİ

Yalçın, Yağızer

Yüksek Lisans., İnşaat Mühendisliği Bölümü

Tez Yöneticisi: Dr. Öğr. Üyesi Onur Pekcan

Eylül 2018, 144 sayfa

Limit denge metodu, şev stabilitesi analizi problemlerinde oldukça bilinen bir yöntemdir. Farklı kabullere dayanan birçok limit denge yöntemi olmakla beraber, bütün yöntemler kayma güvenliğini, iterasyon tabanlı optimizasyona dayalı olarak bulunan kritik kayma yüzeyiyle ilişkilendirmektedir. Bu nedenle, bütün bir kayma analizi, çözümlerin güvenilirliğini ve çözüm zamanını direkt etkileyen, kayma yüzeylerinin (i) oluşturulması, (ii) analizi ve (iii) optimize edilmesi aşamalarını içermektedir. Bu bağlamda, son yirmi yılda, özellikle optimizasyon yöntemlerinin verimini arttırmak için birçok çalışma yapılmıştır. Ancak kayma yüzeyi oluşturmak ve analiz etmek için kullanılan yöntemlerin verimliliği üzerinde çok az durulmuştur. Bu çalışmada, yukarıdaki eksiklikleri gidermek için, genel kayma yüzeylerinin oluşturulması ve analizi konusunda yenilikler içeren Integral Tabanlı Limit Denge Yöntemi (ILEM) önerilmektedir. Optimizasyon sürecine faydalı olması amacıyla, ILEM, test kayma yüzeylerini, ikinci dereceden eğrilerle tanımlayarak kullanılan geometrik parametre sayısını en aza indirgemektedir. Buna ilaveten, bahsi geçen ikinci dereceden fonksiyonlar, limit denge koşullarının diferansiyel denklemler aracılığı ile temsil edilmesine de olanak tanımaktadır. Bununla hakim denklemler elde edilmekte ve integrasyonla kapalı çözümlere ulaşılmaktadır. Böylece ILEM, konvansiyonel limit denge yöntemlerinin dilimlere dayalı çözümleme yapma zorunluluğunu ve bundan kaynaklanan tahmin hatalarını ortadan kaldırmaktadır. Ayrıca, yüksek dereceden sayısal integral alma yöntemleri sayesinde kısa zamanda iyileştirilen doğruluk oranları da bu metodun kaçınılmaz bir sonucudur. ILEM yönteminin güvenilirliği ve verimliliği, bir çok test problemi kullanılarak doğrulanmıştır. Böylelikle, diğer yöntemlere göre ciddi anlamda ilerleme kaydetmeye olanak tanıyan ILEM, iyileştirilmiş bir limit denge yöntemi olarak sunulmaktadır.

Anahtar Kelimeler: Şev Stabilitesi Analizi, Integral Tabanlı Limit Denge Yöntemi, Genel Kayma Yüzeyi, Mühendislik Optimizasyonu

Dedicated to my family…

ACKNOWLEDGEMENTS

First, I would like to express my sincere appreciation to the person who inspired me to specialize in geotechnical engineering, my supervisor, Asst. Prof. Dr. Onur Pekcan. He has been a great influence on me over the years and I feel privileged to have studied under his guidance. His support, encouragement, and friendship are invaluable for me.

I am deeply grateful to Prof. Dr. Oğuzhan Hasançebi who did not only inspire my research interests but also blessed me with his guidance over the years. I truly feel indebted for his support.

I would also like to express my gratitude to the esteemed members of the examining committee, Prof. Dr. Erdal Çokça, Prof. Dr. Seyhan Fırat, and Assoc. Prof. Dr. Zeynep Gülerce. I appreciate their valuable time, constructive remarks, and contributions.

As a proud member of AI2LAB, I wish to thank all my colleagues for sharing this experience with me and especially want to acknowledge Murat Altun who has always been eager to share his extensive knowledge. I am also thankful to Yunus Oruç for his efforts and contributions in the early stages of this study.

I wish to thank Ahmet Bahaddin Ersöz, Türker Teke, Mücahit Gürbüz, Yılmaz Emre Sarıçiçek, Berkan Söylemez, Emir Ahmet Oğuz, Burak Akbaş, Melih Kenanoğlu, Anıl Ekici, and Mert Tunalı for their friendship and Berhan Melek for handing me the torch, I will to pass it on to someone worthy. I want to extend my gratitude and love to Gizem Can, Gülçin Dalgıç, and Makbule Ilgaç, your mere presence gave me joy every day.

My dearest friends, Esma Saraç, Çağlayan Demirci, and Puria Tabiehzad, I feel lucky to have you in my life. Thank you for your continual support and friendship.

Finally, I want to acknowledge my family to whom I owe everything. My mother Selver, my father Ömer, and my brother Yalçıner, I would like to dedicate this thesis to you as a small token of gratitude for your efforts, support, and love.

TABLE OF CONTENTS

APPENDICES

LIST OF TABLES

TABLES

LIST OF FIGURES

FIGURES

LIST OF ABBREVIATIONS

BS	Bishop's Simplified Method
CE	Corps of Engineers Method
DE	Differential Evolution
FM	Fellenius' Method
GLE	General Limit Equilibrium
ILEM	Integrated Limit Equilibrium Method
JS	Janbu's Simplified Method
LEM	Limit Equilibrium Method
LK	Lowe and Karafiath's Method
M1	Malkawi's Surface Generation Method
M2	Cheng's Equal Division Method
M3	Cheng's Variable Division Method
M4	Sun's Cubic Spline Method
MP	Morgenstern-Price Method
SM	Spencer's Method
SQS	Scaled Quadratic Spline Method
QS	Quadratic Spline Method

CHAPTER 1

INTRODUCTION

1.1. Overview

With the gradual expansion of urbanized areas, development of transportation networks in landslide susceptible areas and common application of engineered soil structures such as embankments, cut slopes, and earth retaining walls [1], slope stability analysis has become a vital part of civil engineering practice. In search of reliable analysis procedures, extensive research has been conducted over the past 80 years [2], giving rise to numerous methods that combine the principles of soil mechanics with solution approaches based on analytical techniques or the concepts of continuum/discontinuum mechanics. As a result, contemporary analysis techniques include, but are not limited to, Limit Equilibrium Methods (LEMs), Finite Element Method and Discrete Element Method. Among those, LEMs have been widely preferred owing to their capability to produce reliable results within reasonable computational demand. Given a possible failure surface, these methods utilize static equilibrium conditions to determine the "limit state" soil shear strength parameters and quantify the stability in terms an artificial measure named factor of safety, F_S, which is the ratio between the mobilized and available soil shear strength at the failure limit state. The analysis proceeds with different surfaces and the critical one (i.e. the surface with minimum F_S) is associated with slope system safety. In other words, limit equilibrium procedures require back-calculation of the critical slip surface, hence a complete analysis framework incorporates modules for (i) surface generation/representation, (ii) stability analysis and (iii) surface optimization. Consequently, the reliability and computational efficiency of the framework depends on the capability, as well as the compatibility of these modules.

Surface generation module is perhaps the most underrated yet influential component of a slope stability analysis framework. Most of the available methods and the common practice aim to facilitate the optimization process through simplifying assumptions regarding the surface geometry. For instance, it is a common approach to limit the surface geometry to planar, circular, composite planar-circular or logarithmic spiral shapes, which can be modeled with only a few decision variables. However, these assumptions significantly limit the accuracy of the results as the critical surface often deviates from such simple geometries [3]. Therefore, it is essential that the method is competent to represent any reasonable surface which may assume arbitrary shapes with variable curvature and abrupt transitions (i.e. general slip surfaces). Although these issues are addressed in the literature, there are only a few general surface generation methods to choose from. Furthermore, the available methods generally require excessive numbers of decision variables for accurate surface representation; as a result, they produce challenging optimization problems. Therefore, improved techniques are still in demand.

After their generation, the surfaces are analyzed using a LEM. Although all LEMs share the common features mentioned before, they differentiate with unique assumptions based on force distribution, equilibrium criteria, and sometimes slip surface geometry. A broad classification divides them into two groups as single free-body procedures and procedures of slices. Single free-body procedures include simple methods like Infinite Slope [4], Logarithmic Spiral [5, 6], and Swedish Circle [7, 8]. One characteristic property of these methods is that the underlying assumptions yield formulations where the normal stress along the slip surface is either constant or do not affect the overall equilibrium. As a result, equilibrium equations can be formulated for the whole free-body [2]. Conversely, such a simplification is not possible with other LEMs, hence they discretize the free-body into slices to determine the normal stress distribution. However, discretization itself is not sufficient to resolve such a force system because the number of unknowns becomes greater than the number of available equilibrium and boundary conditions when all inter-slice reactions are accounted for.

Therefore, either simplifications or additional boundary conditions are required to render the problem determinate. In this sense, unique solution schemes were proposed in the literature, giving rise to LEMs known as Fellenius [9], Bishop's simplified and rigorous [10], Janbu's simplified and generalized [11], Lowe and Karafiath's [12], Corps of Engineers [13], Morgenstern-Price [3], Spencer's [14], and Sarma's [15] methods. These methods mainly differ from one another based on the considerations regarding the equilibrium conditions and internal forces, yet it is possible to unify some of them with a common formulation like General Limit Equilibrium (GLE) method [16]. In general, procedures of slices are capable of handling complex slope geometries, variable soil properties, and external loading effects [1] and therefore often preferred over single free-body procedures. However, they are computationally upscale on the account of free-body discretization and individual slice evaluation.

Since LEMs require the location of the critical surface, the analysis proceeds with the surface optimization step where the geometric parameters of the trial solutions are updated with an optimization method. Limit equilibrium approach inherently makes it possible to formulate the analysis procedure as a shape optimization problem with an objective to minimize F_S. The complexity of the problem depends on the combined effect of (i) model constants (e.g. slope geometry, soil profile, groundwater and loading conditions), and (ii) innate characteristics of the selected surface generation method. When simple surface geometries are assumed, the problem becomes sufficiently easy to solve with simple trial and error routines. However, accurate representation of critical surfaces requires general surface generation methods, which produce high-dimensional optimization problems. Considering that the search spaces of these problems often contain multiple local minima [2], implementing robust optimization techniques is essential for the reliability of the analysis framework. This issue has been extensively studied in the literature, and both deterministic and stochastic optimization techniques have been employed. Currently, there is a growing consensus that the modality and dimensionality of slope stability analysis problems make it necessary to adopt global optimization methods, which involve a certain degree of random operations. In that regard, stochastic optimization algorithms such as Genetic Algorithm [17–25], Differential Evolution [26, 27], and Particle Swarm Optimization [28–31] were successfully adopted in the literature.

With multiple factors in effect, the application of LEM requires a clear understanding of the fundamental concepts regarding the surface generation, stability analysis, and surface optimization methods. Limitations imposed by each component can easily engender the overestimation of safety and inevitably result in catastrophic consequences. Therefore, both individual and collective performances of the integrated methods should be assessed when developing an analysis framework.

1.2. Research Objectives

Aiming to develop a reliable and computationally efficient slope stability analysis framework, the present study proposes enhanced surface generation and analysis procedures. Focusing on general slip surfaces and procedures of slices, the defects of the available methods and formulations are identified to specialize the research objectives. Examination of the available general surface generation methods draws the inferences that they; (i) require excessive numbers of decision variables for accurate surface representation, rendering surface optimization a difficult task, (ii) lack the flexibility to converge to complex surface geometries, and (iii) represent the slip surfaces with contiguous linear segments, causing unnecessary loss of accuracy. Similarly, when available LEM formulations are adopted for stability analysis; (i) F_S evaluation becomes computationally upscale on the account of tedious operations to discretize the sliding body and individually evaluate each slice; and (ii) F_S is often overestimated due to the sensitivity of results to the number of slices used in discretization. Based on these arguments, the present study aims to develop advanced methods to generate and analyze general slip surfaces and incorporate them into a proficient slope stability analysis framework.

1.3. Scope of the Study

Addressing the issues mentioned in the preceding section, the present study introduces Integrated Limit Equilibrium Method (ILEM), wherein novel procedures are implemented to generate and analyze general slip surfaces. The surface generation procedure of ILEM incorporates a technique named Scaled Quadratic Spline method (SQS) which utilizes *piecewise* continuous quadratic spline functions for surface representation. The method aims to handle complex geometries with variable curvature and abrupt gradient transitions using a minimal number of decision variables, and hence produces relatively lower-dimensional optimization problems. Furthermore, SQS capacitates a higher accuracy level with smooth curve representation, compared to available methods that adopt linear segments. In addition to this embedment, an enhanced analysis strategy is proposed in ILEM as an extension of SQS. ILEM analysis approach is similar to GLE in the sense that it can be adapted into several LEMs. However, the static equilibrium conditions are formulated based on the quadratic function representation of SQS. The derivation results in two governing equations that consist of definite integrals, which can be integrated analytically to obtain closed-form solutions. Therefore, ILEM can eliminate the errors of slice approximation procedures. Furthermore, the integrals can be evaluated with numerical methods such as *Simpson's 1/3* and *Gauss quadrature* rules to produce adequate results with reasonably low computational effort. Based on these properties, ILEM is introduced as an alternative to the available limit equilibrium formulations.

To validate the reliability of the proposed approach, ILEM surface generation and analysis methods are evaluated individually. First, a benchmark problem set is assembled with the slope stability analysis problems available in the literature. The resulting set includes a total of 11 examples, incorporating a broad range of cases from simple homogeneous slopes to complex soil profiles; with and without the presence of groundwater effect, external and pseudo-static earthquake loading. Then, SQS is combined with GLE formulation and Differential Evolution (DE) optimization algorithm and evaluated in a series of experiments with these problems. Similarly, the general surface generation methods in available literature studies [21, 32, 33] are adopted with the same configuration for performance comparison. The results are interpreted with statistical significance tests to assess the improvement rate of SQS over other methods and additionally evaluated with respect to the commercial slope stability analysis software, *Slide v7* [34]. The results emphasize the capability of SQS and validate the applicability of the proposed analysis procedure.

Accordingly, ILEM analysis procedure is tested in comparison with GLE formulation. For the analyses in this part, the critical slip surfaces obtained in the previous experiments are further analyzed using the closed-form formulation of ILEM and other variants based on numerical integration methods such as *trapezoidal*, *Simpson's 1/3* and *Gauss quadrature* rules. The closed-form solution approach is validated for the procedures of slices proposed by Fellenius, Bishop, Janbu, Lowe and Karafiath, Corps of Engineers, Spencer, and Morgenstern-Price. Then, a computationally efficient ILEM variant is developed based on numerical approximation techniques. Lastly, a comparison is provided to illustrate the improved efficiency of ILEM over GLE.

1.4. Thesis Outline

To deliver the findings and contributions of the study, the rest of the manuscript is organized as follows: Chapter 2 provides detailed information about available surface generation, stability analysis, and optimization techniques, outlining the general framework of limit equilibrium based slope stability analysis procedures. Chapter 3 is dedicated to ILEM surface generation procedure, SQS. The method is conceptually introduced, formulated and validated through comparative benchmark testing with other available surface generation techniques. Chapter 4 presents the unified formulation of ILEM stability analysis procedure. In this chapter, several ILEM variants are developed and a computationally efficient configuration is proposed as an alternative to the available limit equilibrium formulations. Lastly, Chapter 5 summarizes the findings and concludes the study.

CHAPTER 2

LIMIT EQUILIBRIUM CONCEPT FOR SLOPE STABILITY ANALYSIS

The focus of this chapter is to provide the fundamentals of the theory and application of limit equilibrium concept to slope stability analysis problems. Therefore, the scope is constrained with the currently available methods, with an emphasis on procedures of slices and general surface generation techniques. Accordingly, in Section 2.1, limit equilibrium concept is introduced and available analysis methods are discussed in detail. Section 2.2 is dedicated to slip surface generation methods, while Section 2.3 covers the surface optimization strategies proposed in the literature. Furthermore, the methods adopted in the succeeding chapters are formulated in each section.

2.1. Theory of Limit Equilibrium

Limit equilibrium approach assumes that a slope is stable when any free-body inside the soil medium is at rest, implying that the static equilibrium conditions are satisfied. Based on this assumption, LEMs cannot yield a direct measure of system reliability; instead, they analyze multiple paths within the soil profile to determine the critical slip surface. For any surface, the safety level is quantified with a constant named factor of safety, F_S, which is the ratio between the available soil shear strength and the equilibrium shear stress at the slip surface. When the shear strength is expressed with Mohr-Coulomb soil model, the definition of F_S extends to the expressions given in Eqs. (2.1) and (2.2), where F_S is assumed to be constant throughout the slip surface.

$$F_S = \frac{\tau}{s} = \frac{c + \sigma_n \tan\phi}{c_m + \sigma_n \tan\phi_m} \tag{2.1}$$

$$F_S = \frac{c}{c_m} = \frac{\phi}{\phi_m} \tag{2.2}$$

where τ: peak shear stress, s: equilibrium shear stress, σ_n: normal stress, c and ϕ: soil cohesion and friction angle (i.e. subscript "m" denotes the mobilized parameters).

Considering the generic slip surface given in Figure 2.1, it is possible to formulate the equilibrium equations and determine the mobilized shear strength based on the inertial forces, external loads and base reactions. Among those, calculations of inertial and external forces are relatively straightforward. On the other hand, the base reaction is the resultant of two variable stress distributions (i.e. normal stress and shear resistance), hence require additional considerations. The common approach is to divide the free-body into a finite number of slices and derive the equilibrium equations based on the individual effect of each segment. However, the problem becomes statically indeterminate when all internal reactions are accounted for. Considering a body of "*n*" slices, the available equilibrium and boundary conditions are summarized in Table 2.1. For each slice, there are three equilibrium (i.e. horizontal force, vertical force and moment) and one boundary (i.e. Mohr-Coulomb criterion) conditions, resulting in a total of $4n$ equations. On the other hand, the unknowns (i.e. F_S value, the magnitude and location of the base and interface reactions illustrated in Figure 2.1b) add up to $6n$-2 variables as given in Table 2.2. Consequently, the problem is statically indeterminate with a degree of $2n$-2, and therefore requires either simplifications or additional boundary conditions to solve.

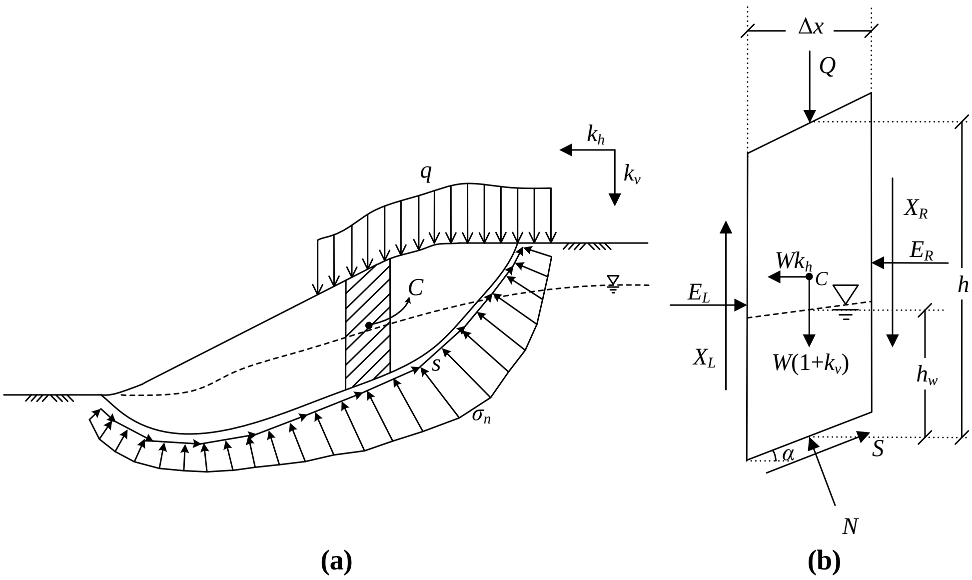

Figure 2.1: Free-body diagram of a generic slip surface
(a) overall diagram **(b)** vertical slice diagram

Table 2.1: Available equilibrium and boundary conditions of LEM

Equations	**Number**
Horizontal force equilibrium	n
Vertical force equilibrium	n
Moment equilibrium	n
Mohr-Coulomb criterion	n
Total	$4n$

Table 2.2: Unknown variables in LEM

Unknowns	**Number**
Normal force at the base of the slice	n
Location of the normal force at the base of the slice	n
Shear force at the base of the slice	n
Interslice normal force	n-1
Interslice shear force	n-1
Location of the interslice force (i.e. line of thrust)	n-1
Factor of safety, F_S	1
Total	$6n$-2

Provided that the indeterminacy problem is handled, limit equilibrium can provide the F_S related to an assumed slip surface. However, a single analysis does not yield a direct measure of system reliability as the stability of the slope is associated with the critical slip surface (i.e. the free-body with the minimum F_S). Therefore, a surface optimization procedure is necessary to minimize the F_S. Without the aid of computers, both individual slice evaluation and surface optimization can translate to be tedious tasks. Suitably, the earlier studies focused on simplifications that either facilitate or eliminate these steps. For instance, methods like Infinite Slope [4], Logarithmic Spiral [5, 6], and Swedish Circle [7, 8] greatly simplify the problem with restricted surface geometries, allowing the formulation of equilibrium equations without free-body discretization. Also known as single free-body procedures, these methods are simple enough to adopt in hand calculations; however, their application is limited to specific slope and slip surface geometries, soil types, loading and groundwater conditions.

In the following decades, the advances in computer technology allowed the practical implementation of methods based on individual slice evaluation, namely, procedures of slices. Procedures of slices are competent to handle complex geometries and loading conditions, hence applicable to a wider range of analysis problems. Despite having simplifications and intuitive assumptions to overcome static indeterminacy, some variants of these methods rigorously satisfy the equilibrium conditions. For instance, procedures of slices like Fellenius' [9], Bishop's simplified [10], Janbu's simplified [11], Lowe and Karafiath's [12] and Corps of Engineers [13] methods ignore some of the equilibrium conditions and internal forces. On the other hand, Bishop's Rigorous [10], Janbu's Generalized [11], Morgenstern-Price [3], Spencer's [14] and Sarma's [15] methods overcome indeterminacy through minor assumptions, rigorously satisfying the equilibrium conditions. Although the underlying assumptions of these methods are slightly different, they can be accommodated within unified formulations like General Limit Equilibrium (GLE) [16].

2.1.1. Single Free-Body Procedures

Despite their limitations, single free-body procedures like Infinite Slope, Logarithmic Spiral, and Swedish Circle can provide a rough estimation of F_S under specific conditions. Although not utilized in this study, these methods are discussed in the following sub-sections to provide a rudimentary understanding of the limit equilibrium concept.

2.1.1.1. Infinite Slope Method

Proposed by Taylor [4], Infinite Slope method considers a fully translational failure mechanism. The method assumes that failure develops along an infinitely long plane, parallel to the ground surface as illustrated in Figure 2.2. Therefore, base normal and shear stresses are constant. Based on this idea, the analysis can be performed on any vertical element by resolving the stresses along the slip direction. The interface reactions can be ignored as the forces on the opposite sides of the element are collinear with equal magnitude.

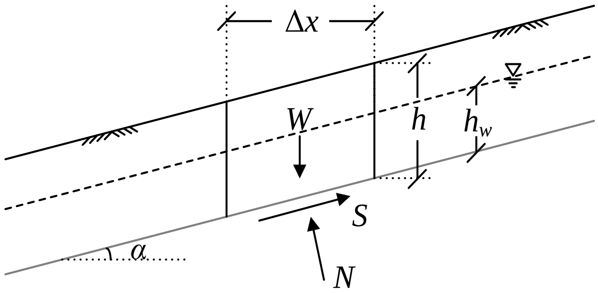

Figure 2.2: Infinite slope analysis

Slice weight, W, and average pore-water pressure, u, are calculated using Eqs. (2.3) and (2.4), respectively. For Eq. (2.4), hydrostatic condition is assumed.

$$W = \gamma h \Delta x \tag{2.3}$$

$$u = \gamma_w h_w \tag{2.4}$$

where γ: unit weight of soil, h: height of slice, γ_w: unit weight of water, h_w: height of slice below the water table, Δx: width of the slice.

Base normal force, N, is calculated considering force equilibrium, using Eq. (2.5).

$$N = W \cos \alpha \tag{2.5}$$

where α: inclination of slice base, measured from horizontal.

Based on the Mohr-Coulomb failure criterion, shear resistance, S, is calculated using Eq. (2.6).

$$S = \frac{c'}{F_S} \cdot \frac{\Delta x}{\cos\alpha} + \frac{\tan\phi'}{F_S} \cdot \left(N - \frac{u\,\Delta x}{\cos\alpha} \right) \tag{2.6}$$

where F_S: factor of safety, c' and ϕ': effective soil cohesion and friction angle, respectively.

To evaluate the factor of safety, F_S, force equilibrium is satisfied along the slip direction. As a result, F_S can be singled out to obtain Eq. (2.7).

$$F_S = \frac{c'\Delta x \sec\alpha + \left(N - \dfrac{u\,\Delta x}{\cos\alpha} \right) \tan\phi'}{W \sin\alpha} \tag{2.7}$$

The given procedure can be adopted for effective stress analysis, yet it is possible to modify the equations to evaluate F_S based on total stresses. In that case, the effect of pore-water pressure is ignored and, c' and ϕ' in Eq. (2.7) are replaced with the undrained shear strength parameters, c_u and ϕ_u.

Although Infinite Slope approach is based on force equilibrium, moment equilibrium is implicitly satisfied since the interface forces cancel out and rest pass through the same point, producing zero net moment. Having a straightforward formulation, the method can provide a quick estimation of F_S for translational failure, and therefore often preferred when the there is a shallow bedrock or a soft soil interlayer. However, its application is limited to cases where the ground surface and soil layers are in parallel alignment. Another issue of Infinite Slope method is that the effect of slip toe and scarp are ignored, hence the method usually underestimates F_S compared to rigorous procedures of slices.

2.1.1.2. Swedish Circle Method

Introduced by Fellenius in 1922 [7], Swedish Circle is one of the earliest slope stability analysis methods, having applications that date back to 1916 [8]. The procedure considers the rotational failure of a circular slip surface around its central axis and utilizes moment equilibrium to determine the F_S. Therefore, the base normal stresses focalize to the center of rotation as illustrated in Figure 2.3. Furthermore, the frictional resistance of soil is ignored (i.e. ϕ=0) to overcome static indeterminacy and eliminate free-body discretization completely. As a consequence, the method is only applicable to circular slip surfaces with cohesive soil interfaces, under fully undrained condition. Considering moment equilibrium with respect to point R, F_S can be derived for a homogeneous soil profile as follows:

$$F_S = \frac{\sum M_{resisting}}{\sum M_{driving}} = \frac{c\,L\,r}{W\,r_x} \tag{2.8}$$

where r: radius of slip circle, L: total arc length, W: total weight of free-body, x_C and x_R: abscissas of gravitational center of mass and rotational axis, respectively.

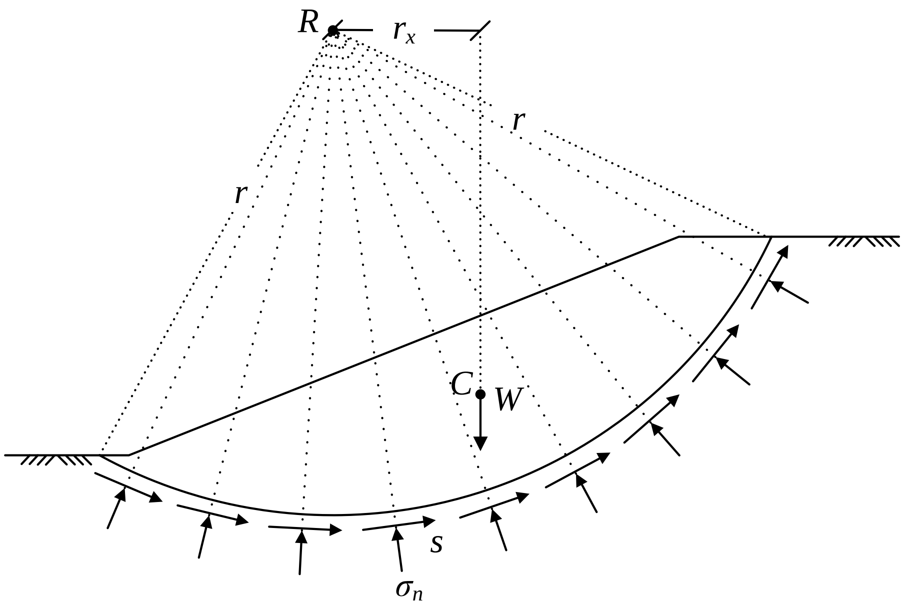

Figure 2.3: Swedish circle analysis

Despite its limitations, Swedish Circle method can handle composite soil profiles through discrete evaluation of resisting forces. Furthermore, the method rigorously satisfies the static equilibrium conditions. Although force equilibrium is not exclusively evaluated, the normal stress distribution can assume any configuration that satisfies the criteria. Swedish Circle is a reliable method within its range of application, however, it often overestimates F_S due to limitations imposed by circular surface assumption.

2.1.1.3. Logarithmic Spiral Method

Similar to other single free-body procedures, Logarithmic Spiral method exploits the slip surface geometry to overcome static indeterminacy. Initially proposed by Taylor [5] and further extended by Frohlich [6], the method employs logarithmic spiral slip surfaces as illustrated in Figure 2.4. The geometry of the spiral is a function of the center of rotation, mobilized friction angle, ϕ_m, the angle of rotation, θ, and the initial radius, r_o, as given in Eqs. (2.9) and (2.10).

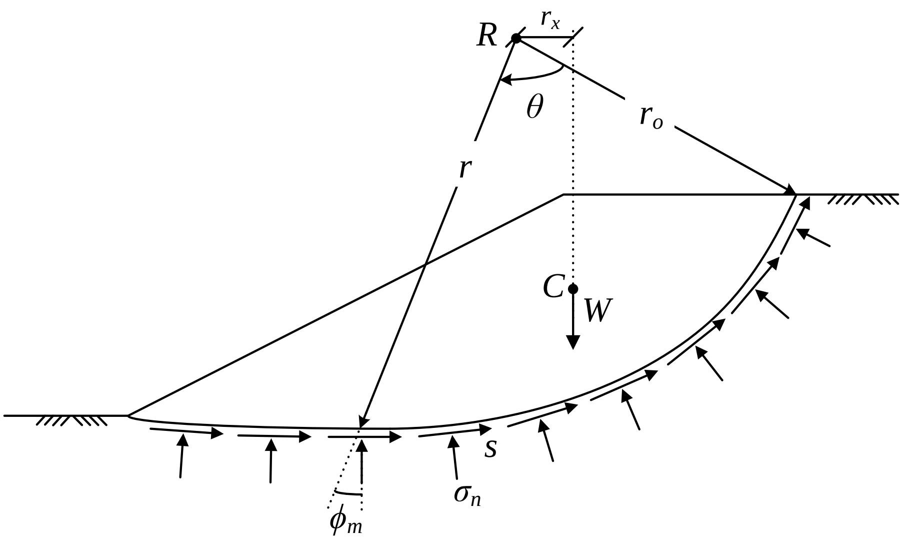

Figure 2.4: Logarithmic spiral analysis

$$\tan\phi_m = \frac{\tan\phi}{F_S} \tag{2.9}$$

$$r = r_o e^{\theta \tan\phi_m} \tag{2.10}$$

Using the proposed geometry, the resultant of the normal stress, σ_n, and the frictional resistance (i.e. $\sigma_n \tan\phi_m$) always passes through the rotational axis, producing zero net moment. Therefore, it is possible to evaluate the F_S based on moment equilibrium by ignoring the contribution of normal stresses, similar to Swedish Circle method. Another similarity with Swedish Circle method is that force equilibrium is satisfied without explicit consideration. However, Logarithmic Spiral method may require several trials to achieve complete equilibrium since the resulting F_S and the one initially assumed to calculate the mobilized friction angle are different. Therefore, an iterative procedure is often adopted to assure the agreement of these two terms. Through this implementation, the method can analyze slopes under both drained and undrained conditions, which is an improvement over Swedish Circle method. In addition, logarithmic spirals are relatively more capable of representing complex slip surface geometries, compared to planar and circular surfaces adopted in other single free-body-procedures. However, the formulation of the method is rather complex, and its application is only possible when the soil profile is homogeneous, or at least friction angle is the same for all layers.

2.1.2. Procedures of Slices and General Limit Equilibrium Method

Procedures of slices have wider application ranges compared to single free-body procedures, being able to handle composite soil profiles under complex loading configurations, in both drained and undrained conditions. Furthermore, most of the available formulations can analyze general slip surfaces, which are more flexible to represent the critical case compared to the simplified approaches presented previously.

In this section, some of the common procedures of slices are conceptually introduced based on General Limit Equilibrium (GLE) formulation, which is proposed by Fredlund et al. [16] to provide a unified formulation for the available approaches. Therefore, GLE is not considered as a separate LEM, rather a generalized form on the existing ones. It is worth mentioning that there are several other unified formulations in the literature [44, 45], however, they are kept out of the scope of this study. The formulation of GLE can be manipulated with slight adjustments to produce results for the procedures of slices proposed by Fellenius, Bishop, Janbu, Lowe and Karafiath, Corps of Engineers, Morgenstern and Price, and Spencer. In its generalized form, the formulation considers vertical force equilibrium to derive the equations for base shear and normal forces. Then, F_S is separately computed for horizontal force and moment equilibrium. In other words, GLE utilizes two separate F_S definitions, which are iteratively equated to satisfy complete equilibrium.

GLE incorporates two major assumptions to overcome static indeterminacy. First, the normal force at the base of each slice is assumed to act towards the middle, which reduces the degree of indeterminacy to n-2 for a body of n slices. In addition, GLE either specifies a direction or a location (i.e. line of thrust) for the interslice forces. All LEMs presented in this section can be formulated with the former assumption, hence it will be the focal point. Based on the approach proposed by Morgenstern and Price [3], the direction of resultant interslice forces can be specified with Eq. (2.11).

$$X/E = \lambda \, f_i(x) \tag{2.11}$$

where X: interslice shear force, E: interslice normal force, λ: a constant scale factor, $f_i(x)$: a prescribed function that dictates the variation of X/E ratio along the slip surface.

Applicable to each slice interface, the boundary condition given in Eq. (2.11) interpolates n-1 equations and one unknown (i.e. constant scale factor, λ) to the problem. Accordingly, the system becomes statically determinate. Based on this approach, GLE method is formulated for the effective stress analysis of the general slip surface given in Figure 2.5, where the slope is subjected to external and pseudo-static earthquake loading. Only the governing equations are provided in this section, and the detailed formulation is provided later in Chapter 4.

The normal and shear forces illustrated in Figure 2.5b are computed using Eqs. (2.12) and (2.13), respectively.

$$N = \frac{W \cdot (1 + k_v) + Q + (X_R - X_L) - (\Delta x \tan\alpha) \cdot \dfrac{c'}{F_S} + (u \Delta x \tan\alpha) \cdot \dfrac{\tan\phi'}{F_S}}{\cos\alpha + \dfrac{\sin\alpha \tan\phi'}{F_S}} \tag{2.12}$$

$$S = \frac{c'}{F_S} \cdot \frac{\Delta x}{\cos\alpha} + \frac{\tan\phi'}{F_S} \cdot \left(N - \frac{u \Delta x}{\cos\alpha} \right) \tag{2.13}$$

where W: weight of slice (i.e. refer to Eq. (2.3)), k_v and k_h: vertical and horizontal seismic coefficients, Q: resultant of external load acting above the slice, X and E: interslice shear and normal forces (i.e. subscripts "L" and "R" given in Figure 2.5b denote left and right-hand sides of slice, respectively), Δx: width of slice, α: inclination of slice base measured from horizontal, u: average pore-water pressure on slice base (i.e. refer to Eq. (2.4)), c' and ϕ': effective soil cohesion and friction angle, respectively.

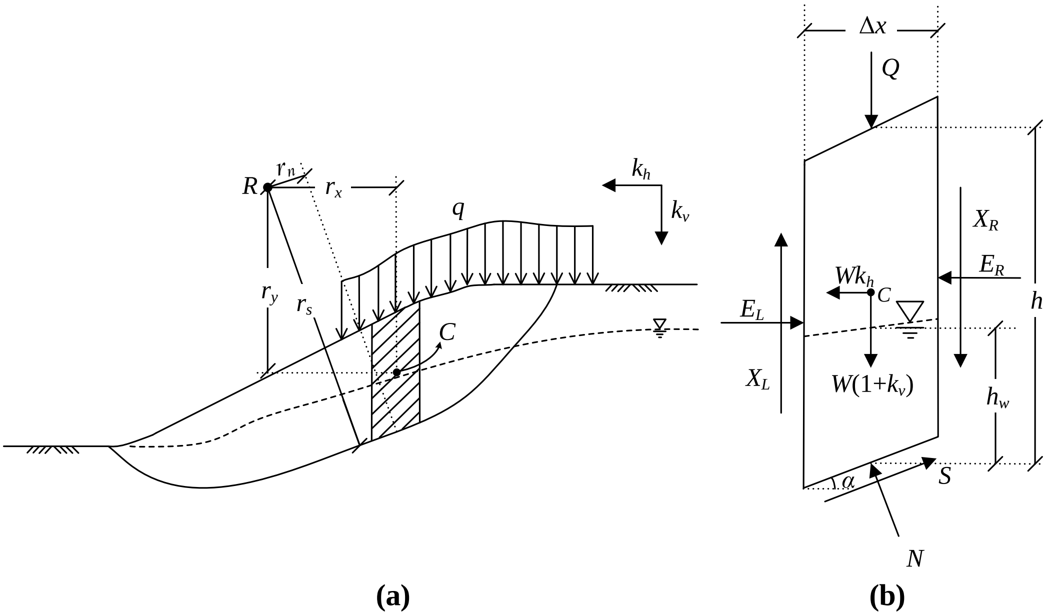

Figure 2.5: General Limit Equilibrium analysis approach
(a) slip surface of a slope under external and seismic loading
(b) free-body diagram of a vertical slice

To satisfy complete force equilibrium, horizontal forces in each slice are summed up, producing the force F_S of GLE, given in Eq. (2.14).

$$F_{S,f} = \frac{\sum\left[\left(c' - u\tan\phi'\right)\cdot \Delta x + \tan\phi' N\cos\alpha\right]}{\sum\left(N\sin\alpha + Wk_h\right)} \tag{2.14}$$

where $F_{S,f}$: force factor of safety.

Similarly, moment equilibrium is satisfied with respect to a common rotational center, point R in Figure 2.5a. As a result, the moment F_S can be determined using Eq. (2.15).

$$F_{S,m} = \frac{\sum\left\{\left[\left(c' - u\tan\phi'\right)\cdot \frac{\Delta x}{\cos\alpha} + N\tan\phi'\right]\cdot r_s\right\}}{\sum\left\{\left[Q + W\cdot\left(1 + k_v\right)\right]\cdot r_x + Wk_h r_y - Nr_n\right\}} \tag{2.15}$$

where $F_{S,m}$: moment factor of safety, r_s, r_x, r_y, and r_n: moment arms in Figure 2.5a.

Although the formulation of GLE is given for effective stress analysis, the equations can be adapted for total stresses by ignoring the effect of pore-water pressure and substituting the undrained parameters into the equations. In the following sub-sections, GLE interpretations of common LEMs are discussed further.

2.1.2.1. Fellenius' Method

Fellenius' method (i.e. also known as Ordinary Method of Slices) is the earliest procedure of slices in the literature. The method was initially proposed as an extension of Swedish Circle method to deal with soils under drained condition. In this procedure, interslice forces are completely ignored and F_S is determined based on moment equilibrium. Contrary to other procedures, Fellenius' method does not satisfy vertical force equilibrium. Instead, the vertical forces are resolved into their components, parallel and perpendicular to the slip surface. The perpendicular component is assumed to be equal to the base normal force that is used to determine the shear resistance. Since this approach is contradictory to the one adopted in GLE, Fellenius' method requires an additional modification. For this method only, the normal force is calculated using the expression given in Eq. (2.16).

$$N = \left[W \cdot \left(1 + k_v\right) + Q\right] \cdot \cos\alpha - W k_h \sin\alpha \tag{2.16}$$

Contrary to the normal force equation given for GLE, Eq. (2.16) is independent of F_S. Therefore, for Fellenius' method, a single step calculation concludes the analysis. Since Fellenius' method does not satisfy force equilibrium, the value of F_S depends on the location of the rotational center, *R*. It is usually acceptable to use the center of the arc as the reference point when circular slip surfaces are adopted [35]. However, such a distinct location is not available for general slip surfaces. Therefore, the application of Fellenius' method is usually not recommended for non-circular slip surfaces. Furthermore, the method often yields unrealistic results, especially for flat slopes with high pore-water pressures [36].

2.1.2.2. *Bishop's Simplified Method*

Similar to Fellenius' approach, Bishop's simplified method ignores horizontal force equilibrium and determines F_S based on moment evaluation. However, base normal forces are calculated based on Eq. (2.12), which ensures vertical force equilibrium. The procedure accounts for interslice forces but ignores the shear components to overcome static indeterminacy (i.e. $\lambda f_i(x)=0$). Based on these assumptions, F_S can be evaluated using Eq. (2.15).

Bishop's simplified method does not guarantee complete force equilibrium, hence F_S is dependent on the point of reference selected for moment calculations, similar to Fellenius' method. However, the results are only affected by the vertical position of the reference point since the free-body is in vertical force equilibrium. Regardless, the application of this procedure is mostly restricted to circular slip surfaces.

2.1.2.3. *Janbu's Simplified Method*

It is apparent that simplified methods that evaluate F_S based on moment equilibrium require a distinct axis of rotation, which is not clearly defined for general slip surfaces. Addressing this issue, Janbu proposed a procedure where F_S is evaluated based on horizontal force equilibrium instead. As a result, the procedure commonly known as Janbu's simplified method ignores moment equilibrium. Assumptions regarding the internal forces are the same as Bishop's, in that, interslice shear forces are ignored (i.e. $\lambda f_i(x)=0$). With this approach, F_S can be evaluated using Eq. (2.14).

Ignoring the shear resistance in the slice interfaces, Janbu's simplified method always underestimates F_S [2] compared to rigorous methods. Accordingly, Janbu proposed correction factors to adjust the results based on experimental data from various slope stability analysis problems.

2.1.2.4. Lowe and Karafiath's Method

Lowe and Karafiath introduced a side force correction within a concept similar to the one proposed by Janbu. In Lowe and Karafiath's method, it is intuitively assumed that the direction of the resultant interslice force in an interface is equal to the average of the ground and slip surface slopes as illustrated with Figure 2.6. Using GLE formulation, this approach is accommodated by setting λ factor to 1 and applying the interslice force function given in Eq. (2.17). Lowe and Karafiath's method is often considered as the most accurate of all force equilibrium methods [2, 37].

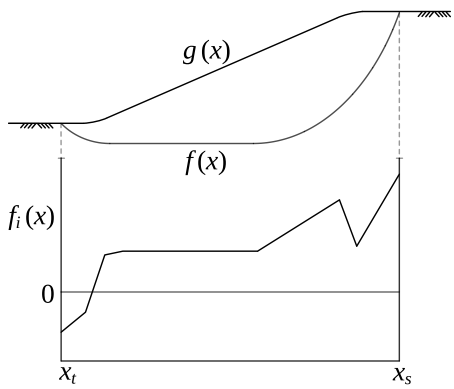

Figure 2.6: Interslice force function of Lowe and Karafiath's method

$$\lambda = 1,\ f_i(x) = \frac{f'(x) + g'(x)}{2} \tag{2.17}$$

where $f(x)$: a function representing the slip surface, $g(x)$: a function representing the ground surface.

2.1.2.5. Corps of Engineers Method

Corps of Engineers method is essentially the same as the one proposed by Lowe and Karafiath. However, in this method, the direction of the interslice force is assumed to be equal to the average ground surface slope. This statement is interpreted in two different ways as (i) the inclination of the chord passing through the slip toe and scarp and (ii) the average ground surface slope above the interface. Therefore, Corps of Engineers method has two variations used in practice as illustrated in Figure 2.7 and given in Eqs. (2.18) and (2.19). Compared to Lowe and Karafiath's internal force assumption, both of these approaches often lead to overestimated F_S values [2, 37].

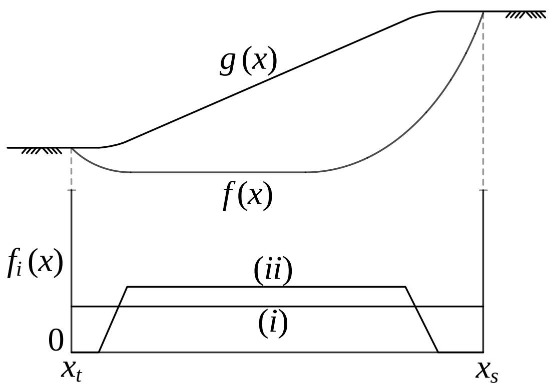

Figure 2.7: Interslice force functions of Corps of Engineers method

$$\textit{Case } (i)\text{:}\ \lambda = 1,\ f_i(x) = \frac{f(x_s) - f(x_t)}{x_s - x_t} \tag{2.18}$$

$$\textit{Case } (ii)\text{:}\ \lambda = 1,\ f_i(x) = g'(x) \tag{2.19}$$

where x_t and x_s: abscissas of slip toe and scarp.

2.1.2.6. Morgenstern-Price and Spencer's Methods

Morgenstern-Price method is possibly the most common rigorous procedure of slices. The method accounts for all internal reactions and equilibrium conditions, hence can be adopted as the generalized form of GLE formulation. In this approach, the direction of interslice force is again dictated with a prescribed function, $f_i(x)$. However, in this case, λ factor is utilized to scale the function, in order to achieve complete equilibrium. As a result, both F_S and λ are unknown variables in Morgenstern-Price method. There are various interslice force functions proposed in the literature (e.g. constant, trapezoid, half-sine, clipped sine functions). However, the F_S computed by Morgenstern-Price method is reasonably insensitive to this selection [3]. Therefore, any reasonable relation can be implemented. Among the available approaches, constant and half-sine functions are commonly preferred in engineering practice [38]. Therefore, these functions are defined in Eqs. (2.20) and (2.21) and further illustrated in Figure 2.8. It should be noted that Spencer's method is a special case of Morgenstern-Price method where the interslice function is constant (i.e. all interslice forces are parallel).

$$\text{Constant function: } f_i(x) = 1 \tag{2.20}$$

$$\text{Half-sine function: } f_i(x) = \sin\left[\pi\left(\frac{x - x_t}{x_s - x_t}\right)\right] \tag{2.21}$$

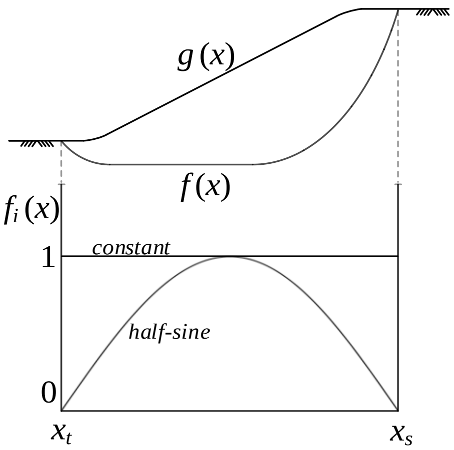

Figure 2.8: Interslice force functions of Morgenstern-Price method

Using one of the abovementioned interslice functions, Morgenstern-Price method analyzes the slip surface based on force and moment equilibrium. As a result, the problem is defined by two governing equations, Eqs. (2.14) and (2.15), and two unknowns, F_S and λ. Since normal force is dependent on F_S, both expressions are recursive (i.e. F_S appears on both sides). Therefore, the system cannot be solved through algebraic operations. Instead, trial and error approaches, graphical procedures or multivariate quasi-Newton root finding methods can be adopted to find the couple that satisfies both equilibrium conditions. For the non-rigorous LEMs proposed by Bishop, Janbu, Lowe and Karafiath, and Corps of Engineers, the solution procedure is comparably simple. The problem is either defined by Eq. (2.14) or (2.15) and the only unknown is F_S. Accordingly, bracketing methods or fixed-point iteration can also be adopted to find F_S, in addition to the methods mentioned previously. Based on the discussions presented in this section, a summary of common procedures of slices are given in Table 2.3.

Table 2.3: Summary and comparison of procedures of slices

Method	Equilibrium Conditions: Vertical Force	Equilibrium Conditions: Horizontal Force	Equilibrium Conditions: Moment	Surface	Comments
Fellenius [9]	✕	✕	✓	Circular	The simplest method of slices; ignores interslice forces; very inaccurate for flat slopes with high pore-water pressures
Bishop's simplified [10]	✓	✕	✓	Circular	Ignores interslice shear forces; accurate within its range of applications
Janbu's simplified [11]	✓	✓	✕	General	Simplest force method; ignores interslice shear forces; always underestimates F_S
Lowe and Karafiath [12]	✓	✓	✕	General	Assumes the magnitude and direction of interslice shear forces; most accurate force equilibrium method
Corps of Engineers [13]	✓	✓	✕	General	Assumes the magnitude and direction of interslice shear forces; often overestimates F_S
Spencer [14]	✓	✓	✓	General	Simplest rigorous method; assumes parallel interslice forces; accurate
Morgenstern-Price [3]	✓	✓	✓	General	Rigorous method; variable interslice force direction; accurate

2.2. Slip Surface Generation

The procedures discussed so far can only evaluate the stability of an assumed slip surface. Therefore, a method is required to generate trial solutions, considering that LEMs associate the slope system safety to that of the critical slip surface. In this section, some of the available surface generation methods are introduced through a classification of available approaches. First, procedures that generate simple surface geometries such as planar, circular and logarithmic spiral are presented in Section 2.2.1. Then, in Section 2.2.2, some of the common general slip surface generation methods are discussed and formulated for the succeeding chapters.

2.2.1. Planar, Circular and Logarithmic Spiral Slip Surfaces

The approaches discussed in this section are based on specified surface geometries that are coupled with specific LEMs or adopted to simplify the surface optimization procedure. A common feature of these approaches is that the resulting surfaces can be represented with at most a few geometric parameters. For instance, planar surfaces used in Infinite Slope analysis are defined by only one geometric parameter, which is the slip surface depth. As a result, a specific surface generation or optimization technique is not necessarily adopted for this method.

In the case of circular and logarithmic spiral surfaces, the geometry can be defined by a center and a radius (i.e. initial radius for logarithmic spirals). Therefore, a two-dimensional analysis optimizes three control variables to determine the critical slip surface. In practice, this procedure is often handled with a grid search routine [37]. The example given in Figure 2.9 illustrates a circular failure analysis. Each node of the grid is a possible center for the critical slip surface. For each center, multiple surfaces are generated and the radius, r, is optimized to minimize F_S. The configuration that yields the minimum F_S is specified as the critical slip surface. For logarithmic spiral surfaces, a similar approach can be adopted as well. Although this approach is relatively simple, the result accuracy is limited as the critical slip surface can significantly deviate from these constrained geometries.

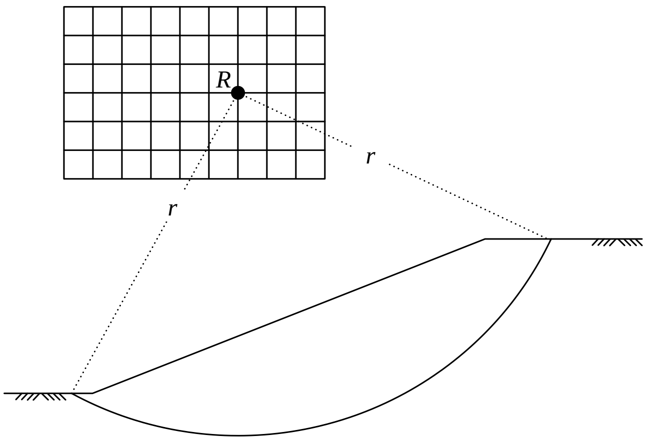

Figure 2.9: Grid search approach for circular failure analysis

2.2.2. General Slip Surfaces

The reliability of limit equilibrium solutions significantly depends on the capability of the implemented surface generation method. To accurately represent the critical case, the method should be flexible to produce any reasonable slip surface, which may incorporate a composition of planar and rotational segments with variable curvature and even abrupt gradient transitions. In this sense, general surface generation methods (i.e. also known as non-circular surface generation methods) eliminate the restrictions imposed by the approaches presented previously. Although this concept is widely accepted, it is not extensively studied in the literature except for the notable efforts of Sun [21], Malkawi [32], Bolton [41], Cheng [33, 39] and Li [42]. In the following sub-sections, the methods proposed by Malkawi, Cheng, and Sun are presented.

2.2.2.1. Malkawi's Method

The method suggested by Malkawi [32] is one of the most effective approaches in the literature, having successful applications to slope stability analysis problems. When generating a slip surface of *n* slices, the formulation requires *2n* geometric parameters, which are normalized between [0, 1]. The parameters can either be chosen randomly or produced by an optimization routine. The method always generates convex surfaces to meet the kinematical admissibility requirement proposed in [28, 32, 39, 40]. Beyond that, no major geometric restrictions are imposed on the surface geometries. The procedure is formulated below, based on the generic surface illustrated in Figure 2.10.

***Step 1*:** Define the horizontal boundary limits of the slip toe and scarp, $V_1(x_1, y_1)$ and $V_{n+1}(x_{n+1}, y_{n+1})$, respectively.

$$x_1 \in \left[x_{1,\min},\ x_{1,\max}\right], \qquad x_{n+1} \in \left[x_{n+1,\min},\ x_{n+1,\max}\right] \tag{2.22}$$

where $x_{1,\min}$ and $x_{n+1,\min}$: minimum limits of x_1 and x_{n+1}, $x_{1,\max}$ and $x_{n+1,\max}$: maximum limits of x_1 and x_{n+1}.

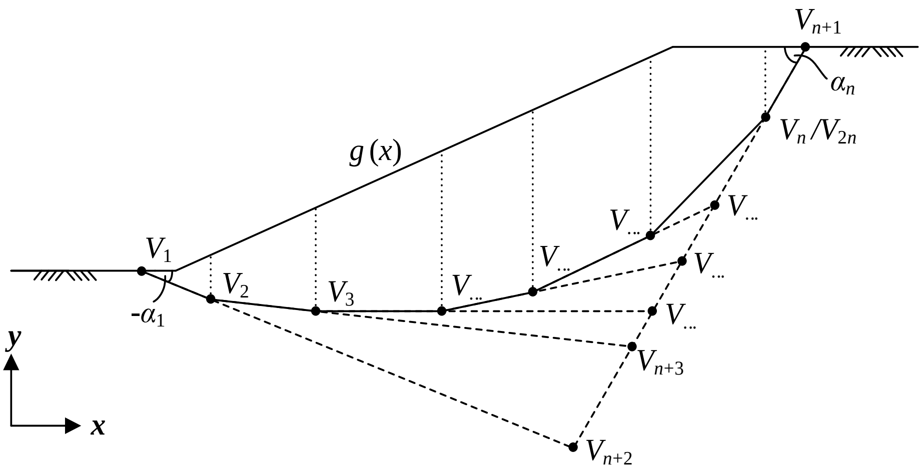

Figure 2.10: Malkawi's surface generation method

***Step 2*:** Prescribe the number of slices, n, and generate a decision vector of $2n$ variables using an optimization method.

$$\mathbf{r} = \left(r_1, ..., r_d, ..., r_{2n}\right) \tag{2.23}$$

r: a decision vector with $2n$ variables, r_d: d^{th} geometric variable of **r**, where $r_d \in [0, 1]$.

***Step 3*:** Determine the positions of $V_1(x_1, y_1)$ and $V_{n+1}(x_{n+1}, y_{n+1})$ using Eqs. (2.24)–(2.27).

$$x_1 = x_{1,\min} + r_1\left(x_{1,\max} - x_{1,\min}\right) \tag{2.24}$$

$$y_1 = g(x_1) \tag{2.25}$$

$$x_{n+1} = x_{n+1,\min} + r_2\left(x_{n+1,\max} - x_{n+1,\min}\right) \tag{2.26}$$

$$y_{n+1} = g(x_{n+1}) \tag{2.27}$$

where $y=g(x)$: the function representing the ground surface.

***Step 4*:** Determine the toe and scarp angles of the surface, denoted as α_1 and α_n respectively, using Eqs. (2.28) and (2.29). It should be noted that the toe angle is limited between -30° and -45° to avoid computational difficulties during the F_S evaluation, in accordance with [43]. However, this approach does not impose any restrictions to the generated surfaces since slice widths are variable. The width of the first slice may converge to zero and practically be replaced by the second slice, allowing any toe angle greater than -30^{o}.

$$\alpha_1 = \frac{\pi}{12}(r_3 - 3) \tag{2.28}$$

$$\alpha_n = \frac{\pi}{2} + r_4\alpha_1 \tag{2.29}$$

Step 5**:** Determine the position of $V_{n+2}(x_{n+2}, y_{n+2})$ analytically by drawing two lines from V_1 and V_{n+1} with angles α_1 and α_n, respectively.

Step 6**:** Determine the position of $V_2(x_2, y_2)$ using Eqs. (2.30) and (2.31).

$$x_2 = x_1 + r_5(x_{n+2} - x_1) \tag{2.30}$$

$$y_2 = y_1 + (x_2 - x_1)\tan\alpha_1 \tag{2.31}$$

Step 7**:** Determine the positions of vertices n+3 to 2n using Eqs. (2.32) and (2.33).

$$x_{i+1} = x_i + r_{i+4-n}(x_{n+1} - x_i) \tag{2.32}$$

$$y_{i+1} = y_i + (x_{i+1} - x_i)\tan\alpha_n \tag{2.33}$$

for $i = n+2, n+3, \ldots, 2n-1$

Step 8**:** Determine the positions of vertices 3 to n-1 using Eqs. (2.34)–(2.36).

$$x_{i+1} = x_i + r_{i+n+2}(x_{i+n+1} - x_i) \tag{2.34}$$

$$\tan\alpha_i = \frac{y_{i+n+1} - y_i}{x_{i+n+1} - x_i} \tag{2.35}$$

$$y_{i+1} = y_i + (x_{i+1} - x_i)\tan\alpha_i \tag{2.36}$$

for $i = 2, 3, \ldots, n-2$

Step 9**:** Assign the coordinates of the V_n using Eq. (2.37). Note that V_n and V_{2n} correspond to the same vertex.

$$x_n = x_{2n},\; y_n = y_{2n} \tag{2.37}$$

2.2.2.2. Cheng's Equal and Variable Division Methods

In their study, Cheng et al. [33] evaluated the performances of various surface generation methods, including the one proposed by Malkawi. The study concluded that Malkawi's method is fairly efficient for problems incorporating stratified soil profiles, yet it may not be applicable to complicated loading cases. Accordingly, they proposed the alternative approaches presented in this section. Cheng's method starts by assigning the slip toe and scarp positions. Then, the slice widths and the base angles are assigned considering the kinematical admissibility requirements. There are two variations of this method, based on (i) equal slice division (i.e. slice width is constant) and (ii) variable slice division (i.e. slice width is variable) which generate a slip surface of n slices using n+1 and $2n$ geometric parameters, respectively. The procedure is formulated below considering the generic slip surface illustrated in Figure 2.11.

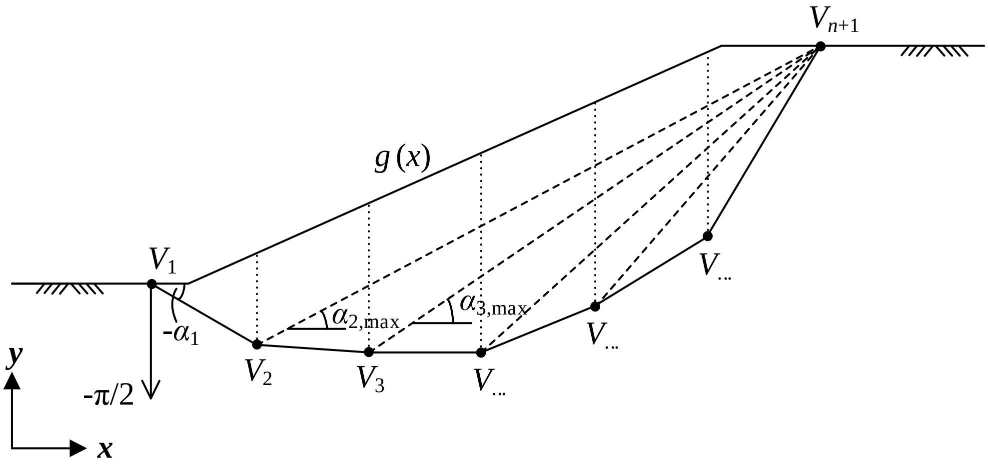

Figure 2.11: Cheng's surface generation methods

***Step 1*:** Define the horizontal boundary limits of the slip toe and scarp, $V_1(x_1, y_1)$ and $V_{n+1}(x_{n+1}, y_{n+1})$, respectively.

$$x_1 \in \left[x_{1,\min},\ x_{1,\max}\right], \qquad x_{n+1} \in \left[x_{n+1,\min},\ x_{n+1,\max}\right] \tag{2.38}$$

where $x_{1,\min}$ and $x_{n+1,\min}$: minimum limits of x_1 and x_{n+1}, $x_{1,\max}$ and $x_{n+1,\max}$: maximum limits of x_1 and x_{n+1}.

Step 2**:** Prescribe the number of slices, n, and select either equal or variable division approach. For equal division approach, generate a decision vector of n+1 variables. For the variable division approach, generate a 2n variables.

$$\text{Equal division: } \mathbf{r} = \left(r_1, ..., r_d, ..., r_{n+1}\right) \tag{2.39}$$

$$\text{Variable division: } \mathbf{r} = \left(r_1, ..., r_d, ..., r_{2n}\right) \tag{2.40}$$

where **r**: a decision vector with either n+1 or 2n variables based on the selected approach, r_d: d^{th} geometric variable of **r**, where, $r_d \in [0, 1]$.

Step 3**:** Determine the positions of $V_1(x_1, y_1)$ and $V_{n+1}(x_{n+1}, y_{n+1})$ using Eqs. (2.41)–(2.44).

$$x_1 = x_{1,\min} + r_1\left(x_{1,\max} - x_{1,\min}\right) \tag{2.41}$$

$$y_1 = g(x_1) \tag{2.42}$$

$$x_{n+1} = x_{n+1,\min} + r_2\left(x_{n+1,\max} - x_{n+1,\min}\right) \tag{2.43}$$

$$y_{n+1} = g(x_{n+1}) \tag{2.44}$$

where $y=g(x)$: the function representing the ground surface.

Step 4**:** Calculate the average slice width, Δx, using Eq. (2.45) and determine abscissas of vertices 2 to n using either Eq. (2.46) or Eq. (2.47), depending on the selected approach.

$$\Delta x = \frac{x_{n+1} - x_1}{n} \tag{2.45}$$

$$\text{Equal division: } x_i = x_{i-1} + \Delta x \text{ for } i = 2, 3, \text{n} \tag{2.46}$$

$$\text{Variable division: } x_i = x_{i-1} + \left(0.5 + r_{i+n}\right)\Delta x \text{ for } i = 2, 3, \text{n} \tag{2.47}$$

Step 5**:** Determine the toe angle of the surface, denoted as α_1, using Eq. (2.48). Note that the toe angle is limited between the ground surface inclination and 90°.

$$\alpha_1 = -\frac{\pi}{2} + r_3\left[g'(x_1) - \frac{\pi}{2}\right] \tag{2.48}$$

Step 6**:** Calculate the ordinate of V_2 using Eq. (2.49).

$$y_i = y_{i-1} + \Delta x \tan \alpha_{i-1} \tag{2.49}$$

Step 7**:** For slices 2 to n-1, determine the minimum and maximum limits of base angles using Eqs. (2.50) and (2.51). Then, calculate the base angles and ordinates using Eqs. (2.52) and (2.53), respectively.

$$\alpha_{i,\min} = \alpha_{i-1} \tag{2.50}$$

$$\alpha_{i,\max} = \tan^{-1}\left[\min\left\{\frac{y_{n+1} - y_i}{x_{n+1} - x_i},\ \frac{g(x_{i+1}) - y_i}{x_{i+1} - x_i}\right\}\right] \tag{2.51}$$

$$\alpha_i = \alpha_{i,\min} + r_{i+2}\left(\alpha_{i,\max} - \alpha_{i,\min}\right) \tag{2.52}$$

$$y_{i+1} = y_i + \Delta x \tan \alpha_i \tag{2.53}$$

for i = 2, 3, n-1

where $\alpha_{i,\min}$ and $\alpha_{i,\max}$: minimum and maximum limits of α_i.

2.2.2.3. Sun's Cubic Spline Method

The common feature of Malkawi's and Cheng's methods is that they require a great number of geometric parameters for accurate surface representation, and thus produce high-dimensional, difficult surface optimization problems. Addressing this issue, Sun [21] proposed a procedure to minimize the number of geometric variables through spline interpolation. The method generates a number of vertices and connects them with continuous cubic spline functions. Then, the resulting free-body is divided into equally spaced vertical slices. Based on the description given by Sun, the method is summarized as follows:

Step 1**:** Construct n_s+1 vertices as represented in Eq. (2.54). The vertices should comply with the constraints given in Eqs. (2.55)–(2.58).

$$V_1(x_1, y_1),\ V_2(x_2, y_2), \ldots,\ V_{n_s+1}\left(x_{n_s+1}, y_{n_s+1}\right) \tag{2.54}$$

Equal horizontal spacing constraint:

$$x_j = x_{j-1} + \frac{\left(x_{n_s+1} - x_1\right)}{n_s} \quad \text{for } j = 2, 3, \ldots, n_s \tag{2.55}$$

Boundary constraints:

$$x_{\min} \le x_j \le x_{\max} \text{ for } j = 1, 3, \ldots, n_s+1 \tag{2.56}$$

$$y_1 = g(x_1),\ y_{n_s+1} = g(x_{n_s+1}) \tag{2.57}$$

Kinematic admissibility constraint:

$$-\frac{\pi}{4} \le \alpha_1 \le \alpha_2 \le \ldots \le \alpha_j \le \ldots \le \alpha_{n_s+1} \le \frac{\pi}{3} \tag{2.58}$$

where n_s: number of splines, $x_{\min}$ and $x_{\max}$: minimum and maximum horizontal limits of vertices, $y=g(x)$: the function representing the ground surface, α_j: inclination of the line passing through vertices j and $j+1$.

***Step 2*:** Perform cubic spline interpolation to connect the vertices. Based on this approach, kinematical admissibility is not guaranteed as cubic spline functions can oscillate to produce concave down segments.

***Step 3*:** Divide the free-body into n vertical slices and process the data to compute slice properties.

Although the general concept of the method is described, an explicit formulation was not given in the study of Sun [21]. In the scope of this study, Sun's method is formulated based on Malkawi's approach through a modification to impose constant slice widths. The resulting procedure requires n_s+1 geometric parameters to generate a surface of n_s splines as formulated in the following pseudocode considering the generic slip surface illustrated in Figure 2.12.

***Step 1*:** Define the horizontal boundary limits of the slip toe and scarp, $V_1(x_1, y_1)$ and $V_{ns+1}(x_{ns+1}, y_{ns+1})$, respectively.

$$x_1 \in \left[x_{1,\min},\ x_{1,\max}\right], \qquad x_{n_s+1} \in \left[x_{n_s+1,\min},\ x_{n_s+1,\max}\right] \tag{2.59}$$

where $x_{1,\min}$ and $x_{ns+1,\min}$: minimum limits of x_1 and x_{ns+1}, $x_{1,\max}$ and $x_{ns+1,\max}$: maximum limits of x_1 and x_{ns+1}.

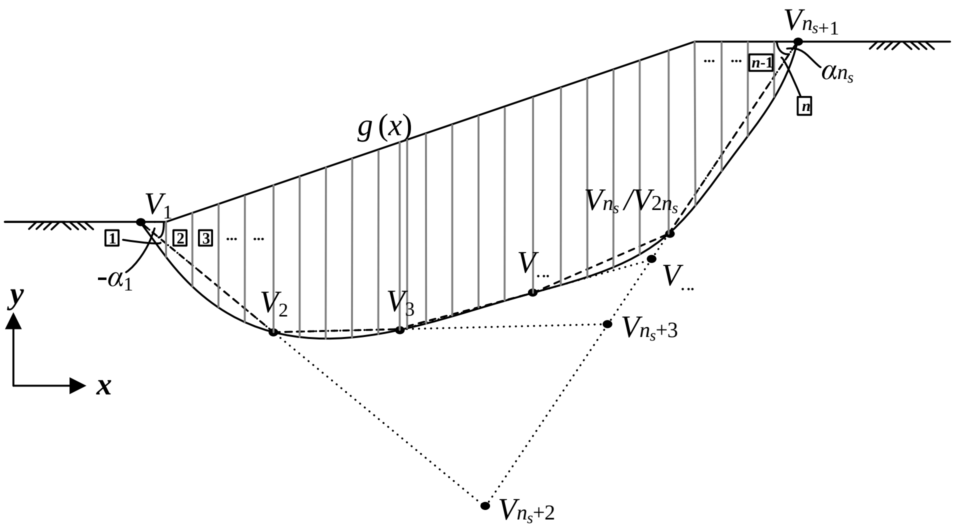

Figure 2.12: Sun's surface generation method

Step 2**:** Prescribe the number of splines, n_s, and generate a decision vector of n_s+1 variables using an optimization method.

$$\mathbf{r} = \left(r_1, ..., r_d, ..., r_{n_s+1}\right) \tag{2.60}$$

r: a decision vector with n_s+1 variables, r_d: d^{th} geometric variable of **r**, where $r_d \in [0,1]$.

Step 3**:** Determine the positions of $V_1(x_1, y_1)$ and $V_{ns+1}(x_{ns+1}, y_{ns+1})$ using Eqs. (2.61)–(2.64).

$$x_1 = x_{1,\min} + r_1\left(x_{1,\max} - x_{1,\min}\right) \tag{2.61}$$

$$y_1 = g(x_1) \tag{2.62}$$

$$x_{n_s+1} = x_{n_s+1,\min} + r_2\left(x_{n_s+1,\max} - x_{n_s+1,\min}\right) \tag{2.63}$$

$$y_{n_s+1} = g(x_{n_s+1}) \tag{2.64}$$

where $y=g(x)$: the function representing the ground surface.

Step 4**:** Calculate the average slice width, Δx, using Eq. (2.65) and determine the abscissas of vertices 2 to n_s using Eq. (2.66).

$$\Delta x = \frac{x_{n_s+1} - x_1}{n_s} \tag{2.65}$$

$$x_j = x_{j-1} + \Delta x \;\text{ for } j = 2, 3, n_s \tag{2.66}$$

Step 5**:** Determine the toe and scarp angles of the surface, denoted as α_1 and α_{ns} respectively. The method limits the base angles -45° and 60°. Therefore, the equations given for Malkawi's method are modified to comply with this requirement.

$$\alpha_1 = \frac{\pi}{12}(r_3 - 3) \tag{2.67}$$

$$\alpha_{n_s} = \frac{\pi}{3} + r_4 \alpha_1 \tag{2.68}$$

Step 6**:** Determine the position of $V_{ns+2}(x_{ns+2}, y_{ns+2})$ analytically by drawing two lines from V_1 and V_{ns+1} with angles α_1 and α_{ns}, respectively.

Step 7**:** Determine the ordinates of V_2 and V_{ns} using Eqs. (2.69) and (2.70).

$$y_2 = y_1 + (x_2 - x_1)\tan\alpha_1 \tag{2.69}$$

$$y_{n_s} = y_{n_s+1} - (x_{n_s+1} - x_{n_s})\tan\alpha_{n_s} \tag{2.70}$$

Step 8**:** Determine the positions of vertices n_s+3 to 2n_s-1 using Eqs. (2.71) and (2.72).

$$x_{j+1} = x_j + r_{j+3-n_s}(x_{n_s+1} - x_j) \tag{2.71}$$

$$y_{j+1} = y_j + (x_{j+1} - x_i)\tan\alpha_{n_s} \tag{2.72}$$

for $j = n_s+2, n_s+3, \ldots, 2n_s-2$

Step 9**:** Determine the ordinates of vertices 3 to n_s-1 using Eqs. (2.73) and (2.74).

$$\tan\alpha_j = \frac{y_{j+n_s+1} - y_j}{x_{j+n_s+1} - x_j} \tag{2.73}$$

$$y_{j+1} = y_j + (x_{j+1} - x_j)\tan\alpha_j \tag{2.74}$$

for $j = 2, 3, \ldots, n_s-2$

Step 10**:** Perform cubic spline interpolation to connect the vertices. The boundary conditions of the splines were not clearly specified by Sun. Therefore, the study possibly employed natural splines.

Step 11**:** Divide the free-body into *n* vertical slices as illustrated in Figure 2.12 and process the data to compute slice properties.

2.3. Surface Optimization and Differential Evolution Algorithm

Each surface generation method presented in the previous section requires input decision vectors containing the geometric parameters of the trial slip surfaces. These parameters are essentially the problem variables that are optimized in order to minimize F_S. When general slip surface generation methods are employed, the analysis procedures translate into high-dimensional optimization problems. Considering that the search spaces of these problems often contain multiple local minima, implementing a global optimization technique is vital to produce reliable results. In other words, the optimization method should be capable of exploring the search space and avoid/escape local minima through random operations. In this sense, stochastic optimization algorithms are often preferred over other alternatives.

Despite the above arguments, deterministic approaches based on conjugate-gradient technique [46], dynamic programming [47, 48], alternating-variable search [49, 50], simplex method [51–54], Powell, Broyden-Fletcher-Goldfarb-Shanno and Davidon-Fletcher-Powell algorithms [53] were adopted in the earlier studies due to relatively high computational cost of stochastic search techniques.

After this era, structured random procedures based on Monte Carlo simulation were proposed for the problem by Greco [55] and Malkawi et al. [32, 56]. Following the rapid advent of computer technology, deterministic techniques were suppressed by the development of nature-inspired stochastic optimization algorithms named metaheuristics and became obsolete for the problem. Generally inspired by the random concepts observed in biology, physics, material science, social studies, etc., metaheuristic algorithms imitate some phenomena within an iterative framework to converge to a solution. The random nature of these algorithms help them avoid local optima in complex problems, hence they are favored over deterministic techniques in a broad range of engineering applications, including slope engineering. Among the available metaheuristic algorithms, Genetic Algorithm has numerous implementations to slope stability problems [17–25]. Variants of another evolutionary algorithm, Differential Evolution, were adopted in [26, 27]. Swarm intelligence algorithms are also popular with applications of Particle Swarm Optimization, Artificial Fish Swarm Algorithm and Cuckoo Search [28–31]. Furthermore, there are notable studies based on Harmony Search [29, 33], Simulated Annealing and Tabu Search [29], Ant Colony Optimization [57, 58], Gravitational Search Algorithm [59, 60], Artificial Bee Colony Optimization [61], Immunised Evolutionary Programming [58], and Imperialistic Competitive Algorithm [62]. In this study, the specific focus will be on Differential Evolution algorithm.

Inspired by Darwin's principles of natural selection and evolution, Storn and Price [63] introduced Differential Evolution (DE) algorithm for continuous variable optimization problems. The algorithm initializes with a randomly generated population of individuals (i.e. decision vectors) and performs successive operations named (i) mutation, (ii) crossover, and (iii) selection. These operations basically simulate evolution within the search space of an optimization problem, in order to improve the quality of the individuals (i.e. slip surfaces). For each member of the population, DE arbitrarily selects and combines the genes (i.e. variables in the decision vector) of three individuals named "donors" to produce a mutant vector. Then, in the crossover phase, the individuals exchange some of their genes (i.e. geometric parameters of the surfaces) with their mutants to produce new members. In the selection phase, the fitness values (i.e. F_S of the surfaces) of the new members are compared with their predecessors. The individuals that produce better quality solutions replace their predecessors to form the next generation of individuals. This procedure is repeated until a specified termination criterion is met. DE has two control parameters; (i) crossover rate, $CR \in [0, 1]$ and, (ii) mutation factor, $F \in [0, 1]$, which are constant factors that can be tuned to manipulate the search behavior of the algorithm. These concepts and their mathematical implementations in the algorithm are given in the following pseudocode and further illustrated in the flowchart given in Figure 2.13.

Step 1 - Initialization**:** Generate a random population of *"K"* individuals, where the position of each individual in the search space is represented by the design vector $\mathbf{r}^k$ defined in Eq. (2.75).

$$\mathbf{r}^k = \left(r_1^k, ..., r_d^k, ..., r_D^k\right) \quad \text{for } k = 1, 2, \ldots, K \tag{2.75}$$

where D: dimension of the problem, $r^k{}_d$: the position of the k^{th} individual on the d^{th} dimension.

Step 2 - Evaluation**:** Evaluate the fitness of each individual.

Step 3 - Mutation**:** For each individual, randomly select three donors from the population and generate a mutant vector, using Eq. (2.76).

$$\mathbf{v}^k = \mathbf{r}^{r1} + F \cdot \left(\mathbf{r}^{r2} - \mathbf{r}^{r3}\right) \quad \text{for } k = 1, 2, \ldots, K \tag{2.76}$$

$$\mathbf{v}^k = \left(v_1^k, ..., v_d^k, ..., v_D^k\right) \tag{2.77}$$

where $\mathbf{v}^k$: mutant vector of the k^{th} individual, $\mathbf{r}^{r1}$**,** $\mathbf{r}^{r2}$ and $\mathbf{r}^{r3}$: randomly selected donor vectors (i.e. $r1$, $r2$, $r3 \in \{1, 2, \ldots, K\}$), F: mutation factor, $v^k{}_d$: the position of $\mathbf{v}$ on the d^{th} dimension.

Step 4 - Crossover**:** Perform crossover operation to produce trial decision vectors, $\mathbf{u}^k$, using Eq. (2.78).

$$u_d^k = \begin{cases} v_d^k, & if \quad R_d^k \le CR \ or \ d = i^k \\ x_d^k, & if \quad R_d^k > CR \ and \ d \ne i^k \end{cases} \quad \text{for } d = 1, 2, \ldots, D \ \text{ and } k = 1, 2, \ldots, K \tag{2.78}$$

where $u^k{}_d$: the position of $\mathbf{u}^k$ on the d^{th} dimension, $R^k{}_d$: uniformly distributed random number $\in [0, 1]$, i^k: randomly chosen index $\in \{1, 2, \ldots, D\}$, CR: crossover rate.

Step 5 - Selection**:** Evaluate the fitness of each trial decision vector $\mathbf{u}^k$ and compare with the fitness of $\mathbf{r}^k$, keep the best one in the population.

Step 6 - Termination**:** Stop iterations if the termination criteria are satisfied. If not, return to Step 3. It is common to control the termination with a prescribed number of maximum iterations, T.

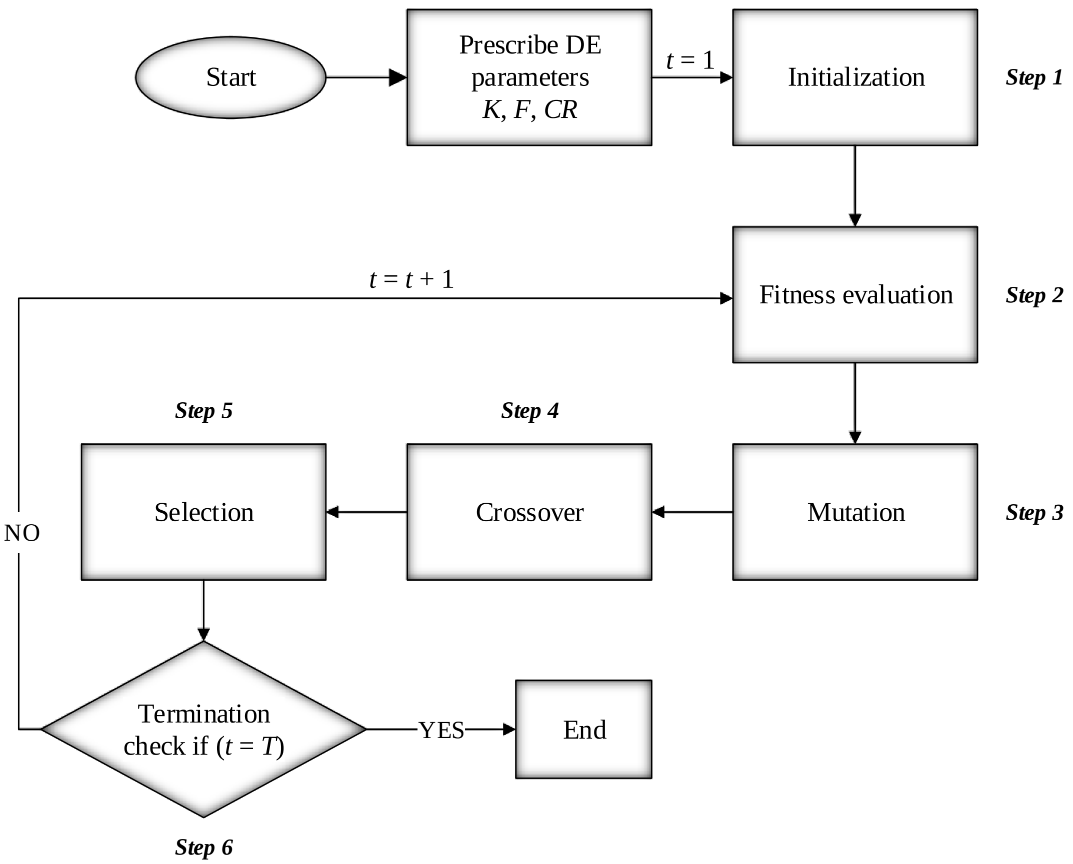

Figure 2.13: Flowchart of Differential Evolution algorithm

CHAPTER 3

INTEGRATED LIMIT EQUILIBRIUM METHOD - PART I: SURFACE GENERATION

In this chapter, the surface generation module of Integrated Limit Equilibrium Method, namely, Scaled Quadratic Spline method (SQS) is introduced and proposed as an alternative to the available approaches. In Section 3.1, the general principles and the aim of SQS are discussed and the method is formulated. Section 3.2 comprises a series of numerical experiments that validate the improved performance of SQS over other surface generation methods in the literature. To emphasize the capability of the proposed method more clearly, the results are further evaluated in comparison with a common commercial stability analysis software. Lastly, a summary of the findings and discussions are given in Section 3.3.

3.1. Scaled Quadratic Spline Method

The proposed surface generation procedure, Scaled Quadratic Spline (SQS) method is conceptually similar to Sun's cubic spline approach [21]. In both methods, the slip surfaces are represented with nonlinear spline functions instead of linear segments, aiming to (i) eliminate the unnecessary accuracy loss and (ii) minimize the number of geometric parameters required for accurate surface representation. With this idea in mind, Sun proposed a procedure with cubic spline interpolation, which has some deficiencies based on the observations made in this study. The first issue with Sun's Cubic Spline Method is that the formulation lacks an explicit constraint to produce admissible surfaces. The method suggests a criterion, given in Eq. (2.58), to assure that the lines passing through the spline nodes form a convex surface. Although this measure implicitly controls the feasibility of the surfaces, it is still possible to produce deficient geometries, as illustrated in Figure 3.1. In some cases, cubic splines may oscillate to produce non-convex surfaces as their geometries are entirely dictated by the alignment of the nodes. Another issue with Sun's approach is related to the applied spline boundary conditions. A cubic surface produced by conventional procedures inherently has continuous first and second derivatives at each node, which is not necessarily a favorable feature for slope stability analysis. The critical slip surfaces often incorporate sudden gradient transitions under external loading or in cases where the soil profile is stratified.

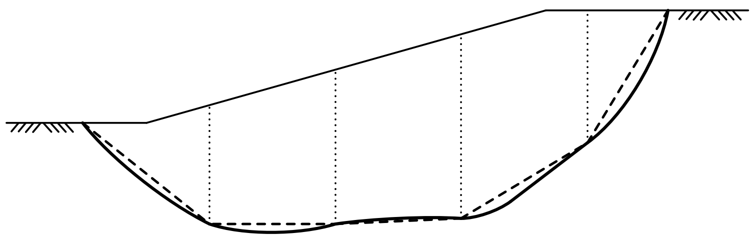

Figure 3.1: Kinematically inadmissible slip surface

Addressing the abovementioned issues, SQS is proposed as a simple, yet efficient alternative to the available surface generation methods. In SQS, spline nodes are generated using the approach proposed by Malkawi [32]. Then, the surface is constructed with *piecewise* continuous quadratic splines as illustrated in Figure 3.2.

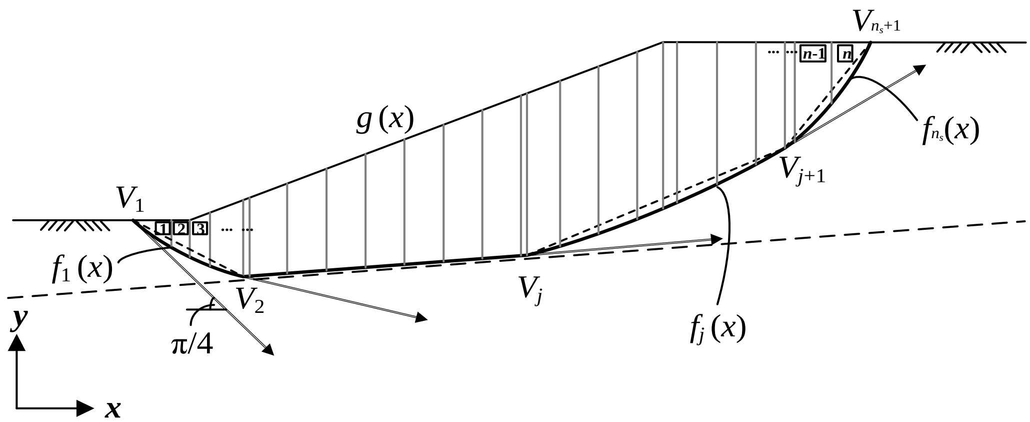

Figure 3.2: Scaled Quadratic Spline Method – general view of a slip surface

For each segment, three boundary conditions are required to calculate the spline coefficients, *"a_f"*, *"b_f"*, and *"d_f"* given in Eq (3.1).

$$f_j(x) = (a_f)_j x^2 + (b_f)_j x + (d_f)_j \tag{3.1}$$

where $f_j(x)$: quadratic spline function representing the j^{th} segment of the surface.

The first two boundary conditions come from the positions of end nodes, vertices V_j and V_{j+1} in Figures 3.2 and 3.3. The last boundary condition is prescribed with the derivative of $f_j(x)$ at its first node, $f_j'(x_j)$. For continuous spline interpolation, this value is already known and equal to the derivative of the preceding spline at the same node, $f_{j-1}'(x_j)$. On the other hand, SQS utilizes $f_{j-1}'(x_j)$ as a lower limit of $f_j'(x_j)$, while the upper limit is taken as the slope of the linear segment between the end nodes (i.e. reference line produced with Malkawi's procedure), denoted as "m_j" in Figure 3.3. Additionally, another lower limit value is implemented to prevent a negative inflection on the second node, V_{j+1}. From the resulting range, SQS assigns a value to $f_j'(x_j)$ using a scale factor between 0 and 1. In other words, the spline geometry is scaled between that of a continuous spline and a linear segment. Through these considerations, SQS always produces convex surfaces. Moreover, the proposed approach stimulates sudden gradient transitions and linear segments to provide the flexibility to deal with geometrically complex problems. To produce a surface represented with n_s splines, the procedure requires $3n_s$ geometric parameters and can be described based on Figures 3.2 and 3.3 as follows:

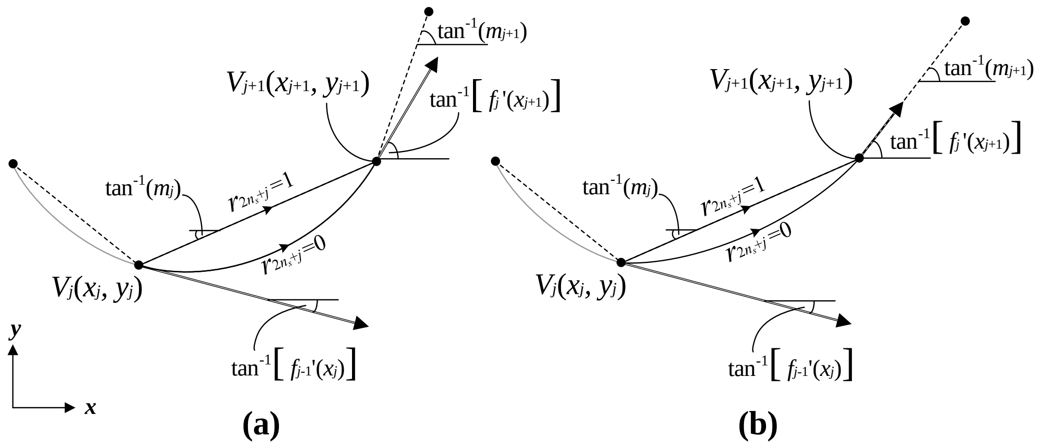

Figure 3.3: Scaled Quadratic Spline Method – close up of splines

***Step 1*:** Prescribe the number of splines, n_s, and generate a decision vector of $3n_s$ variables using an optimization method.

$$\mathbf{r} = (r_1,\ldots,r_d,\ldots,r_{3n_S}) \tag{3.2}$$

where $\mathbf{r}$: a decision vector with $3n_s$ variables, r_d: d^{th} geometric variable of $\mathbf{r}$, $r_d \in [0,1]$.

***Step 2*:** Generate n_s+1 nodal points for quadratic spline interpolation. Employ Malkawi's procedure using the geometric parameters r_1 through r_{2ns}, and take the following into consideration:

(i) In "*Step 4*" of Malkawi's procedure, slip toe inclination is restricted in a range between -30° and -45°. To provide more flexibility, SQS considers a wider range between 0° and -45°.

(ii) In the same step, scarp inclination is determined with an expression based on toe angle. SQS formulation considers scarp inclination as an independent parameter.

Based on these arguments, SQS adopts Malkawi's procedure by replacing Eqs. (2.28) and (2.29) with Eqs. (3.3) and (3.4), respectively.

$$\alpha_1 = \frac{\pi}{4}\left(r_3 - 1\right) \tag{3.3}$$

$$\alpha_{n_s} = \frac{\pi}{4}\left(2 - r_4\right) \tag{3.4}$$

***Step 3*:** Consecutively for each spline: determine the lower and upper limits of $f_j'(x_j)$ using Eqs. (3.5)–(3.8); determine $f_j'(x_j)$ using Eq. (3.9); calculate the spline coefficients using Eqs. (3.10)–(3.12).

$$\left[f_j'(x_j)\right]_{L1} = \begin{cases} -1 & , j = 1 \\ f_{j-1}'(x_j) & , j > 1 \end{cases} \tag{3.5}$$

$$\left[f_j'(x_j)\right]_{L2} = \begin{cases} 2m_j - m_{j+1} & , j < n_s \\ \left[f_j'(x_j)\right]_{L1} & , j = n_s \end{cases} \tag{3.6}$$

$$\left[f_j'(x_j)\right]_{L} = \max\left\{ \left[f_j'(x_j)\right]_{L1},\ \left[f_j'(x_j)\right]_{L2} \right\} \tag{3.7}$$

$$\left[f_j'(x_j)\right]_{U} = m_j \tag{3.8}$$

$$f_j'(x_j) = \left[f_j'(x_j)\right]_{L} + r_{2n_s+j} \cdot \left\{ \left[f_j'(x_j)\right]_{U} - \left[f_j'(x_j)\right]_{L} \right\} \tag{3.9}$$

$$(a_f)_j = \frac{f_j'(x_j) - m_j}{x_{j+1} - x_j}\text{, if } (a_f)_j < \tau_{a_f} \text{ set } (a_f)_j = 0 \tag{3.10}$$

$$(b_f)_j = m_j - (a_f)_j \cdot \left(x_j + x_{j+1}\right) \tag{3.11}$$

$$(d_f)_j = y_j - (a_f)_j \cdot (x_j)^2 - (b_f)_j \cdot x_j \tag{3.12}$$

$$\text{where } f_j(x) = (a_f)_j x^2 + (b_f)_j x + (d_f)_j \tag{3.13}$$

$$\text{for } j = 1, 2, \ldots, n_s$$

where $f_j\,'(x_j)$: function representing the j^{th} quadratic spline, m_j: slope of j^{th} reference line, $[f_j\,'(x_j)]_L$ and $[f_j\,'(x_j)]_U$: lower and upper limits of $f_j\,'(x_j)$, τ_{af}: threshold value for a_f (i.e. τ_{af} is set to 10^{-4} in this study).

***Step 4*:** Divide the free-body into n vertical slices as illustrated in Figure 3.2 and process the data to compute slice properties.

Note that there are two lower limits of $f_j\,'(x_j)$, given in Eqs. (3.5) and (3.6). Eq. (3.5) is based on the terminal gradient of the preceding spline, hence not applicable in the first node. Accordingly, for the first spline, this limit is utilized to keep the slip toe inclination above -45°. Eq. (3.6) is applied to prevent a negative inflection at the second node of each spline, and can be derived by equating $f_j\,'(x_{j+1})$ to the slope of the succeeding reference line, m_{j+1}. Therefore, this boundary condition is not applicable to the last spline. The maximum of the values obtained with Eqs. (3.5) and (3.6) are used as the lower limit of $f_j\,'(x_j)$, given in Eq. (3.7). In Figures 3.3a and 3.3b, the governing limits are based on Eq. (3.5) and (3.6), respectively. Lastly, a threshold value is defined for a_f in Eq. (3.10). Denoted as "τ_{af}", the threshold stimulates linearity and helps with the convergence issues encountered later in Chapter 4.

In addition to SQS, a simplified version of the formulation is also adopted in the numerical experiments. In this simplified variant named Quadratic Spline Method (QS), Eqs. (3.5)–(3.9) are only applied to the first spline function to specify the initial boundary condition. The rest of the splines are constructed continuously without the scaling operation. As a result, QS utilizes $2n_s$+1 geometric parameters as opposed to SQS which requires $3n_s$ parameters. A summary of QS and SQS methods are given in Table 3.1, together with the surface generation methods presented in Chapter 2. It should be noted that the following sections refer to these methods with the abbreviations given in this table.

Table 3.1: Summary and comparison of surface generation methods

Abbreviation: Method	**D**	**Comments**
M1: Malkawi [32]	$2n$	Guarantees kinematical admissibility; allows variable slice width
M2: Cheng's Equal Division [33]	$n+1$	Guarantees kinematical admissibility; keeps slice width constant
M3: Cheng's Variable Division [33]	$2n$	Guarantees kinematical admissibility; allows variable slice width
M4: Sun's Cubic Spline [21]	n_s+1	Promotes kinematical admissibility but does not guarantee it; keeps spline width constant; reduces problem dimension; may not be efficient to handle stratified soil profiles and external loading
QS: Quadratic Spline	$2n_s+1$	Promotes kinematical admissibility but does not guarantee it; allows variable spline width; reduces problem dimension; may not be efficient to handle stratified soil profiles and external loading
SQS: Scaled Quadratic Spline	$3n_s$	Guarantees kinematical admissibility; allows variable spline width; reduces problem dimension; aims to handle complex cases by allowing discontinuous function derivative and stimulating linearity

where D: dimension of the problem (i.e. the number of geometric parameters), n: number of slices, n_s: number of splines.

3.2. Numerical Experiments

To validate the efficiency of ILEM surface generation module, SQS, a series of numerical experiments are performed with a set of benchmark slope stability analysis problems assembled from the literature. The problem set includes six different geometric models, comprising cases with homogeneous and stratified soil profiles. Furthermore, additional configurations with groundwater effect, surcharge, and pseudo-static earthquake loading are considered for some of the examples, resulting in a total of 11 benchmark problems.

The analysis framework is completed with General Limit Equilibrium (GLE) formulation and Differential Evolution (DE) algorithm. The same configuration is also employed with the other surface generation methods (i.e. M1–M4 and QS, given in Table 3.1), in order to evaluate the performance of SQS comparatively. The control parameters of each module are summarized in Table 3.2 and briefly discussed in the following paragraph.

Table 3.2: Parameters settings of the framework components

Module	Method	Parameter
Surface generation	SQS, QS, M4	Number of splines, $n_s \in \{3, 4,\dots, 10\}$ Number of slices, $n \in \{10, 20,\dots, 100\}$
	M1, M2, M3	Number of slices, $n \in \{10, 20,\dots, 100\}$
Stability analysis	GLE - Spencer	Effective stress analysis Error tolerance for F_S and λ, $\varepsilon_{tol}=10^{-5}$
Surface optimization	DE	Mutation factor, F=0.5 Crossover rate, CR=0.9 Population size, K=50 Maximum iteration, T=1000 Number of independent runs = 30

GLE is adopted based on Morgenstern-Price approach with constant interslice force function, given in Eq. (2.20), which is commonly known as Spencer's method. The resulting formulation produces a 2×2 system of nonlinear equations with Eqs. (2.14) and (2.15) and unknowns, F_S and λ. To solve the system, Broyden's multivariate quasi-Newton root finding method [64] is adopted with an error tolerance of $\varepsilon_{tol}=10^{-5}$ for both unknowns. For DE algorithm, the control parameters (i.e. mutation factor "F" and crossover rate "CR") are tuned based on a preliminary study with the settings proposed in the literature. Considering the example problems adopted in this study, the configuration used in [65, 66] is adopted as an efficient parameter setting for all surface generation methods presented in the manuscript. Accordingly, DE is implemented with mutation factor F=0.5 and crossover rate CR=0.9, using a population of K=50 individuals and maximum T=1000 iterations for each analysis. Due to the stochastic nature of DE, each problem is analyzed in 30 independent runs to obtain the statistical performance measures. For the surface generation methods, the main control parameter is either the number of slices or number of splines, both of which identify the dimension of the problem. Since the performance of each method depends on this selection, a parametric study is performed to assess the most efficient configurations. Accordingly, the experiments comprise the analysis of benchmark problems with number of splines varying between 3 and 10 (i.e. where applicable) and number of slices between 10 and 100.

To deliver the findings and validate the applicability of SQS, the following sub-sections are organized as follows: Section 3.2.1 presents the benchmark problems in terms of slope geometry, soil profile and loading condition and gives concise discussions about the expected failure mechanisms. Section 3.2.2 includes the parametric sensitivity analyses of the surface generation methods. In Section 3.2.3, the methods are compared in terms of statistical performance, capability to minimize F_S, and convergence efficiency. Then, in Section 3.2.4, the capability of SQS is emphasized through a comparison with the renowned commercial analysis software, *Slide* [34].

3.2.1. Benchmark Problems

Example 1, adopted from Fredlund and Krahn [67], evaluates the stability of a 12.2 m high slope with 1:2 face inclination, as illustrated in Figure 3.4. The soil profile is dry and idealized as a single homogeneous cohesive soil unit with the parameters given in Table 3.3. External loading and seismic effects are not considered, hence the slope is analyzed under gravitational loads only.

Example 2 is taken from Yamagami and Ueta [53] and is similar to the previous problem. The example deals with a 10 m wide - 5 m high simple slope geometry with a dry homogeneous soil profile as illustrated in Figure 3.5. Yamagami and Ueta analyzed this example under gravitational loads only. Additionally, in this study, the slope is further analyzed considering a 3.5 m wide surcharge of 75 kPa, placed 5 m away from the crest of the slope. In the following sections, experiments without and with the external loading are denoted as *Cases* (*i*) and (*ii*), respectively.

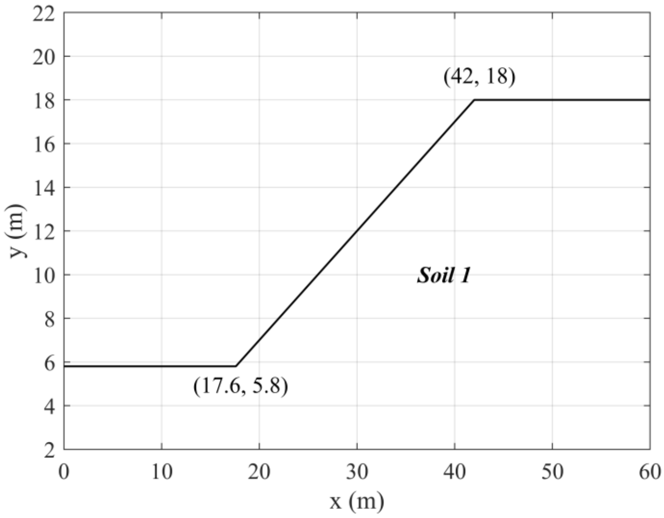

Figure 3.4: *Example 1* – slope geometry and soil profile

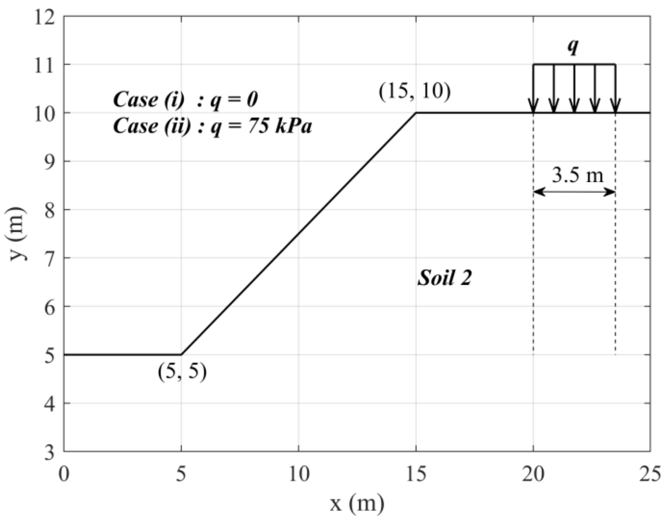

Figure 3.5: *Example 2* – slope geometry and soil profile

In *Example 3*, which was originally studied by Zolfaghari [20], a 17 m wide - 8.5 m high, multi-layered dry slope is analyzed. As illustrated in Figure 3.6, the soil profile is idealized into four discrete units with the parameters given in Table 3.3. The preliminary examination of this problem indicates that there is a thin soft soil deposit (i.e. *Soil 3.3*) between relatively stiffer layers, which may induce a partially translational failure.

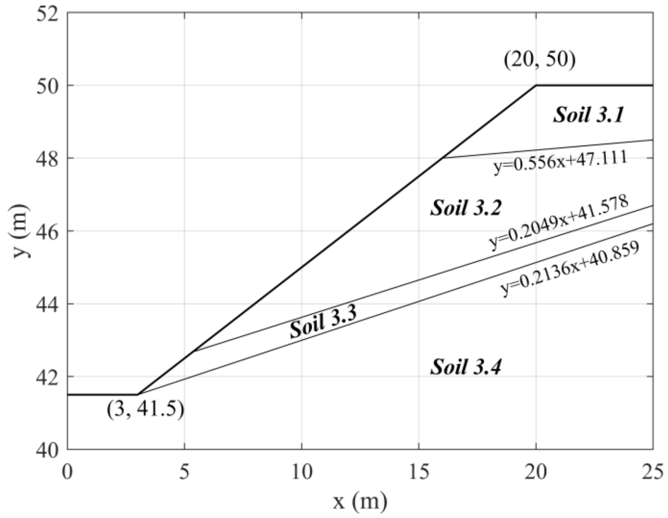

Figure 3.6: *Example 3* – slope geometry and soil profile

Adopted from Arai and Tagyo [46], *Example 4* considers a 30 m wide dry slope with 1:2 face inclination. Illustrated in Figure 3.7, the soil profile comprises parallel aligned three layers. The base soil is a relatively stiff material and the interlayer soil is considerably weak, which will possibly limit the critical slip surface to stay within the upper layers. Considering that the interlayer deposit is relatively thick, either a "rotational" or a deep translational failure is expected.

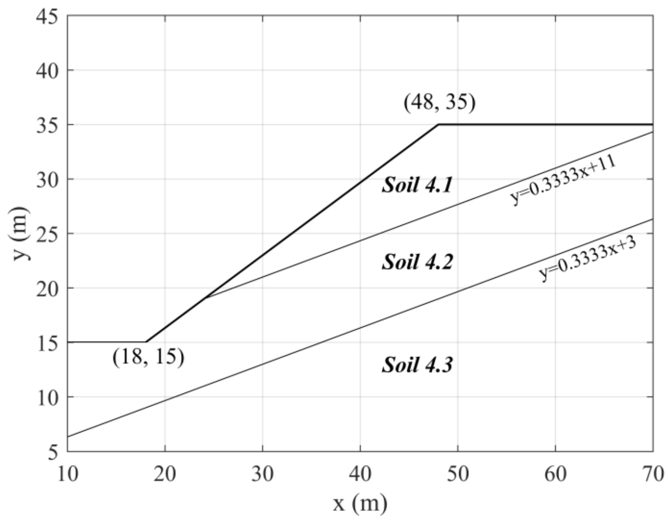

Figure 3.7: *Example 4* – slope geometry and soil profile

Example 5 is introduced by Zolfaghari [20], and incorporates a dry infinite slope with stratified soil profile as shown in Figure 3.8. There are three soil layers, including an interlayer soft soil deposit. The problem is analyzed under static loads in *Case* (*i*). Then, a pseudo-static earthquake analysis is conducted with horizontal seismic coefficient, k_h=0.1 in *Case* (*ii*). For practical purposes, the width of the critical slip surface is limited to 100 m since the slope displays a fully translational failure. Otherwise, the surface width would tend to infinity and promote divergence.

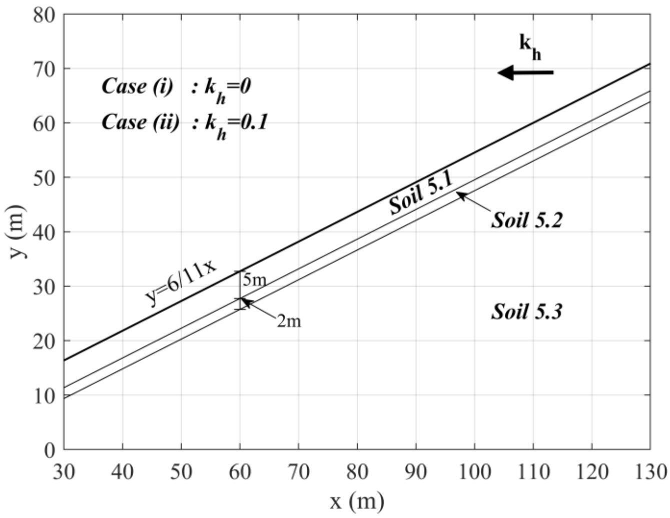

Figure 3.8: *Example 5* – slope geometry and soil profile

Example 6, also taken from Zolfaghari [20], examines a slope with complex soil profile under groundwater and seismic effects, as illustrated in Figure 3.9. The slope is analyzed for four different configurations, which are summarized as follows; *Case* (*i*): there is no earthquake load and no pore-water pressure, *Case* (*ii*): there is no earthquake load but hydrostatic pore-water pressure exists due groundwater, *Case* (*iii*): there is a pseudo-static earthquake load with k_h=0.1, but no pore-water pressure, *Case* (*iv*): there is both pseudo-static earthquake loading with k_h=0.1 and hydrostatic pore-water pressure due to groundwater.

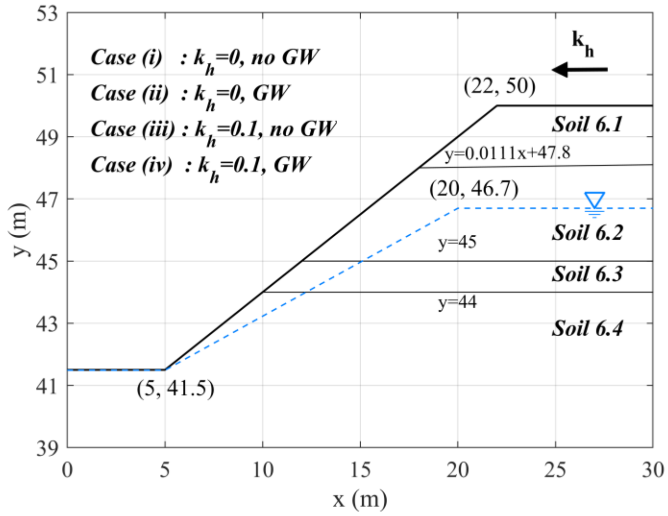

Figure 3.9: *Example 6* – slope geometry and soil profile

All surface generation methods presented in this manuscript require boundary conditions to limit the horizontal position of slip toe and scarp, denoted as “x_t” and “x_s”, respectively. For each benchmark problem, these values are intuitively selected and summarized in Table 3.3, together with the soil parameters.

Table 3.3: Model boundaries and soil parameters

Problem	$[x_{t\min}, x_{t\max}]$	$[x_{s\min}, x_{s\max}]$	Soil	γ (kN/m³)	c' (kPa)	ϕ' (°)
Example 1	$[0, 17.6]^m$	$[42, 60]^m$	*1*	18.83	28.75	20
Example 2	$[0, 5]^m$	$[15, 25]^m$	*2*	17.64	9.8	10
Example 3	$[0, 10]^m$	$[20, 30]^m$	*3.1*	19	15	20
			3.2	19	17	21
			3.3	19	5	10
			3.4	19	35	28
Example 4	$[10, 25]^m$	$[48, 70]^m$	*4.1*	18.82	29.4	12
			4.2	18.82	9.8	5
			4.3	18.82	294	40
Example 5	$[30, 30]^m$	$[35, 130]^m$	*5.1*	18.63	32.5	17
			5.2	18.63	29.4	10
			5.3	18.63	49	27
Example 6	$[0, 15]^m$	$[22, 30]^m$	*6.1*	18.63	14.7	20
			6.2	18.63	16.7	21
			6.3	18.63	4.9	10
			6.4	18.63	34.3	28

Soil numbering is based on the figures. Unit weight of water, γ_w, is taken as 9.81 kN/m³ when necessary.

3.2.2. Parametric Sensitivity Analyses

The main purpose of the parametric study presented in this section is to maximize the statistical performances of the surface generation methods. To develop a suitable methodology for each, a distinction is made between the methods that represent the slip surfaces using (i) slices and (ii) splines. The former group includes M1, M2, and M3, in which the only parameter is the number of slices. For the latter group, including M4, QS, and SQS, both numbers of splines and slices are expected to affect the results. Therefore, slightly different procedures are adopted to assess the performances of these groups of methods, in the following sub-sections. Throughout the analyses, GLE and DE are adopted with the parameter settings given in Table 3.2, and for each experiment, median F_S obtained from 30 independent runs are used as the basis of comparison.

3.2.2.1. Slice-Based Methods

First, it should be mentioned that GLE formulation overestimates the F_S, provided that the step size used in free-body discretization is not sufficiently small. Therefore, any analysis framework that incorporates GLE is inherently biased towards higher numbers of slices. However, when slice-based surface generation methods like M1, M2, and M3 are adopted, such an approach produces high-dimensional optimization problems, which are considerably more difficult to handle. Accordingly, it is necessary to compromise a certain degree of precision to better exploit the capability of these methods. Investigating this issue, the performances of M1, M2, and M3 are evaluated with variable number of slices, n.

For $n \in \{10, 20,\ldots, 100\}$, the performance of M1 is summarized in Table 3.4, in terms of median F_S of 30 independent runs for all examples. In this table, bold notation denotes the best parameter configuration for each example, while the overall performances of the configurations are represented through the mean value of the relative error, ε_R, calculated using Eq. (3.14). As an example, the relative error of n=20 slice analysis for *Example 1* is calculated as (1.9972-1.9942)/1.9942×100=0.15%. Average of the relative errors for all benchmark problems is 0.75%.

$$(\varepsilon_R)_n = \frac{(F_{s,\text{med}})_n - \min\{\mathbf{F}_{s,\text{med}}\}}{\min\{\mathbf{F}_{s,\text{med}}\}} \times 100 \tag{3.14}$$

where $(F_{S,\text{med}})_n$: median F_S obtained for an example using n slices, and $\mathbf{F}_{S,\text{med}}=\{(F_{S,\text{med}})_{10}, (F_{S,\text{med}})_{20}, \ldots, (F_{S,\text{med}})_{100}\}$.

Based on the approach given above, M1 is most efficient with 40 slices, which produces the lowest mean ε_R at 0.27%. It is notable that the success rate of M1 decreases with increasing number of slices. Using 60 slices, more than half the analyses did not converge to a feasible solution for *Example 6 Cases* (*i*) and (*ii*). Above 60 slices, this issue is encountered in all experiments.

Table 3.4: Sensitivity of M1 to the number of slices

n→	***10***	***20***	***30***	***40***	***50***	***60***	***70***	***80***	***90***	***100***
Example 1	1.9968	1.9972	**1.9942**	1.9961	1.9947	1.9944	NC	NC	NC	NC
Example 2 (*i*)	1.3342	1.3328	1.3331	**1.3327**	1.3331	1.3339	NC	NC	NC	NC
Example 2 (*ii*)	1.0068	1.0065	1.0063	**1.0030**	1.0054	1.0059	NC	NC	NC	NC
Example 3	1.0928	1.0939	**1.0928**	1.0935	1.0930	1.0957	NC	NC	NC	NC
Example 4	0.4173	0.4173	0.4170	**0.4168**	0.4171	0.4187	NC	NC	NC	NC
Example 5 (*i*)	1.0744	1.0845	1.0731	1.0639	**1.0590**	1.0827	NC	NC	NC	NC
Example 5 (*ii*)	**0.8736**	0.9127	0.9357	0.8802	0.9056	0.8968	NC	NC	NC	NC
Example 6 (*i*)	1.3392	1.3367	**1.3367**	1.3409	1.3386	1.3400	NC	NC	NC	NC
Example 6 (*ii*)	1.2122	1.2135	**1.2104**	1.2122	1.2204	NC	NC	NC	NC	NC
Example 6 (*iii*)	1.0532	1.0513	**1.0476**	1.0476	1.0531	1.0502	NC	NC	NC	NC
Example 6 (*iv*)	0.9442	**0.9422**	0.9423	0.9531	0.9542	NC	NC	NC	NC	NC
Mean ε_R (%)	0.30	0.75	0.81	**0.27**	0.62	NC	NC	NC	NC	NC

The results are given in terms of median F_S of 30 independent runs.

Similarly, the outcomes of the sensitivity analysis of M2 are summarized in Table 3.5. In this case, the results are unanimously in favor of 20 slice configuration, which achieves the best statistical outcomes for the benchmark problems. It is worth mentioning that M2 does not suffer from divergence issues like M1. However, its performance is significantly sensitive to the number of slices. The mean difference between the median F_S obtained with 20 slices and 30 slices exceed 10%, which is a considerably high deviation for slope stability analysis. The differences significantly increase when higher values are adopted.

Using M3, the results are similar to those obtained with M2 in the sense that the performance of the method is significantly influenced by the dimensionality of the problem. As illustrated in Table 3.6, M3 is most efficient with lower numbers of slices, 10 being the best alternative considering the resulting mean ε_R value. Thereafter, the error increases monotonically.

Table 3.5: Sensitivity of M2 to the number of slices

***n*→**	***10***	***20***	***30***	***40***	***50***	***60***	***70***	***80***	***90***	***100***
Example 1	2.0072	**1.9920**	1.9998	2.0112	2.0318	2.0445	2.0474	2.0658	2.1049	2.1345
Example 2 (*i*)	1.3319	**1.3251**	1.3276	1.3334	1.3382	1.3515	1.3649	1.3945	1.3796	1.4176
Example 2 (*ii*)	1.0158	**1.0083**	1.0162	1.0294	1.0542	1.0793	1.0986	1.1190	1.1373	1.1414
Example 3	2.1321	**1.1886**	1.8154	1.7212	1.7086	1.7586	1.7816	1.8794	1.8932	1.9918
Example 4	0.4197	**0.4177**	0.5699	0.5557	0.5487	0.5453	0.5428	0.5418	0.5401	0.5397
Example 5 (*i*)	1.3112	**1.1978**	1.3171	1.6368	2.0215	1.9007	1.8428	1.7946	1.7611	1.7545
Example 5 (*ii*)	1.1252	**1.0025**	1.0837	1.3117	1.4124	1.3622	1.3394	1.3100	1.3141	1.3167
Example 6 (*i*)	1.3984	**1.3795**	1.4443	1.7301	2.1934	2.1867	2.1996	2.2028	2.2231	2.2456
Example 6 (*ii*)	1.2609	**1.2561**	1.2900	1.5003	2.1431	2.1527	2.1615	2.1492	2.1945	2.2200
Example 6 (*iii*)	1.1040	**1.0941**	1.1387	1.3321	1.3515	1.3597	1.3942	1.4199	1.4473	1.5154
Example 6 (*iv*)	0.9898	**0.9784**	1.0001	1.0719	1.1945	1.2700	1.3303	1.3683	1.4265	1.4965
Mean ε_R (%)	9.76	**0.00**	11.12	20.47	33.41	33.52	34.27	35.33	36.65	39.36

Table 3.6: Sensitivity of M3 to the number of slices

***n*→**	***10***	***20***	***30***	***40***	***50***	***60***	***70***	***80***	***90***	***100***
Example 1	**1.9911**	1.9920	1.9998	2.0187	2.0323	2.0322	2.0588	2.0705	2.0969	2.1093
Example 2 (*i*)	1.3301	**1.3252**	1.3292	1.3330	1.3390	1.3454	1.3720	1.3736	1.4034	1.4117
Example 2 (*ii*)	1.0026	**1.0010**	1.0058	1.0411	1.0514	1.0971	1.1004	1.1256	1.1386	1.1395
Example 3	**1.1335**	1.6450	1.6149	1.6108	1.6807	1.7218	1.7802	1.8546	1.8941	1.9473
Example 4	**0.4148**	0.4161	0.5444	0.5396	0.5369	0.5354	0.5349	0.5347	0.5347	0.5346
Example 5 (*i*)	1.1760	**1.1413**	1.2698	1.5927	1.7043	1.6685	1.6431	1.6285	1.6305	1.6237
Example 5 (*ii*)	0.9804	**0.9756**	1.0027	1.2809	1.2508	1.2301	1.2377	1.2615	1.2777	1.2962
Example 6 (*i*)	**1.3656**	1.3814	1.4211	2.0959	2.1243	2.1279	2.1449	2.1785	2.1900	2.2329
Example 6 (*ii*)	**1.2393**	1.2461	1.2955	1.6539	2.0539	2.0906	2.1020	2.1178	2.1731	2.1660
Example 6 (*iii*)	**1.0784**	1.0813	1.1184	1.3241	1.3335	1.3710	1.3893	1.4083	1.4702	1.5137
Example 6 (*iv*)	0.9737	**0.9710**	0.9908	1.1964	1.2159	1.2688	1.2970	1.3557	1.4454	1.5277
Mean ε_R (%)	**0.39**	4.31	9.39	25.63	30.32	31.70	32.98	35.02	37.79	39.83

3.2.2.2. Spline-Based Methods

For the spline-based methods, M4, QS, and SQS, the parametric analyses are conducted in two stages. First, for each method, the number of slices, n, is kept constant at 40 and the benchmark problems are analyzed with numbers of splines, n_s, ranging between 3 and 10 (i.e. $n_s \in \{3, 4, \ldots, 10\}$). Using the most efficient configuration from these analyses, the methods are further evaluated with $n \in \{10, 20, \ldots, 100\}$. Using spline-based methods, the complexity of the optimization problem is not directly influenced from the number of slices. Therefore, the outcomes are expected to be in favor of higher values.

The results obtained with M4 for different n_s values are given in Table 3.7. First, it is noticed that parameter selection is less influential on the performance of M4, compared to the previous methods. For all benchmark problems, except for *Example 3* and *Example 5 Case* (*ii*), adoption of 4 to 10 splines can yield F_S values in the same order of magnitude. Considering the mean ε_R values, M4 is most efficient with 6 splines.

Table 3.7: Sensitivity of M4 to the number of splines

***n*=40** n_s →	***3***	***4***	***5***	***6***	***7***	***8***	***9***	***10***
Example 1	1.9848	1.9796	**1.9789**	1.9790	1.9802	1.9838	1.9902	1.9905
Example 2 (*i*)	1.3256	1.3238	1.3228	**1.3227**	**1.3227**	1.3228	1.3229	1.3229
Example 2 (*ii*)	1.0461	1.0208	1.0159	1.0168	1.0162	**1.0140**	1.0190	1.0162
Example 3	2.2963	1.1654	1.1481	**1.1477**	1.5167	1.5018	1.4783	1.4614
Example 4	0.4183	0.4160	0.4158	0.4152	0.4140	0.4143	**0.4132**	0.4140
Example 5 (*i*)	1.4603	1.2227	1.1639	1.1076	1.0775	**1.0682**	1.0708	1.0791
Example 5 (*ii*)	1.2332	1.0350	0.9759	0.9265	0.8887	**0.8832**	0.9168	1.0929
Example 6 (*i*)	1.3828	1.3680	**1.3524**	1.3527	1.3525	1.3528	1.3641	1.3641
Example 6 (*ii*)	1.2652	1.2389	1.2254	1.2257	**1.2130**	1.2218	1.2228	1.2394
Example 6 (*iii*)	1.0867	1.0688	1.0644	1.0614	1.0674	**1.0611**	1.0680	1.0739
Example 6 (*iv*)	0.9875	0.9604	0.9513	0.9536	0.9521	**0.9492**	0.9508	0.9547
Mean ε_R (%)	17.67	3.62	1.99	**0.99**	3.18	2.92	3.31	5.27

Based on the outcomes given in Table 3.7, n_s is kept constant at 6 and M4 is evaluated with n ranging between 10 and 100. The results given in Table 3.8, indicate that the method favors higher numbers of slices. Ideally, the mean ε_R would decrease monotonically with increasing *n*, yet there are some deviations in the results which are most probably related to the stochastic nature of the implemented optimization algorithm, DE. Regardless, *n* is selected as 70 for M4, considering the improved results over other configurations.

Table 3.8: Sensitivity of M4 to the number of slices

n_s=6 | *n* →	10	20	30	40	50	60	70	80	90	100
Example 1	1.9936	1.9841	1.9803	1.9790	1.9798	1.9785	1.9789	1.9785	**1.9783**	1.9787
Example 2 (*i*)	1.3352	1.3254	1.3233	1.3227	1.3225	1.3223	1.3222	1.3222	1.3222	**1.3221**
Example 2 (*ii*)	1.0169	1.0180	1.0173	1.0168	1.0165	1.0163	1.0162	1.0161	**1.0160**	**1.0160**
Example 3	1.1587	1.1594	1.1388	1.1477	1.2034	1.1431	1.1365	1.1372	**1.1357**	1.1385
Example 4	0.4171	0.4165	0.4156	0.4152	0.4159	**0.4150**	0.4152	0.4158	0.4151	**0.4150**
Example 5 (*i*)	1.1135	1.1260	1.1080	1.1076	1.1561	1.1032	1.1041	1.1059	**1.1021**	1.1063
Example 5 (*ii*)	**0.9208**	0.9987	0.9281	0.9265	0.9435	0.9283	0.9281	0.9261	0.9270	0.9270
Example 6 (*i*)	1.3785	1.3661	1.3568	1.3527	1.3678	1.3499	**1.3486**	1.3516	1.3534	1.3496
Example 6 (*ii*)	1.2511	1.2471	1.2315	1.2257	1.2381	1.2322	1.2218	1.2266	1.2243	**1.2213**
Example 6 (*iii*)	1.0811	1.0904	1.0676	1.0614	1.0801	1.0691	1.0651	**1.0593**	1.0637	1.0653
Example 6 (*iv*)	0.9804	0.9677	0.9515	0.9536	0.9693	0.9526	**0.9510**	0.9669	0.9530	0.9512
Mean ε_R (%)	1.36	1.97	0.38	0.30	1.83	0.32	**0.14**	0.33	0.15	0.16

Similarly, QS is evaluated with variable n_s and the results are summarized in Table 3.9. The results indicate that QS is less sensitive to the selection of n_s, compared to M4. The mean ε_R value only deviates by 0.17% considering the range between 4 and 7 splines. Among those, the best results are obtained with 6 splines, which is exactly the same as M4. This may indicate that quadratic order functions are sufficiently flexible to represent the critical slip surfaces.

Table 3.9: Sensitivity of QS to the number of splines

n=40 | n_s →	3	4	5	6	7	8	9	10
Example 1	1.9800	1.9786	**1.9785**	**1.9785**	1.9786	**1.9785**	1.9789	1.9796
Example 2 (*i*)	1.3231	1.3231	**1.3230**	**1.3230**	**1.3230**	**1.3230**	1.3233	1.3237
Example 2 (*ii*)	1.0145	1.0127	1.0041	**1.0015**	1.0026	1.0053	1.0059	1.0096
Example 3	1.1023	1.1003	**1.1002**	1.1056	1.1008	1.1245	1.1115	1.1449
Example 4	0.4130	0.4122	**0.4118**	**0.4118**	**0.4118**	**0.4118**	0.4122	0.4124
Example 5 (*i*)	1.0345	**1.0189**	1.0274	1.0245	1.0276	1.0395	1.0516	1.0447
Example 5 (*ii*)	0.8760	0.8544	0.8571	0.8556	0.8621	**0.8542**	0.8835	0.8970
Example 6 (*i*)	1.3495	1.3439	1.3439	1.3395	**1.3381**	1.3423	1.3473	1.3487
Example 6 (*ii*)	1.2100	1.2095	1.2062	**1.2047**	1.2066	1.2091	1.2072	1.2130
Example 6 (*iii*)	1.0610	1.0587	1.0541	**1.0527**	1.0537	1.0537	1.0589	1.0626
Example 6 (*iv*)	0.9484	0.9447	0.9453	**0.9396**	0.9433	0.9460	0.9467	0.9525
Mean ε_R (%)	0.82	0.29	0.25	**0.12**	0.24	0.55	0.95	1.50

Regarding the sensitivity of QS to n value, the results are reasonably close to the expectations. Given in Table 3.10, the median F_S values obtained with QS tend to decrease with increasing number of slices, and the maximum among the adopted values, 100 slices, yields the best results.

Table 3.10: Sensitivity of QS to the number of slices

n_s=6 | n →	*10*	*20*	*30*	*40*	*50*	*60*	*70*	*80*	*90*	*100*
Example 1	1.9960	1.9824	1.9793	1.9785	1.9779	1.9778	1.9780	1.9779	1.9779	**1.9775**
Example 2 (*i*)	1.3353	1.3257	1.3239	1.3230	1.3226	1.3226	1.3223	1.3225	**1.3222**	1.3229
Example 2 (*ii*)	1.0088	1.0058	1.0020	1.0015	1.0013	1.0015	1.0020	1.0017	1.0017	**1.0009**
Example 3	1.1012	1.1001	1.0987	1.1056	1.0989	1.1009	1.0997	1.1022	1.1036	**1.0980**
Example 4	0.4145	0.4124	0.4119	0.4118	0.4119	0.4119	**0.4117**	0.4118	0.4118	0.4118
Example 5 (*i*)	1.0294	1.0265	1.0306	1.0245	1.0237	1.0336	**1.0194**	1.0230	1.0238	1.0235
Example 5 (*ii*)	0.8575	0.8634	**0.8503**	0.8556	0.8556	0.8534	0.8652	0.8514	0.8526	0.8519
Example 6 (*i*)	1.3452	1.3448	1.3421	1.3395	1.3404	1.3401	1.3404	1.3380	1.3389	**1.3373**
Example 6 (*ii*)	1.2099	1.2106	1.2074	1.2047	1.2089	1.2067	**1.2045**	1.2074	1.2077	1.2056
Example 6 (*iii*)	1.0529	1.0540	**1.0494**	1.0527	1.0542	1.0497	1.0515	1.0527	1.0507	1.0547
Example 6 (*iv*)	0.9438	0.9440	0.9444	0.9396	0.9433	**0.9392**	0.9394	0.9423	0.9394	0.9426
Mean ε_R (%)	0.67	0.51	0.24	0.23	0.25	0.23	0.23	0.18	0.17	**0.15**

Lastly, the proposed surface generation method, SQS, is evaluated with the same procedure as M4 and QS. Presented in Table 3.11, the outcomes of the analysis with variable numbers of splines highlight the statistical soundness of the method. Compared to the M4 and QS, SQS is significantly less sensitive to this parameter. The minimum ε_R values are obtained with 6 and 7 splines, and the mean ε_R deviates at most by 0.02% within the range between 6 and 9 splines. The number of splines in SQS is fixed to 6 for the following analyses.

The outcomes of SQS obtained with varying number of slices, given in Table 3.12, are somewhat similar to those of M4. Although the results are in favor of higher values, there are some deviations, possibly resulting from the stochastic nature of DE algorithm. Within the considered range, 70 slice configuration is statistically the best alternative with a mean ε_R value of 0.05%.

Table 3.11: Sensitivity of SQS to the number of splines

n=40	***n_s →***	***3***	***4***	***5***	***6***	***7***	***8***	***9***	***10***
Example 1		1.9792	**1.9785**	1.9788	**1.9785**	1.9786	**1.9785**	1.9787	1.9789
Example 2 (*i*)		1.3230	1.3230	1.3234	1.3230	1.3230	1.3231	**1.3227**	1.3229
Example 2 (*ii*)		1.0012	**0.9988**	0.9990	0.9991	0.9993	0.9991	0.9990	0.9990
Example 3		1.1022	1.0995	1.0911	**1.0898**	1.0902	1.0907	1.0901	**1.0898**
Example 4		0.4129	0.4116	**0.4114**	**0.4114**	**0.4114**	**0.4114**	0.4115	**0.4114**
Example 5 (*i*)		1.0231	1.0145	1.0143	1.0158	**1.0127**	1.0144	1.0149	1.0157
Example 5 (*ii*)		0.8513	0.8474	0.8457	0.8457	**0.8447**	0.8448	0.8461	0.8458
Example 6 (*i*)		1.3458	1.3401	1.3349	**1.3342**	1.3372	1.3382	1.3356	1.3365
Example 6 (*ii*)		1.2119	1.2062	1.2043	**1.2012**	1.2022	1.2019	1.2019	1.2019
Example 6 (*iii*)		1.0611	1.0523	1.0526	1.0500	1.0475	**1.0456**	1.0489	1.0499
Example 6 (*iv*)		0.9466	0.9437	0.9391	**0.9344**	0.9368	0.9384	0.9356	0.9371
Mean ε_R (%)		0.74	0.36	0.18	**0.08**	**0.08**	0.10	0.10	0.13

Table 3.12: Sensitivity of SQS to the number of slices

n_s=6	***n →***	***10***	***20***	***30***	***40***	***50***	***60***	***70***	***80***	***90***	***100***
Example 1		1.9954	1.9823	1.9795	1.9785	1.9782	1.9780	1.9782	1.9778	1.9779	**1.9777**
Example 2 (*i*)		1.3343	1.3259	1.3240	1.3230	1.3228	**1.3223**	**1.3223**	**1.3223**	1.3225	1.3224
Example 2 (*ii*)		1.0062	1.0000	0.9994	0.9991	0.9990	0.9991	**0.9988**	**0.9988**	0.9997	0.9991
Example 3		1.0928	1.0917	1.0910	**1.0898**	1.0938	1.0917	1.0902	1.0936	**1.0898**	1.0905
Example 4		0.4140	0.4123	0.4116	0.4114	0.4113	**0.4112**	**0.4112**	0.4113	0.4114	**0.4112**
Example 5 (*i*)		1.0164	1.0139	1.0146	1.0158	**1.0121**	1.0145	1.0149	1.0133	1.0135	1.0165
Example 5 (*ii*)		0.8453	0.8451	0.8461	0.8457	0.8452	**0.8443**	**0.8443**	0.8459	0.8448	0.8448
Example 6 (*i*)		1.3403	1.3381	1.3360	1.3342	1.3353	1.3356	1.3345	1.3351	**1.3340**	1.3376
Example 6 (*ii*)		1.2060	1.2062	1.2056	1.2012	1.2037	1.2031	**1.2002**	1.2028	1.2045	1.2033
Example 6 (*iii*)		1.0512	1.0503	1.0502	1.0500	1.0475	1.0505	1.0466	1.0488	**1.0461**	1.0464
Example 6 (*iv*)		0.9401	0.9422	0.9416	**0.9344**	0.9377	0.9363	0.9353	0.9376	0.9392	0.9393
Mean ε_R (%)		0.56	0.31	0.25	0.11	0.13	0.13	**0.05**	0.15	0.11	0.15

In light of the sensitivity analyses given in this section, the most efficient parameter configurations for the surface generation methods are assessed and summarized in Table 3.13.

Table 3.13: Parameter settings of surface generation methods

	M1	**M2**	**M3**	**M4**	**QS**	**SQS**
Number of splines, n_s	-	-	-	6	6	6
Number of slices, n	40	20	10	70	100	70

3.2.3. Comparison of Surface Generation Methods

In this section, the outcomes of the benchmark analyses are evaluated in further detail to gain insight about the capability, computational efficiency and statistical reliability of each surface generation method. Accordingly, a comparative study is performed based on the results obtained with the parameter settings given in Table 3.13. In the following sub-sections, each benchmark problem is investigated separately, and then the results are utilized in statistical significance tests to assess the most reliable surface generation method.

3.2.3.1. Example 1

The outcomes for *Example 1* are given in Table 3.14, summarizing the statistical performances of the surface generation methods. The results are reported in terms of statistical parameters like minimum, median, maximum, mean and standard deviation values, which are calculated based on the F_S values obtained from 30 independent analyses. The outcomes indicate that spline-based methods (i.e. M4, QS, and SQS) are effective to deal with *Example 1*. Among those, QS performs slightly better than M4 and SQS, finding the minimum F_S as 1.9771. The statistical parameters also highlight QS as the best alternative, however, the differences compared to M4 and SQS are arguably small. On the other hand, M1, M2, and M3 are not as competitive, despite achieving practically similar results.

Table 3.14: *Example 1* – statistical comparison of surface generation methods

	M1	**M2**	**M3**	**M4**	**QS**	**SQS**
$F_{S,\mathrm{min}}$	1.9878	1.9833	1.9898	1.9777	**1.9771**	1.9773
$F_{S,\mathrm{med}}$	1.9961	1.9920	1.9911	1.9789	**1.9775**	1.9782
$F_{S,\mathrm{max}}$	2.0195	2.0202	2.0007	2.0022	**1.9789**	1.9799
$F_{S,\mathrm{mean}}$	1.9976	1.9954	1.9923	1.9808	**1.9778**	1.9784
St. Dev.	7.E-03	1.E-02	3.E-03	5.E-03	**6.E-04**	1.E-03

The critical slip surface located by each method is illustrated in Figure 3.10. Similar to the previous findings, M4, QS, and SQS are in strong agreement such that the critical surfaces located by these methods are almost identical. On the other hand, M1, M2, and M3 slightly deviate from these results, estimating relatively deeper critical paths.

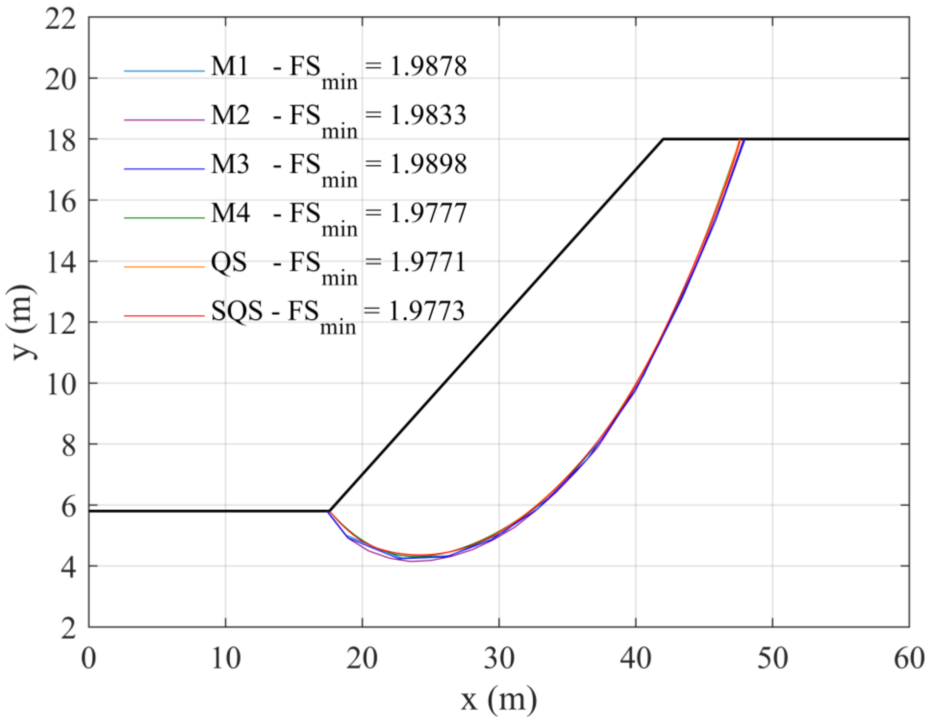

Figure 3.10: *Example 1* – comparison of critical slip surfaces

The last evaluation for *Example 1* regards the computational efficiency of the methods. Accordingly, for each method, the analysis progress is illustrated in the convergence graph given in Figure 3.11, where the x and y-axes represent the number of iterations and median F_S of 30 independent runs, respectively. First, it is noticeable that the initial populations generated by M3 are significantly better than those of other methods. However, M3 achieves limited improvement and fails to produce results that are comparable to those of M4, QS, and SQS. An important finding is that the convergence of QS, which is statistically the best method for *Example 1*, requires over twice the iterations required with other methods. On the other hand, the analyses with M4 and SQS mature in less than 100 iterations, which is relatively low. As a result, M4 and SQS may be preferred over QS in order to achieve computationally efficient solutions.

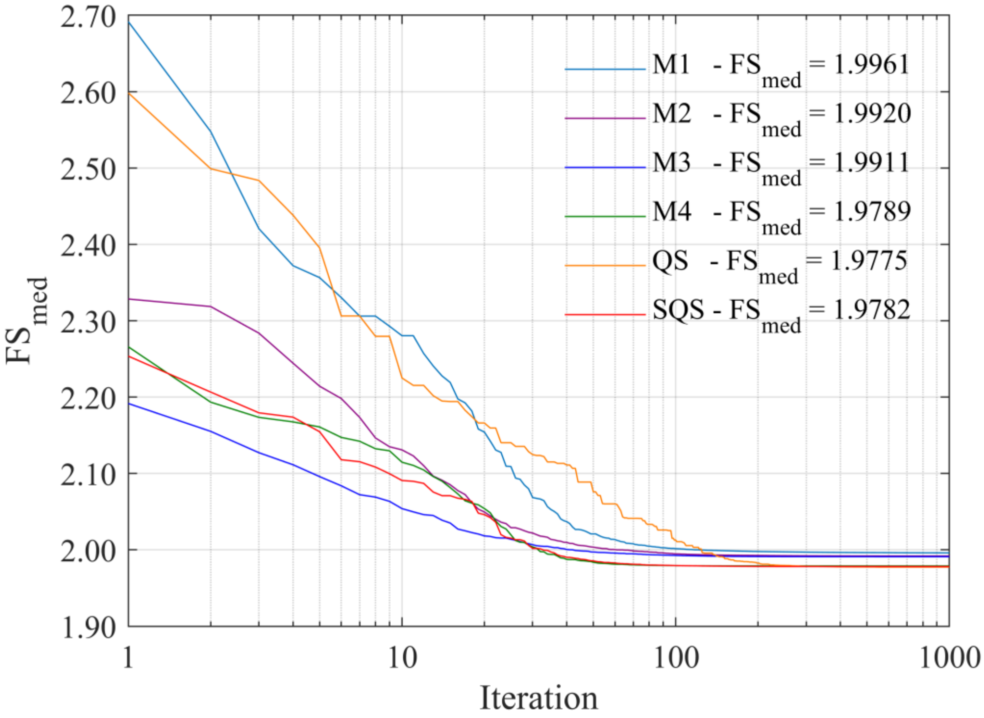

Figure 3.11: *Example 1* – the convergence of surface generation methods

3.2.3.2. Example 2

The statistical results of *Example 2* are given in Table 3.15 for both cases of the benchmark problem. For *Case* (*i*), which incorporates a homogeneous soil profile under no external loading, the outcomes further validate the efficiency of spline-based methods to deal with simple problems. Similar to *Example 1*, M4, QS, and SQS exhibit competitive statistical performances, improving the results of M1, M2 and M3. The minimum F_S is reported as 1.3219 based on the analyses with QS. However, M4 and SQS are able to find similar results. For Case (*ii*), which additionally considers surcharge loading, the outcomes are strictly in favor of SQS considering all statistical measures, as well as minimum F_S reported as 0.9976. Although QS can find similar results in some occurrences, it is statistically inferior compared to SQS, while M4 fails to produce competitive results. It is also noteworthy to mention that M1, M2, and M3 perform fairly better than M4 for this problem.

Table 3.15: *Example 2* – statistical comparison of surface generation methods

		M1	M2	M3	M4	QS	SQS
Case (*i*)	$F_{S,\text{min}}$	1.3280	1.3240	1.3298	1.3222	**1.3219**	1.3220
	$F_{S,\text{med}}$	1.3327	1.3251	1.3301	**1.3222**	1.3229	1.3223
	$F_{S,\text{max}}$	1.3419	1.3295	1.3332	1.3273	**1.3240**	**1.3240**
	$F_{S,\text{mean}}$	1.3334	1.3257	1.3303	**1.3226**	1.3230	**1.3226**
	St. Dev.	3.E-03	2.E-03	**7.E-04**	1.E-03	9.E-04	**7.E-04**
Case (*ii*)	$F_{S,\text{min}}$	1.0012	1.0058	1.0013	1.0160	0.9978	**0.9976**
	$F_{S,\text{med}}$	1.0030	1.0083	1.0026	1.0162	1.0009	**0.9988**
	$F_{S,\text{max}}$	1.0108	1.0226	1.0074	1.0340	1.0281	**1.0051**
	$F_{S,\text{mean}}$	1.0046	1.0097	1.0031	1.0175	1.0020	**0.9995**
	St. Dev.	3.E-03	4.E-03	**2.E-03**	4.E-03	6.E-03	**2.E-03**

The critical slip surfaces for *Cases* (*i*) and (*ii*) are demonstrated in Figures 3.12 and 3.13, respectively. For *Case* (*i*), the resulting surfaces are in good agreement and the main difference is the smoothness obtained with the spline-based methods. On the other hand, there are visible deviations between the estimations obtained for *Case* (*ii*). Regardless, all methods except for M4 estimate a curvilinear critical path with a triangular wedge below the surcharge area, as illustrated in Figure 3.13. The underlying reason behind the failure of M4 may be attributed to the simplifying assumptions within the formulation of the method. M4 keeps the spline widths constant and uses continuous interpolation. As a result, the surfaces lack the flexibility to represent the sudden transition observed in *Case* (*ii*). QS overcomes this issue by allowing variable spline widths, in that a spline in QS can assume infinitesimal width and high curvature to allow an abrupt transition. On the other hand, SQS basically encourages such surfaces through the scaling operation.

The convergence graphs of *Example 2*, given in Figures 3.14 and 3.15, further illustrate the efficiency of SQS. Although M4 converges slightly faster than SQS in *Case* (*i*), the method significantly deviates from the optimum solution in *Case* (*ii*). On the other hand, QS is computationally the most inefficient alternative among the spline-based methods, while M1, M2, and M3 are reasonably cost-effective despite their limitations.

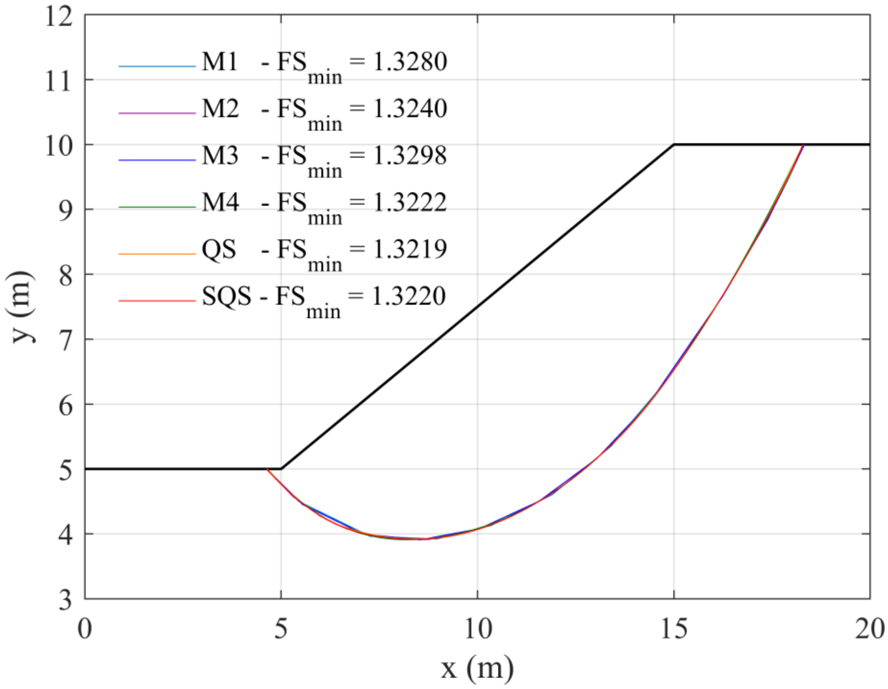

Figure 3.12: *Example 2 Case* (*i*) – comparison of critical slip surfaces

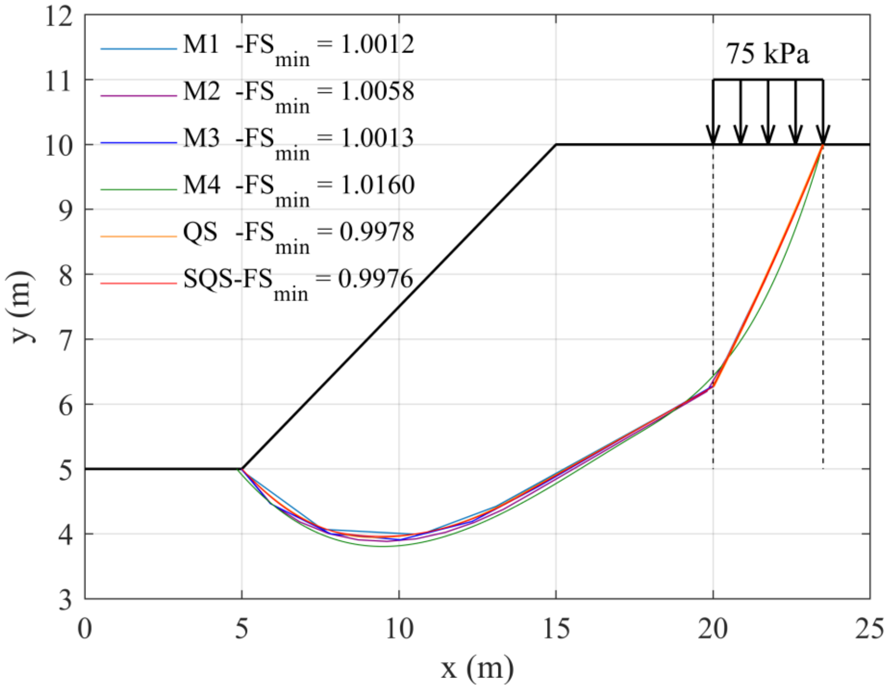

Figure 3.13: *Example 2 Case* (*ii*) – comparison of critical slip surfaces

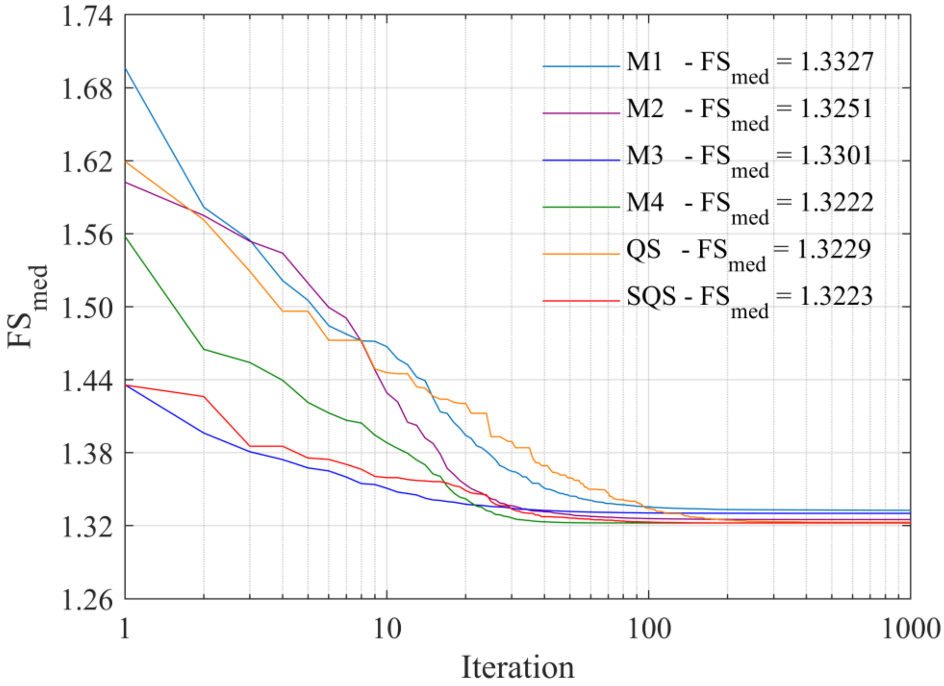

Figure 3.14: *Example 2 Case* (*i*) – the convergence of surface generation methods

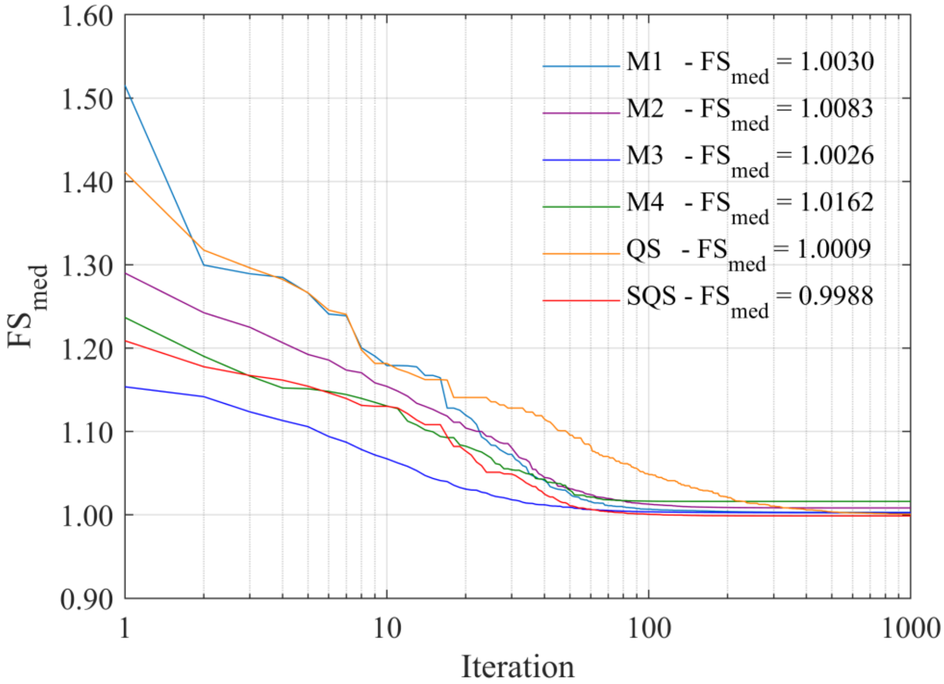

Figure 3.15: *Example 2 Case* (*ii*) – the convergence of surface generation methods

3.2.3.3. Example 3

Based on the results given in Table 3.16, *Example 3* has proven to be a challenging problem for the surface generation methods. Among those, M2, M3, and QS have shown severe deviations as indicated by the reported mean and maximum F_S values. Although M1 is more competent than these methods, SQS is the best alternative considering all performance measure. It is notable to mention that the median F_S of SQS is better than the minimum of all methods, except for QS. The most critical slip surface is also obtained with SQS, with a corresponding F_S value of 1.0878.

Table 3.16: *Example 3* – statistical comparison of surface generation methods

	M1	**M2**	**M3**	**M4**	**QS**	**SQS**
$F_{S,\mathrm{min}}$	1.0904	1.1152	1.1157	1.1175	1.0893	**1.0878**
$F_{S,\mathrm{med}}$	1.0935	1.1886	1.1335	1.1365	1.0980	**1.0902**
$F_{S,\mathrm{max}}$	1.1203	1.5419	1.2325	1.7087	1.4351	**1.1049**
$F_{S,\mathrm{mean}}$	1.0954	1.2394	1.1406	1.1804	1.1408	**1.0933**
St. Dev.	7.E-03	1.E-01	3.E-02	1.E-01	1.E-01	**6.E-03**

The critical slip surfaces, given in Figure 3.16, illustrate that all methods indicate a deep translational failure within the soft soil interlayer. The surfaces produced by QS and SQS are in strong correlation. M1 slightly deviates from these methods, while M2, M3 and M4 estimate the position of the slip toe about 1 to 1.5 m away from the most critical surface.

The convergence graphs, given in Figure 3.17, highlight M1 and SQS as the best alternatives for *Example 3*. The analyses with M2, M3, and QS require significantly higher computational cost – about twice the iterations required with M1 and SQS. Lastly, the analyses with M2 fail to mature within 1000 iterations.

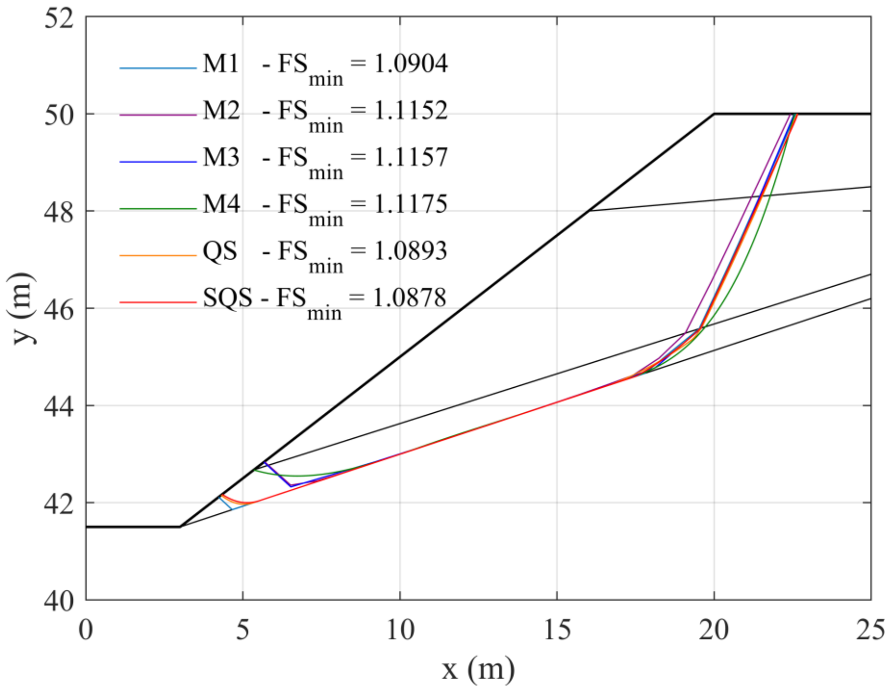

Figure 3.16: *Example 3* – comparison of critical slip surfaces

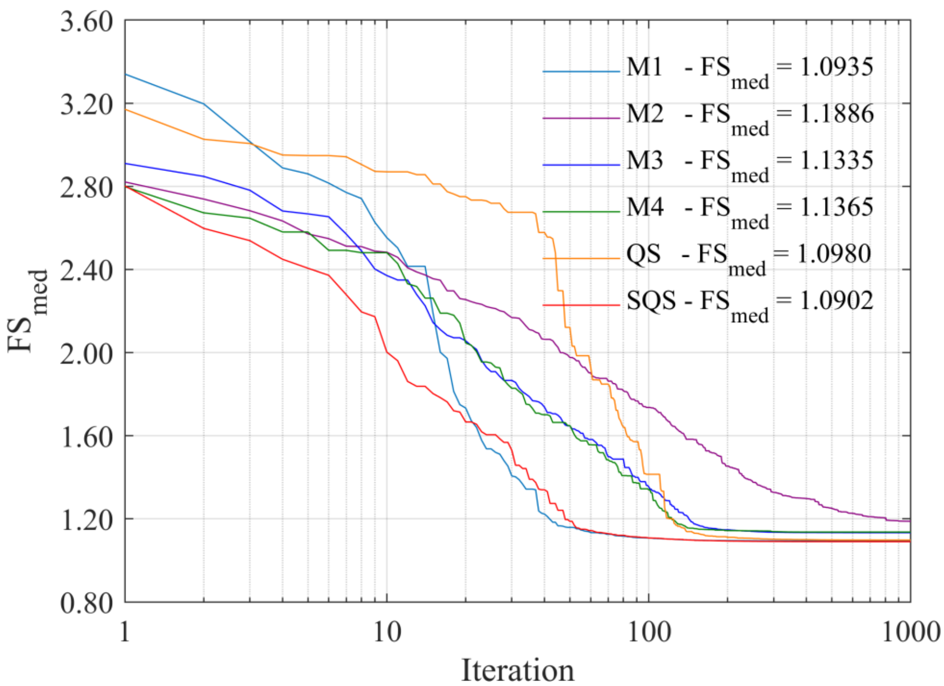

Figure 3.17: *Example 3* – the convergence of surface generation methods

3.2.3.4. *Example 4*

Dealing with *Example 4*, both QS and SQS are effective to produce improved results over the other methods. Among those, SQS performs slightly better than QS based on the statistical parameters given in Table 3.17, while both methods report the minimum F_S as 0.4110. M3 and M4 exhibit consistent performances, however, their accuracy is limited.

Table 3.17: *Example 4* – statistical comparison of surface generation methods

	M1	**M2**	**M3**	**M4**	**QS**	**SQS**
$F_{S,\mathrm{min}}$	0.4157	0.4121	0.4136	0.4149	**0.4110**	**0.4110**
$F_{S,\mathrm{med}}$	0.4168	0.4177	0.4148	0.4152	0.4118	**0.4112**
$F_{S,\mathrm{max}}$	0.4225	0.4215	0.4169	0.4160	0.4124	**0.4122**
$F_{S,\mathrm{mean}}$	0.4175	0.4172	0.4148	0.4152	0.4118	**0.4113**
St. Dev.	2.E-03	2.E-03	7.E-04	**3.E-04**	**3.E-04**	**3.E-04**

The critical slip surfaces illustrated in Figure 3.18, indicate a somewhat rotational failure mechanism. All methods estimate that the slip and slope toes coincide. However, the scarp locations can vary as much as 1.5 m. It is also noticeable that the critical slip surfaces produced by all methods, except for M4, include a discontinuity at the interface between the uppermost and middle soil layers, which illustrates the limitations imposed in the formulation of M4.

The convergence graphs, given in Figure 3.19, indicate that the computational effort required to analyze *Example 4* is more or less similar for all surface generation methods. Furthermore, most methods produce near-optimum solutions with their initial populations, indicating that the geometric and soil properties of this example produce a relatively easier optimization problem compared to the previous ones.

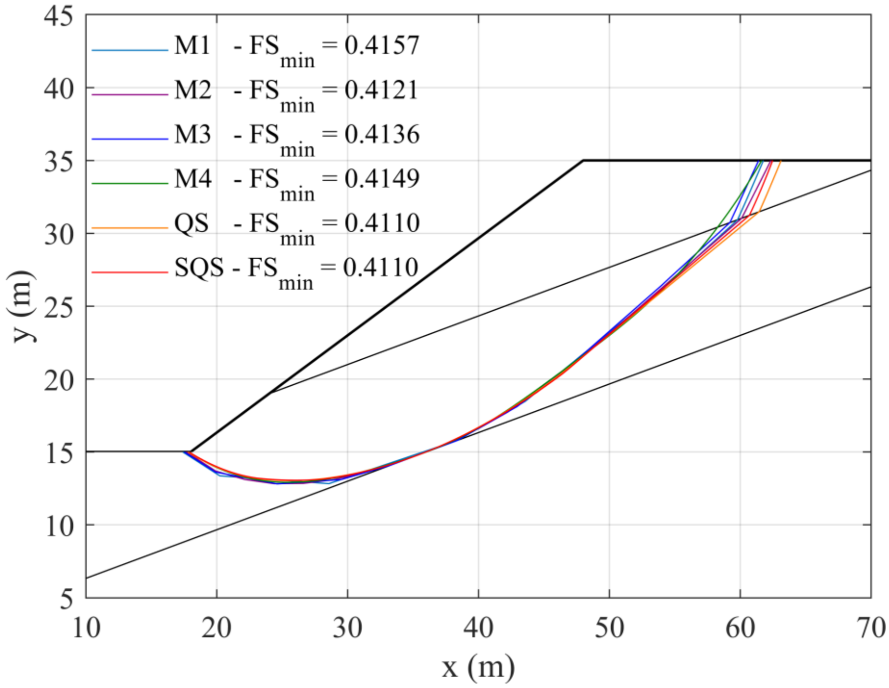

Figure 3.18: *Example 4* – comparison of critical slip surfaces

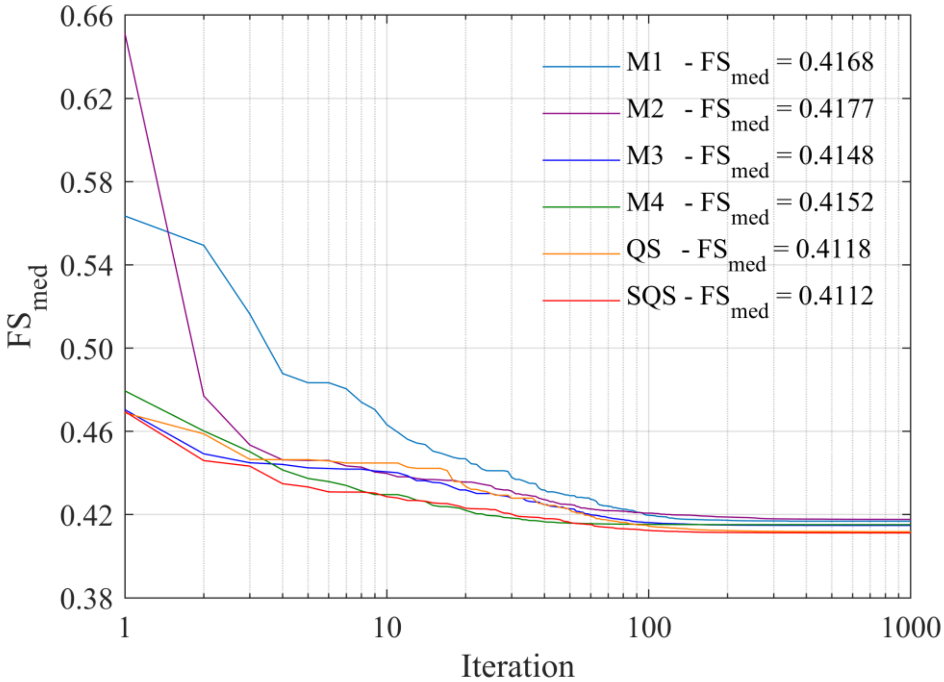

Figure 3.19: *Example 4* – the convergence of surface generation methods

3.2.3.5. *Example 5*

In *Example 5*, the slope is analyzed under static loads in Case (*i*) and further evaluated considering pseudo-static earthquake loading in Case (*ii*). The results of the analyses, presented in Table 3.18, indicate that M2, M3, and M4 fail to locate the critical surface for both cases. M1 is capable to find near-optimum solutions, however, cannot improve the results of QS and SQS, which produce the most critical slip surfaces. For Case (*i*), the minimum F_S is reported with QS as 1.0096, while SQS yields the minimum value for Case (*ii*) as 0.8400. In either case, the minimum F_S values of these two methods differ only slightly. However, it should be noted that SQS is statistically the better alternative.

Example 5 is presumably the most awkward of all the benchmark problems presented in this manuscript. As illustrated in Figures 3.20 and 3.21, the failure is translational. Furthermore, the search space of the problem does not contain any strong local minima considering the distinct soft soil band. However, the critical slip surface is extremely flat with a wide linear segment in the middle. Therefore, the problem mostly tests the capabilities of the surface generation methods. In this sense, M2, M3, and M4 fail in both cases of the problem. On the other hand, M1, QS, and SQS are observed to be flexible enough to represent the critical surfaces.

Table 3.18: *Example 5* – statistical comparison of surface generation methods

		M1	**M2**	**M3**	**M4**	**QS**	**SQS**
Case (*i*)	$F_{S,\mathrm{min}}$	1.0187	1.1319	1.1080	1.0975	**1.0096**	1.0101
	$F_{S,\mathrm{med}}$	1.0639	1.1978	1.1760	1.1041	1.0235	**1.0149**
	$F_{S,\mathrm{max}}$	1.1813	1.5908	1.2785	1.1371	1.1305	**1.0779**
	$F_{S,\mathrm{mean}}$	1.0730	1.2370	1.1805	1.1079	1.0398	**1.0199**
	St. Dev.	4.E-02	1.E-01	4.E-02	**1.E-02**	4.E-02	**1.E-02**
Case (*ii*)	$F_{S,\mathrm{min}}$	0.8461	0.9647	0.9542	0.9251	0.8408	**0.8400**
	$F_{S,\mathrm{med}}$	0.8802	1.0025	0.9804	0.9281	0.8519	**0.8443**
	$F_{S,\mathrm{max}}$	0.9745	1.1541	1.0308	0.9514	0.9461	**0.8791**
	$F_{S,\mathrm{mean}}$	0.8954	1.0087	0.9851	0.9313	0.8628	**0.8469**
	St. Dev.	5.E-02	4.E-02	2.E-02	8.E-03	3.E-02	**8.E-03**

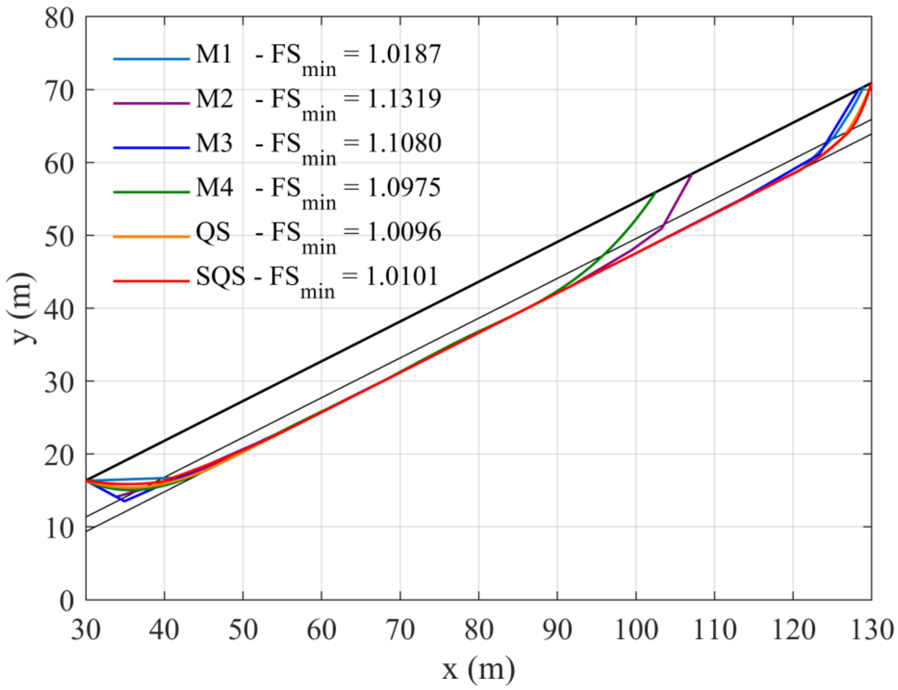

Figure 3.20: *Example 5 Case* (*i*) – comparison of critical slip surfaces

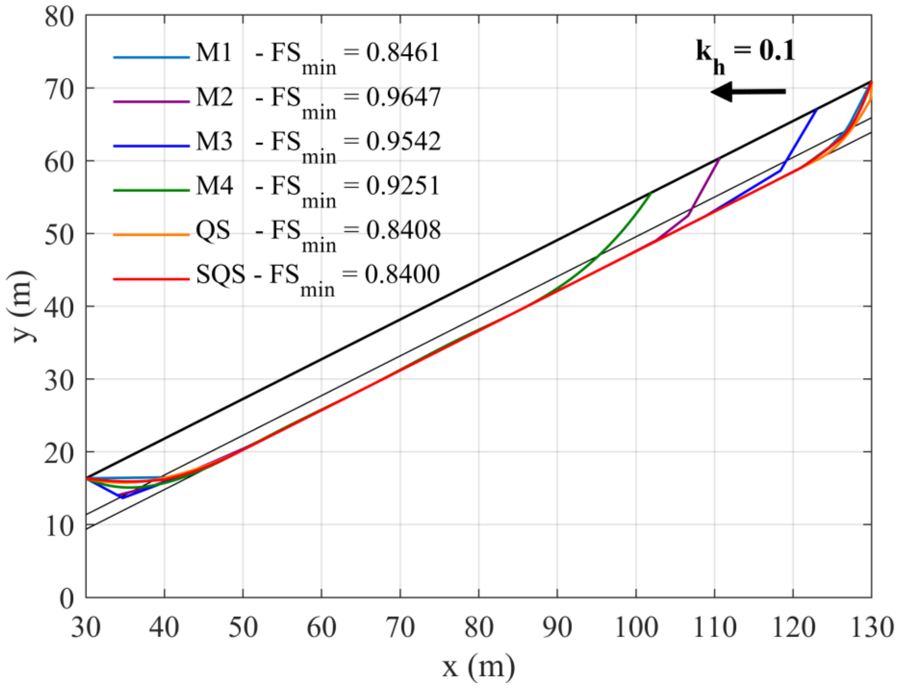

Figure 3.21: *Example 5 Case* (*ii*) – comparison of critical slip surfaces

Convergence graphs for *Cases* (*i*) and (*ii*) are given in Figures 3.22 and 3.23, respectively. Considering both examples, the computational cost of SQS is relatively higher compared to the previous experiments. However, the analyses fully converge in about 200 to 300 iterations, which is either similar to or better than the other methods.

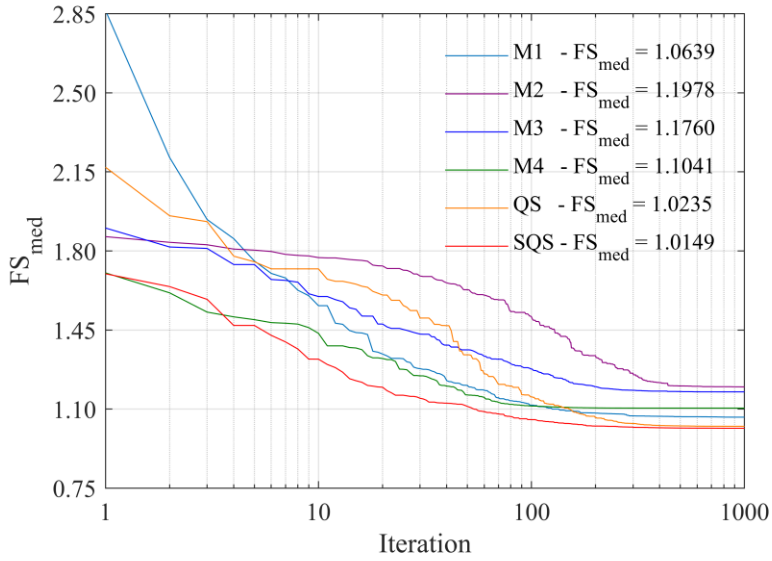

Figure 3.22: *Example 5 Case* (*i*) – the convergence of surface generation methods

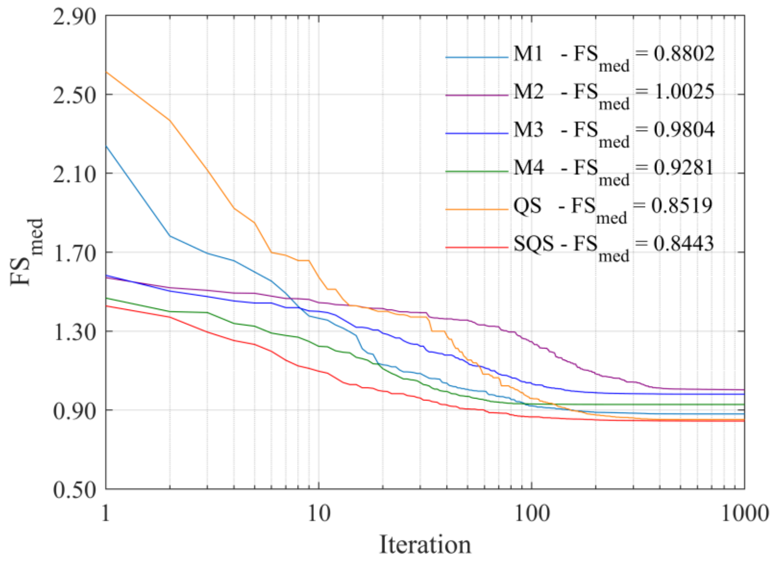

Figure 3.23: *Example 5 Case* (*ii*) – the convergence of surface generation methods

3.2.3.6. Example 6

The last example considers four configurations with different loading and groundwater conditions as summarized in Figure 3.9. The results of the experiments, given in Table 3.19, further emphasize the capability of SQS, which yields the best statistical outcomes as well as the minimum F_S values for all cases. Using SQS, the minimum F_S values for *Cases* (*i*) through (*iv*) are obtained as 1.3303, 1.1971, 1.0419 and 0.9317, respectively. QS often finds similar results but deviates more than SQS, especially in the cases with seismic loading (i.e. *Cases* (*iii*) and (*iv*)). Considering the other methods, M1 is the most competitive alternative, while M2, M3, and M4 often produce inferior solutions.

Table 3.19: *Example 6* – statistical comparison of surface generation methods

		M1	**M2**	**M3**	**M4**	**QS**	**SQS**
Case (*i*)	$F_{S,\mathrm{min}}$	1.3312	1.3514	1.3490	1.3392	1.3304	**1.3303**
	$F_{S,\mathrm{med}}$	1.3409	1.3795	1.3656	1.3486	1.3373	**1.3345**
	$F_{S,\mathrm{max}}$	1.3710	1.4166	1.3892	1.3829	1.3599	**1.3467**
	$F_{S,\mathrm{mean}}$	1.3429	1.3832	1.3677	1.3522	1.3382	**1.3371**
	St. Dev.	9.E-03	2.E-02	9.E-03	1.E-02	**6.E-03**	**6.E-03**
Case (*ii*)	$F_{S,\mathrm{min}}$	1.2022	1.2120	1.2197	1.2045	1.1985	**1.1971**
	$F_{S,\mathrm{med}}$	1.2122	1.2561	1.2393	1.2218	1.2056	**1.2002**
	$F_{S,\mathrm{max}}$	1.2285	1.3700	1.2687	1.3282	1.2119	**1.2091**
	$F_{S,\mathrm{mean}}$	1.2162	1.2636	1.2429	1.2477	1.2064	**1.2016**
	St. Dev.	1.E-02	4.E-02	2.E-02	5.E-02	5.E-03	**4.E-03**
Case (*iii*)	$F_{S,\mathrm{min}}$	1.0424	1.0703	1.0643	1.0559	1.0422	**1.0419**
	$F_{S,\mathrm{med}}$	1.0476	1.0941	1.0784	1.0651	1.0547	**1.0466**
	$F_{S,\mathrm{max}}$	1.0776	1.1766	1.0987	1.3269	1.0639	**1.0596**
	$F_{S,\mathrm{mean}}$	1.0514	1.0949	1.0775	1.0928	1.0538	**1.0471**
	St. Dev.	1.E-02	2.E-02	9.E-03	8.E-02	7.E-03	**4.E-03**
Case (*iv*)	$F_{S,\mathrm{min}}$	0.9335	0.9595	0.9472	0.9430	0.9320	**0.9317**
	$F_{S,\mathrm{med}}$	0.9531	0.9784	0.9737	0.9510	0.9426	**0.9353**
	$F_{S,\mathrm{max}}$	0.9662	1.1029	0.9983	0.9770	0.9688	**0.9432**
	$F_{S,\mathrm{mean}}$	0.9516	0.9908	0.9746	0.9526	0.9456	**0.9367**
	St. Dev.	1.E-02	4.E-02	2.E-02	8.E-03	1.E-02	**4.E-03**

The critical slip surfaces obtained with each method are illustrated in Figures 3.24–3.27 for *Cases* (*i*) through (*iv*), respectively. Considering *Case* (*i*), a partially translational failure mechanism is observed above the relatively stiff base soil layer. The most visible differences are observed for M2 and M3, which locate the slip toe about 1 m away from the other methods. Furthermore, the approximation of M4 is slightly different than M1, QS, and SQS, considering the deviations around the interface between the soft soil band and the upper layer. Similar observations are made for the other cases illustrated in Figures 3.25–3.27.

The convergence graphs, given in Figures 3.28–3.31, support the findings of the previous experiments. For each case, the convergence rate of SQS is significantly better than the other methods, which promotes SQS as a computationally efficient surface generation method. Although QS can find comparable terminal values, the scaling operation in SQS facilitates the optimization process significantly.

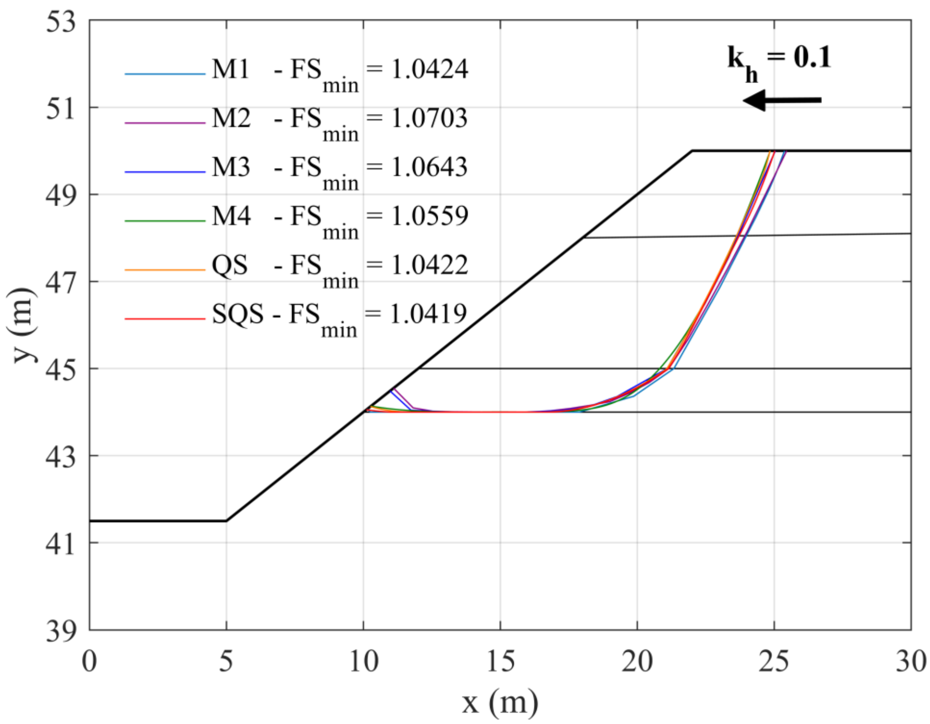

Figure 3.24: *Example 6 Case* (*i*) – comparison of critical slip surfaces

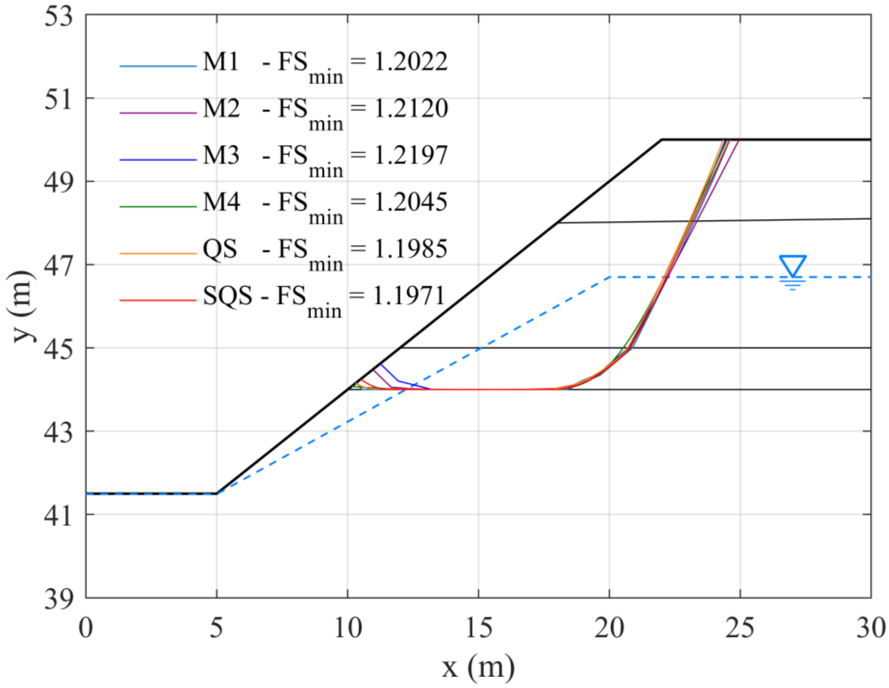

Figure 3.25: *Example 6 Case* (*ii*) – comparison of critical slip surfaces

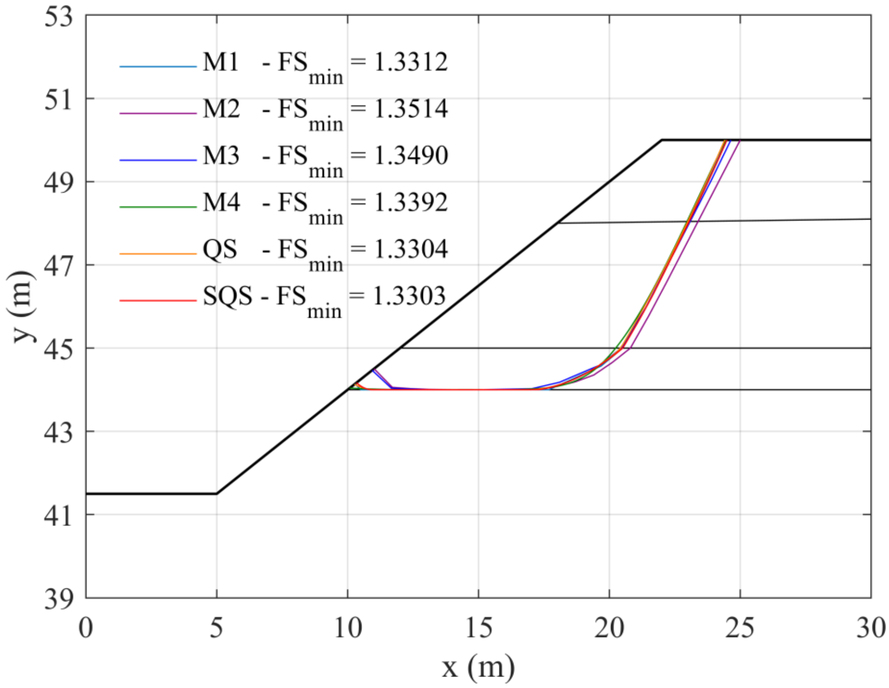

Figure 3.26: *Example 6 Case* (*iii*) – comparison of critical slip surfaces

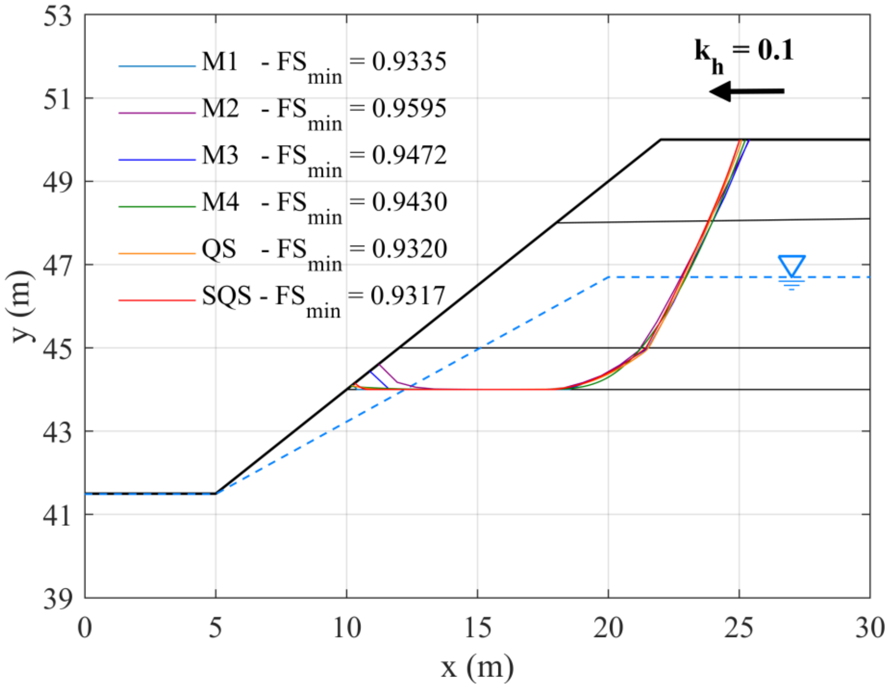

Figure 3.27: *Example 6 Case* (*iv*) – comparison of critical slip surfaces

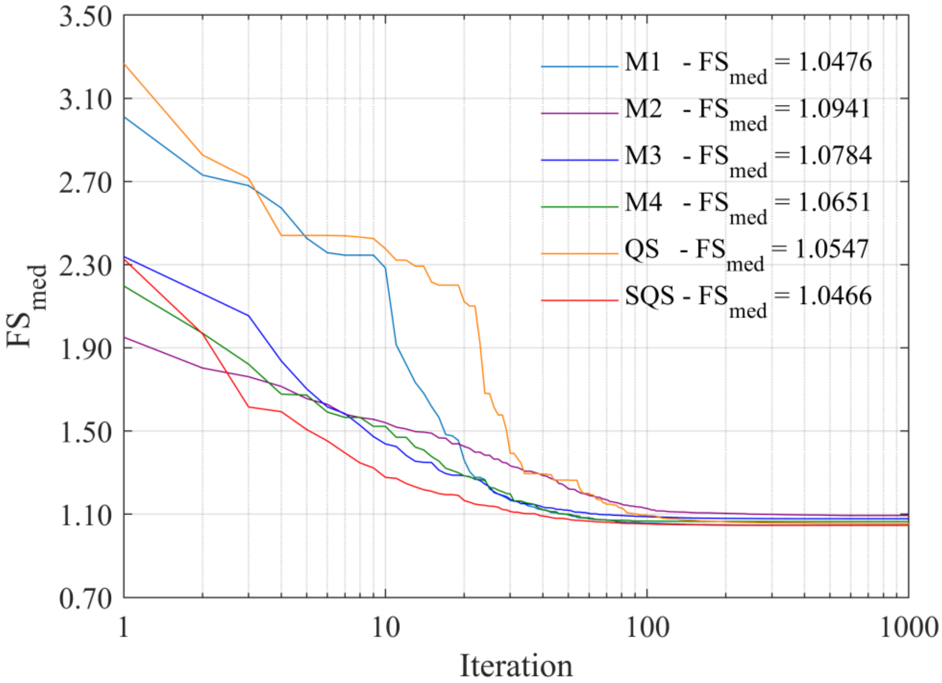

Figure 3.28: *Example 6 Case* (*i*) – the convergence of surface generation methods

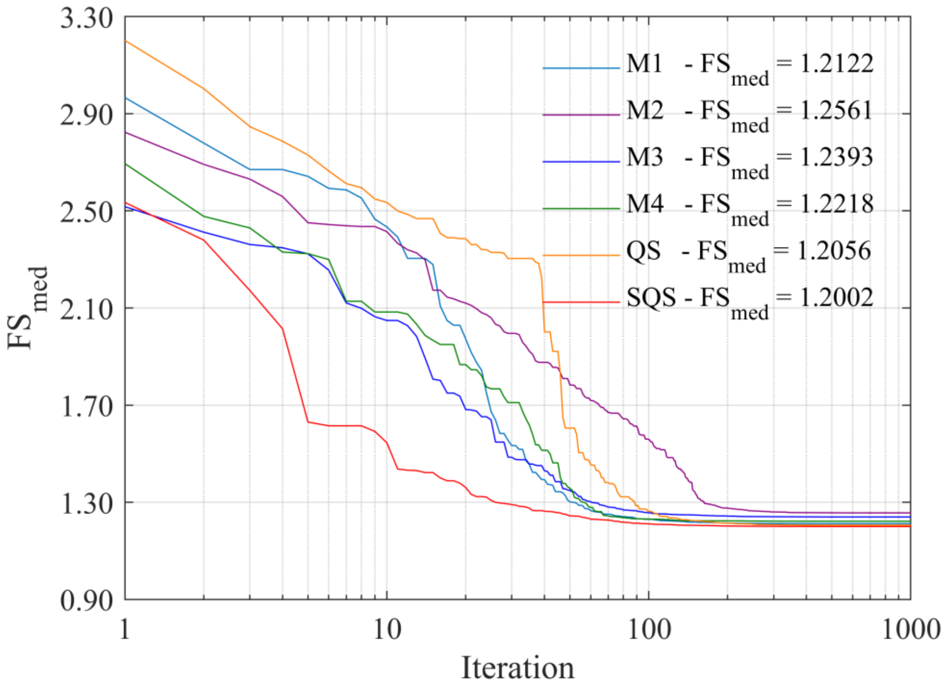

Figure 3.29: *Example 6 Case* (*ii*) – the convergence of surface generation methods

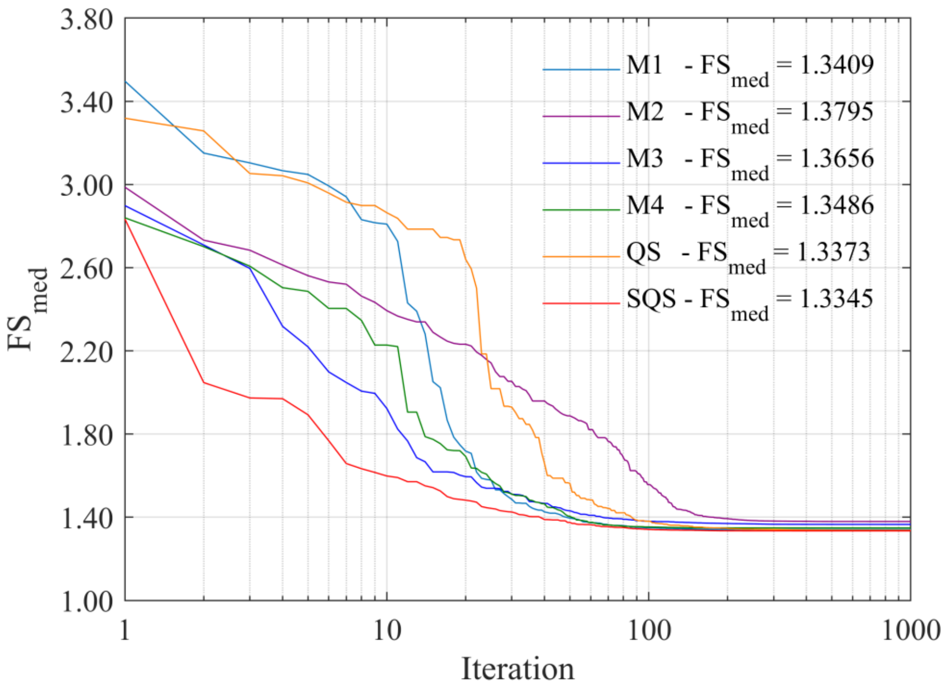

Figure 3.30: *Example 6 Case* (*iii*) – the convergence of surface generation methods

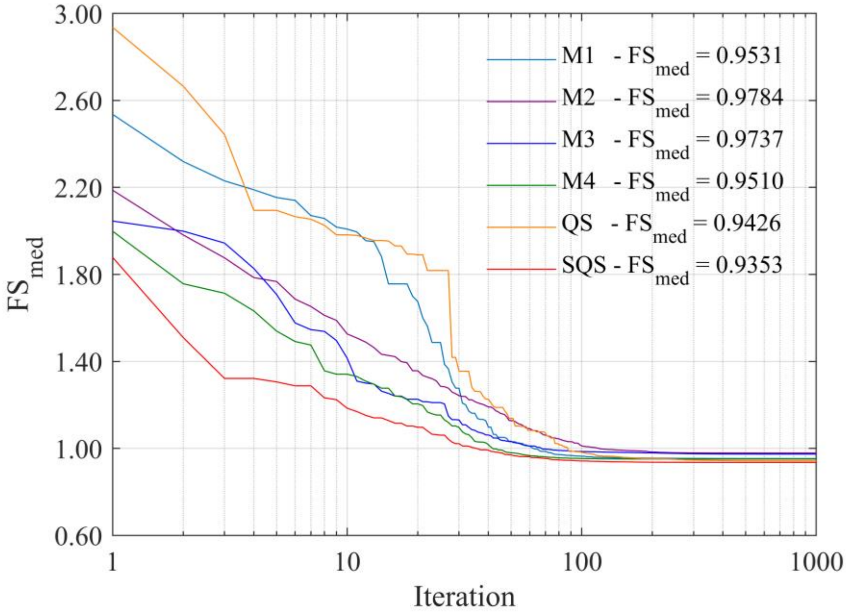

Figure 3.31: *Example 6 Case* (*iv*) – the convergence of surface generation methods

3.2.3.7. Statistical Significance Tests

The experiments presented so far propound SQS as a proficient and statistically reliable alternative to the existing surface generation methods. To validate this claim and encapsulate the findings of the experiments, a comparative analysis is performed to assess the statistical significance of the improvements achieved with SQS. Accordingly, SQS is paired with each surface generation method separately and evaluated using Wilcoxon signed-rank comparison [68] to test the hypothesis that "*the pairwise difference between the results of SQS and the opposing method has a median F_S value equal to zero*". The confidence interval is kept at 95% (i.e. α=0.05) and it is reasoned that the method with lower median F_S performs significantly better than the other if the hypothesis is rejected. The tests are performed based on the results of 30 independent analyses of each benchmark problem, resulting in a total of 11 cases.

The outcomes of the significance tests are summarized in Table 3.20, in terms of p-values and indications to denote the favorable method for each example. The notation is explained as follows; (i) the examples where SQS significantly improves the opposing method are denoted with "⊕", (ii) the examples where the opposing method significantly improves SQS are denoted with "⊖", and (iii) the examples where the differences between the results are not significant are denoted with "⊙". Compared to M1 and M4, SQS exhibits significant improvement in 10 of the 11 instances, and the differences are observed to be insignificant in one case for each method. The improvement rate of SQS over M2 and M3 is 100%. The only method that exhibits improvement over SQS is QS, which is only observed for *Example 1*. Furthermore, it is noteworthy to mention that the results of these two methods are similar in *Example 2* Case (*i*). Both of these examples consider the analysis of simple slope geometries with homogeneous soil profiles under gravitational loads only. For such simple cases, QS may be preferred over SQS. On the other hand, SQS is more effective for complex problems as it produces significant improvement in 8 out of the 9 cases that either incorporate stratified soil profiles or consider external loading.

Table 3.20: Summary of signed-rank tests

SQS vs. →	**M1**	**M2**	**M3**	**M4**	**QS**
Example 1	1.73E-06 ⊕	1.73E-06 ⊕	1.73E-06 ⊕	4.72E-02 ⊕	2.30E-02 ⊖
Example 2 (i)	1.73E-06 ⊕	1.73E-06 ⊕	1.73E-06 ⊕	6.73E-01 ⊙	6.56E-02 ⊙
Example 2 (ii)	4.07E-05 ⊕	1.73E-06 ⊕	7.69E-06 ⊕	1.73E-06 ⊕	3.38E-03 ⊕
Example 3	2.62E-01 ⊙	1.73E-06 ⊕	1.73E-06 ⊕	1.73E-06 ⊕	1.25E-04 ⊕
Example 4	1.73E-06 ⊕	1.73E-06 ⊕	1.73E-06 ⊕	1.73E-06 ⊕	3.72E-05 ⊕
Example 5 (i)	3.52E-06 ⊕	1.73E-06 ⊕	1.73E-06 ⊕	1.73E-06 ⊕	1.17E-02 ⊕
Example 5 (ii)	5.22E-06 ⊕	1.73E-06 ⊕	1.73E-06 ⊕	1.73E-06 ⊕	1.83E-03 ⊕
Example 6 (i)	9.84E-03 ⊕	1.73E-06 ⊕	1.73E-06 ⊕	2.88E-06 ⊕	6.29E-01 ⊙
Example 6 (ii)	3.18E-06 ⊕	1.73E-06 ⊕	1.72E-06 ⊕	3.88E-06 ⊕	1.71E-03 ⊕
Example 6 (iii)	4.07E-02 ⊕	1.73E-06 ⊕	1.73E-06 ⊕	1.73E-06 ⊕	4.53E-04 ⊕
Example 6 (iv)	6.98E-06 ⊕	1.73E-06 ⊕	1.73E-06 ⊕	1.73E-06 ⊕	2.41E-04 ⊕
Summary:	**10⊕;0⊖;1⊙**	**11⊕;0⊖;0⊙**	**11⊕;0⊖;0⊙**	**10⊕;0⊖;1⊙**	**8⊕;1⊖;2⊙**

The results are in terms of p-values. ⊕: SQS shows significant improvement, ⊖: opposing method shows significant improvement, ⊙: the difference is not significant in 95% confidence interval.

3.2.4. Comparison of SQS with Commercial Analysis Software

In this section, the reliability of the analysis framework is verified and the efficiency of SQS is further investigated through a comparison with the renowned slope stability analysis software, *Slide v7* [34]. First, the program is calibrated into the analysis settings used for SQS. Analysis option is selected as "*GLE/Morgenstern-Price*", interslice force function is specified as "*Constant*", groundwater option is selected as "*Water Surfaces*" and the error tolerance for F_S is set to 10^{-5}. Using this configuration, the critical slip surfaces produced with SQS are analyzed for result verification. The outcomes, given in Appendix A, indicate that the results reported in the previous sections are in perfect agreement with the software. The agreement of the results allows a comparative performance evaluation between the proposed framework and *Slide* analysis software. Accordingly, the benchmark problems are analyzed using the software with the following settings: surface type is selected as "*non-circular*", search method is specified as "*Cuckoo Search*", the number of slices for F_S evaluation is set to 100 (i.e. convergence of *Slide v7* is not sensitive to the number of slices) and the surface optimization settings are kept at the default configurations. The software does not report statistical results, hence a comparison is only possible in terms of minimum F_S and the λ values. Given in Table 3.21, the results further emphasize the capability of SQS, which yields a slightly improved F_S value for each experiment.

Table 3.21: Comparison of SQS and *Slide v7*

	SQS		**Slide v7**	
	$F_{S,\min}$	λ	$F_{S,\min}$	λ
Example 1	**1.9773**	0.3026	1.9920	0.3031
Example 2 (i)	**1.3220**	0.2497	1.3252	0.2499
Example 2 (ii)	**0.9976**	0.2874	1.0018	0.2918
Example 3	**1.0878**	0.0719	1.0904	0.7010
Example 4	**0.4110**	0.2430	0.4140	0.2332
Example 5 (i)	**1.0101**	0.4531	1.0207	0.4431
Example 5 (ii)	**0.8400**	0.5680	0.8457	0.5674
Example 6 (i)	**1.3303**	0.1384	1.3321	0.1385
Example 6 (ii)	**1.1971**	0.0703	1.1980	0.0706
Example 6 (iii)	**1.0419**	0.4141	1.0436	0.4136
Example 6 (iv)	**0.9317**	0.3323	0.9329	0.3397

The critical slip surfaces located with SQS and *Slide v7* are illustrated in Figure 3.32. For the experiments except for *Example 2 Case* (*ii*) and *Example 4*, the critical paths are exact matches. The main difference in all cases is the smoothness of the surfaces generated with SQS.

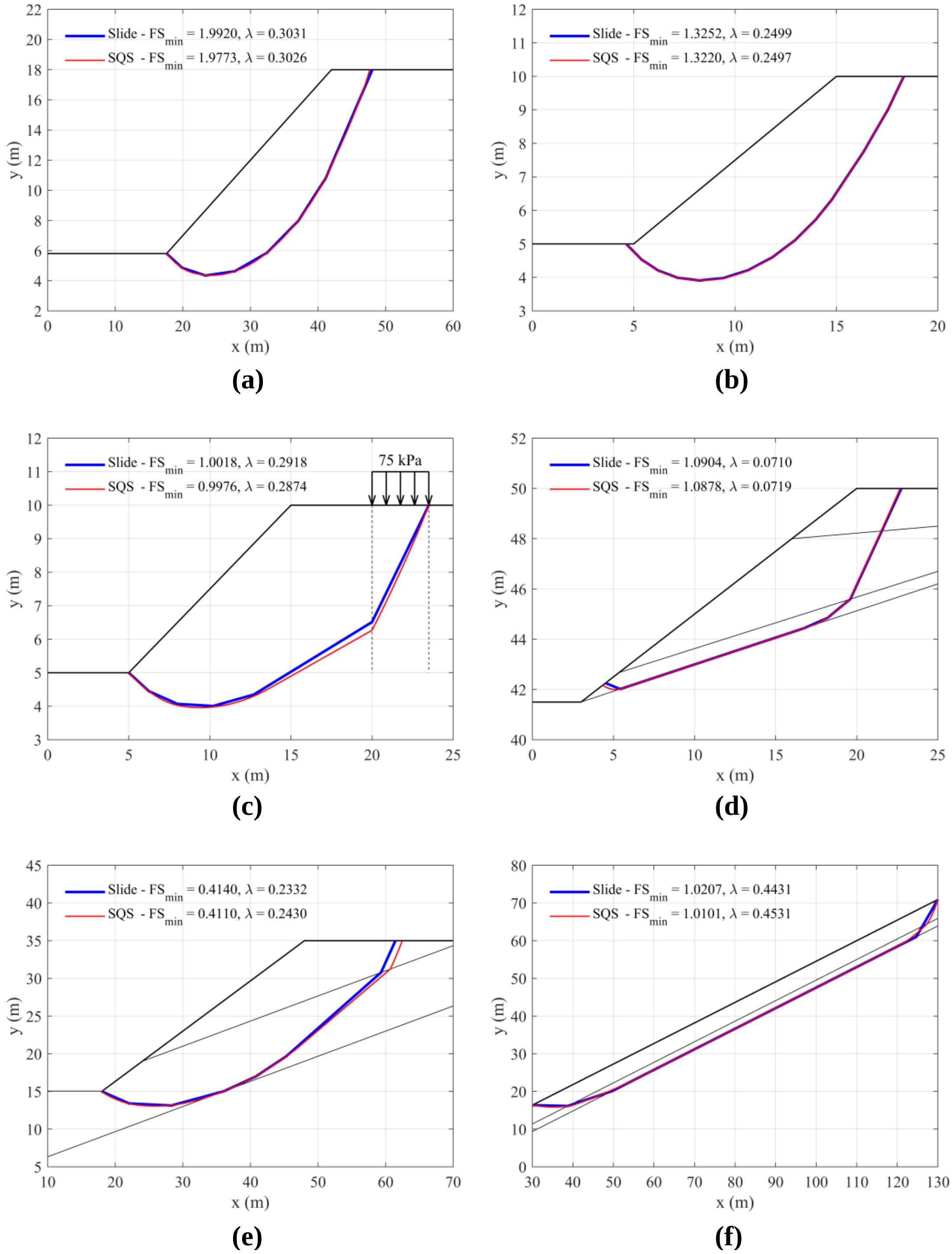

Figure 3.32: Comparison of SQS and *Slide v7* – critical slip surfaces
(a) *Example 1* **(b)** *Example 2* (*i*) **(c)** *Example 2* (*ii*)
(d) *Example 3* **(e)** *Example 4* **(f)** *Example 5* (*i*)

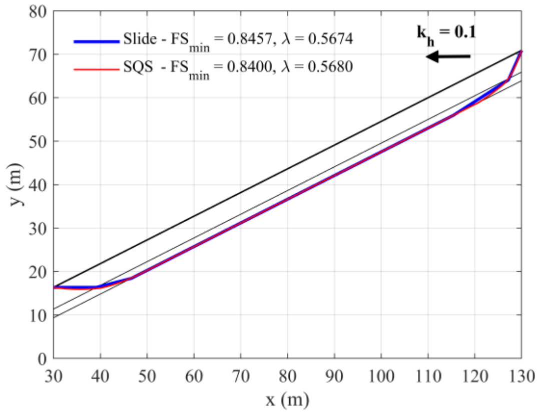

(g)

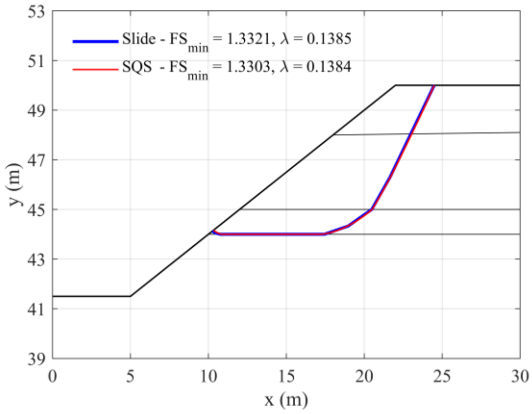

(h)

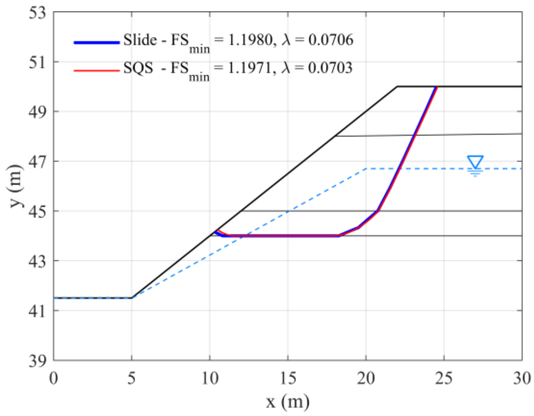

(i)

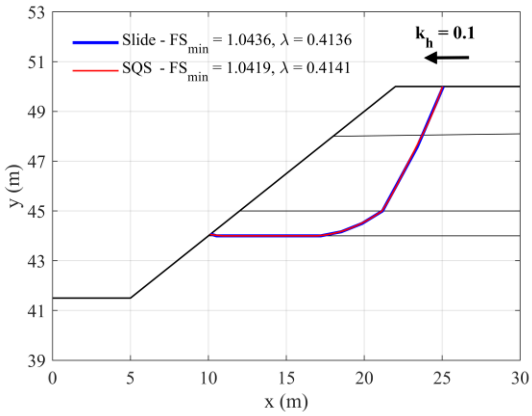

(j)

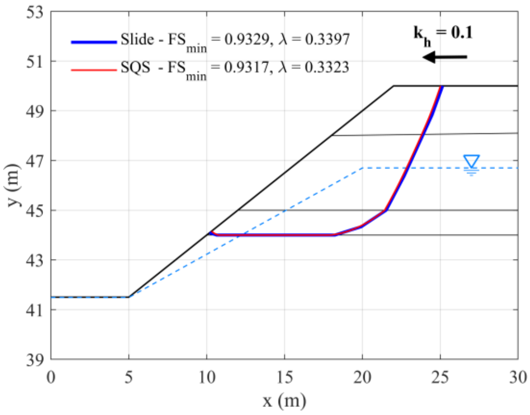

(k)

Figure 3.32 (cont'd): Comparison of SQS and *Slide v7* – critical slip surfaces
(g) *Example 5* (*ii*) **(h)** *Example 6* (*i*) **(i)** *Example 6* (*ii*)
(j) *Example 6* (*iii*) **(k)** *Example 6* (*iv*)

3.3. Discussion of Results

The experiments in this chapter provide an elaborate assessment of the available surface generation procedures and the alternative methods developed in scope of the present study. First, a parametric study is conducted to better understand and exploit the capabilities of these methods, which are broadly classified into two groups as slice and spline-based methods. Slice-based methods like the ones proposed by Malkawi (i.e. M1) and Cheng (i.e. M2 and M3) utilize discrete lines to represent the slip surfaces. Therefore, they require a great number of segments, and consequently geometric parameters for accurate surface representation. Consequently, the convergence rates of these methods are greatly influenced by the resulting dimensionality. On the other hand, spline-based approaches, Sun's method (i.e. M4) and the ones developed in this study (i.e. QS and SQS), seem to overcome this issue. Using any of these methods, a few spline functions are sufficient for accurate surface representation. Accordingly, the resulting surface optimization problems include marginally low numbers of decision variables.

In light of these internal observations, the methods are comparatively evaluated based on result accuracy, statistical soundness, and computational efficiency. For simple slopes with homogeneous soil profiles, all spline approaches are favorable over slice-based methods. However, the capability of Sun's cubic spline method is comparably limited for complex cases with stratified soil profiles or external loading. For such problems, slice-based methods like M1 can be more reliable. Regardless, quadratic spline approaches, QS and SQS, are proficient based on result accuracy and statistical reliability. Furthermore, it is notable that the critical slip surfaces are always reported with either of these methods. The difference between QS and SQS is still significant. The scaling operation proposed in SQS seems to improve the capability of the quadratic spline approach in all aspects, especially in terms of convergence efficiency. SQS usually requires less than half the iterations required with QS, in addition to finding better approximations for the location of the critical slip surfaces. However, it should be noted that QS is slightly better than SQS for simple problems, despite its questionable convergence rates. Regardless, the statistical assessments of the results emphasize the enhanced performance of SQS over QS, as well as the other methods.

Lastly, a verification study is performed with the commercial slope stability analysis software, *Slide*. The outcomes confirm the computational implementations and give further insight into the potential of the proposed method. Even when applied with a conventional optimization algorithm (i.e. Differential Evolution) without problem specific modifications, SQS is able to improve the widely used software, *Slide*. Considering the collective of these findings, the surface generation module of Integrated Limit Equilibrium Method, SQS, is proposed as a reliable surface generation method that can individually be regarded as an enhancement over available procedures.

CHAPTER 4

INTEGRATED LIMIT EQUILIBRIUM METHOD - PART II: STABILITY ANALYSIS

In this chapter, the stability analysis module of Integrated Limit Equilibrium Method, ILEM, is introduced and proposed as a refined alternative to the existing limit equilibrium formulations. In Section 4.1, the analysis problem and the governing equations are derived using quadratic order relations and solution strategies are proposed based on analytical and numerical evaluation methods. Then, the resulting ILEM variants are verified in terms of computational efficiency and result precision in Section 4.2, including a comparison with the renowned GLE formulation. Then, the findings are summarized and discussed in Section 4.3.

4.1. Integrated Limit Equilibrium Method

To elucidate the objective of developing ILEM analysis procedure, it is necessary to refer to Chapter 2 where the limit equilibrium methods were broadly classified into two categories as single free-body procedures and procedures of slices. Among those, procedures of slices are often preferred over the others, owing to their wider ranges of applications and ability to accommodate general slip surfaces. The downside of using procedures of slices is that achieving a satisfactory level of precision requires a considerable computational cost on the account of extensive operations to discretize and evaluate the soil body.

Addressing this issue, a different solution approach is suggested in ILEM as an extension of the proposed surface generation method, SQS. Accordingly, equilibrium conditions are formulated based on quadratic order surface representation. Then, the resulting equations are derived into definite integrals that can either be integrated analytically to find closed-form solutions or accurately approximated with high-order numerical integration methods, both of which eliminate free-body discretization. The underlying assumptions and the range of application of ILEM are exactly the same as procedures of slices and the formulation unifies several LEMs, similar to GLE. However, the proposed method requires neither individual slice evaluation nor free-body discretization, hence resembles a single free-body procedure. In other words, ILEM incorporates the positive features of both lineages of limit equilibrium methods. These ideas and their implementations in ILEM are given in the following sub-sections.

Section 4.1.1 makes an introduction with the basic definitions and representation of geometric problem variables with quadratic order relations. In Section 4.1.2, the governing equations are formulated considering the equilibrium conditions. Then in Section 4.1.3, the governing equations are analytically derived into closed-form solutions for F_S evaluation. Furthermore, numerical approximation methods and their implementation in the literature are briefly discussed. Section 4.1.4 outlines the implementation process of ILEM, including further considerations for complex problems. Lastly, in Section 4.1.5, ILEM interpretation of common LEMs is discussed and a solution approach is given for each method.

4.1.1. Basic Definitions and Geometric Variables

Before commencing with the formulation, it is necessary to give the explicit definitions of the geometric variables. As there are quite a few of them that appear in the formulation, this entire sub-section is dedicated to giving the simple definitions illustrated in Figure 4.1. The notation in Figure 4.1 follows the one adopted in Chapter 3. However, in this case, the surfaces and the distributed surcharge loading, given in Figure 4.1a, are represented with quadratic order polynomials as given in Eqs. (4.1)–(4.4).

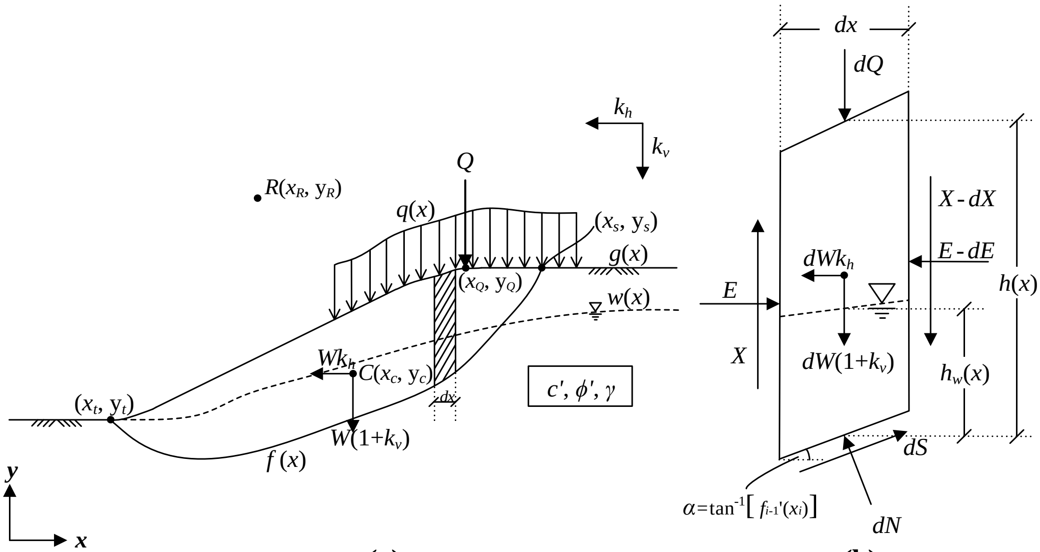

Figure 4.1: Integrated Limit Equilibrium Method analysis approach
(a) slip surface of a slope under external and seismic loading
(b) free-body diagram of an infinitesimal element

$$y_f = f(x) = a_f x^2 + b_f x + d_f \tag{4.1}$$

$$y_g = g(x) = a_g x^2 + b_g x + d_g \tag{4.2}$$

$$y_w = w(x) = a_w x^2 + b_w x + d_w \tag{4.3}$$

$$q(x) = a_q x^2 + b_q x + d_q \tag{4.4}$$

where $f(x)$, $g(x)$, $w(x)$: functions representing the failure surface, ground surface, and groundwater table elevations, and $q(x)$: the magnitude of the distributed surcharge.

The height values illustrated in Figure 4.1b are calculated using Eqs. (4.5) and (4.6) and the base inclination is obtained from the first-order derivative of $f(x)$ as given in Eq. (4.7). Note that h_w assumes negative values if the water level is below the slip surface. In such a case, the function h_w should be set to zero.

$$h(x) = g(x) - f(x) = a_h x^2 + b_h x + d_h \tag{4.5}$$

$$h_w(x) = w(x) - f(x) = a_w x^2 + b_w x + d_w \tag{4.6}$$

$$\alpha(x) = \tan^{-1}\left[f'(x)\right] = \tan^{-1}\left[2a_f x + b_f\right] \tag{4.7}$$

where $h(x)$ and $h_w(x)$: functions representing the height of soil and water above the failure surface, respectively, and $\alpha(x)$: inclination of the failure surface, measured from horizontal.

Using these definitions it is possible to determine the total weight of the free-body, W, with Eq. (4.8), and locate its center of gravity, $C(x_C, y_C)$, using Eqs. (4.9) and (4.10). Note that these expressions are derived considering a homogeneous soil profile and single-function representation. These definitions are extended for complex cases, later in Section 4.1.4.

$$W = \int_{x_t}^{x_s} \gamma\, h \cdot dx = \gamma \cdot \left(\frac{a_h x^3}{3} + \frac{b_h x^2}{2} + d_h x \right) \Bigg|_{x_t}^{x_s} \tag{4.8}$$

$$x_C = \frac{1}{W} \cdot \int_{x_t}^{x_s} x \cdot \gamma\, h \cdot dx = \frac{\gamma}{W} \cdot \left(\frac{a_h x^4}{4} + \frac{b_h x^3}{3} + \frac{d_h x^2}{2} \right) \Bigg|_{x_t}^{x_s} \tag{4.9}$$

$$y_C = \frac{1}{W} \cdot \int_{x_t}^{x_s} y_m \cdot \gamma\, h \cdot dx = \frac{\gamma}{W} \cdot \left(\begin{array}{l} \frac{a_m a_h x^5}{5} + \frac{(a_m b_h + a_h b_m) \cdot x^4}{4} + \frac{(a_m d_h + b_m b_h + a_h d_m) \cdot x^3}{3} \\ + \frac{(b_m d_h + b_h d_m) \cdot x^2}{2} + d_m d_h x \end{array} \right) \Bigg|_{x_t}^{x_s} \tag{4.10}$$

$$\text{where } y_m = m(x) = \frac{g(x) + f(x)}{2} = a_m x^2 + b_m x + d_m \tag{4.11}$$

Lastly, the resultant external load, Q, and its point of application on the x-axis, x_R, are calculated using Eqs. (4.12) and (4.13), respectively.

$$Q = \int_{x_t}^{x_s} q \cdot dx = \left(\frac{a_q x^3}{3} + \frac{b_q x^2}{2} + d_q x \right) \Bigg|_{x_t}^{x_s} \tag{4.12}$$

$$x_Q = \frac{1}{Q} \cdot \int_{x_t}^{x_s} x \cdot q \cdot dx = \frac{1}{Q} \cdot \left(\frac{a_q x^4}{4} + \frac{b_q x^3}{3} + \frac{d_q x^2}{2} \right) \Bigg|_{x_t}^{x_s} \tag{4.13}$$

4.1.2. Formulation of Equilibrium Conditions

The derivation of equilibrium equations in ILEM is similar to the approach previously adopted in GLE. The main difference is that the formulation given in this section is based on an infinitesimal element, as illustrated in Figure 4.1. Note that in the following formulation, all the forces and geometric parameters are treated as dependent variables (i.e. as a function of *x*), whereas soil parameters are assumed to be constant. Furthermore, the groundwater table, slip and ground surfaces are represented by single continuous functions. Later in Section 4.1.4, an extension is provided to accommodate complex cases as mentioned previously. The method is formulated considering fully drained conditions. However, it can be adapted to analyze a slope in undrained condition by ignoring the pore pressure and replacing the effective stress parameters, c' and ϕ', with the total stress parameters, c_u and ϕ_u.

For the infinitesimal element given in Figure 4.1b, weight, *dW*, surcharge load, *dQ*, and base uplift force, *dU*, are calculated using Eqs. (4.14)–(4.16).

$$dW = \gamma\, h dx \tag{4.14}$$

$$dQ = q dx \tag{4.15}$$

$$dU = \frac{\gamma_w h_w}{\cos\alpha} dx \tag{4.16}$$

Considering the infinitesimal element, force equilibrium in horizontal direction gives an expression to calculate the change of internal normal force, *dE* in Eq. (4.17).

$$dE = dN \sin\alpha + dWk_h - dS \cos\alpha \tag{4.17}$$

where *dN* and *dS*: normal and shear reactions on the base of the infinitesimal element.

Similarly, vertical force equilibrium yields an expression for the change of internal shear force, *dX* in Eq. (4.18).

$$dX = dW \cdot \left(1 + k_v\right) + dQ - dN \cos\alpha - dS \sin\alpha \tag{4.18}$$

To overcome static indeterminacy, Morgenstern-Price internal force assumption is applied. As a result, a relation can be written between *dE* and *dX* as follows:

$$X/E = \lambda\, f_i(x) \tag{4.19}$$

$$dX = \lambda\, f_i E - \lambda\left(f_i + f_i' dx\right)\cdot\left(E - dE\right) = \lambda dE f_i^* - \lambda E f_i' dx \tag{4.20}$$

$$f_i' = \frac{df_i}{dx} \tag{4.21}$$

$$f_i^* = f_i + f_i' dx \tag{4.22}$$

where f_i*: the value of internal force function on the right-hand side of the infinitesimal element.

Substituting Eq. (4.20) into Eq. (4.18) and combining with Eq. (4.17) eliminates *dE* and *dX* from the equations, and yields an expression between base shear and normal forces, denoted as *dS* and *dN* in Eq. (4.23), respectively.

$$\left\{\begin{aligned} & dS\cdot\left[\sin\alpha - \lambda f_i^*\cos\alpha\right] + dN\cdot\left[\lambda f_i^*\sin\alpha + \cos\alpha\right] \\ & + dW\cdot\left[\lambda f_i^* k_h - k_v - 1\right] - dQ - \lambda E f_i' dx \end{aligned}\right\} = 0 \tag{4.23}$$

When Mohr-Coulomb strength model is considered, another relation is obtained between *dS* and *dN* in Eq. (4.24).

$$dS = \frac{c'}{F_S}\frac{dx}{\cos\alpha} + \frac{\tan\phi'}{F_S}\left(dN - dU\right) \tag{4.24}$$

Substituting Eq. (4.16) into Eq. (4.24) and dividing both sides by the infinitesimal thickness, *dx*, yields the equation for base shear stress, $s(x)$ in Eq. (4.25).

$$s(x) = \frac{dS}{dx} = \frac{c'}{F_S\cos\alpha} + \frac{\tan\phi'}{F_S}\left(\sigma_n - \frac{\gamma_w h_w}{\cos\alpha}\right) \tag{4.25}$$

$$\text{where } \sigma_n(x) = \frac{dN}{dx} \tag{4.26}$$

Then, Eqs. (4.14), (4.15) and (4.24) are substituted into Eq. (4.23). The resulting equation is arranged to single out *dN*. Dividing both sides by *dx* results in an equation for base normal stress, $\sigma_n(x)$, given in Eq. (4.27).

$$\sigma_n(x) = \frac{dN}{dx} = \frac{\gamma h \cdot \left(k_v + 1 - \lambda f_i^* k_h\right) + \left(\frac{c' - \gamma_w h_w \tan\phi'}{F_S}\right) \cdot \left(\lambda f_i^* - \tan\phi'\right) + q + \lambda E f_i'}{\cos\alpha \cdot \left(1 - \frac{\lambda f_i^* \tan\phi'}{F_S}\right) + \sin\alpha \cdot \left(\frac{\tan\phi'}{F_S} + \lambda f_i^*\right)} \tag{4.27}$$

Although the equations given so far are sufficient to satisfy internal force equilibrium, it is necessary to check overall equilibrium explicitly. Based on Eqs. (4.25) and (4.27), both normal and shear stress distributions are dependent on the internal normal force variation, $E(x)$, which may assume an infinite number of configurations. It is already known that E is zero at the entrance and exit points of the slip surface since the interfaces disappear at these locations. Therefore, the boundary conditions in Eqs. (4.28) and (4.29) must be applied to guarantee complete force equilibrium. Note that internal shear force, X, is linearly dependent on E based on the interslice force assumption given in Eq. (4.19). Therefore, the boundary conditions for the internal shear forces are not considered separately.

$$E(x = x_t) = 0 \tag{4.28}$$

$$E(x = x_s) = 0 \tag{4.29}$$

The boundary condition in Eq. (4.28) is directly applied to Eq. (4.27) and the total change of interslice normal force is set to zero by integrating both sides of Eq.(4.17) as follows:

$$\int_{x_t}^{x_s} dE = \int_{x_t}^{x_s} \sin\alpha \cdot dN + k_h \cdot \int_{x_t}^{x_s} dW - \int_{x_t}^{x_s} \cos\alpha \cdot dS = 0 \tag{4.30}$$

The resulting expression is basically the summation of the horizontal components of the external, inertial and base reaction forces. The integral of dW is equal to the total weight of the sliding body, denoted with “W” in Figure 4.1a. The forces dN and dS can be replaced with $\sigma_n(x)dx$ and $s(x)dx$, respectively to obtain Eq. (4.31).

$$\sum H = Wk_h + \int_{x_t}^{x_s} \sigma_n \sin\alpha \cdot dx - \int_{x_t}^{x_s} s\cos\alpha \cdot dx = 0 \tag{4.31}$$

The above equation can be combined with Eq. (4.25) and arranged into Eq. (4.32), which is similar to the "force F_s" of GLE formulation given in Eq. (2.14).

$$F_S = \frac{\int_{x_t}^{x_s} \left(c' - \gamma_w h_w \tan\phi'\right) \cdot dx + \int_{x_t}^{x_s} \sigma_n \tan\phi' \cos\alpha \cdot dx}{Wk_h + \int_{x_t}^{x_s} \sigma_n \sin\alpha \cdot dx} \tag{4.32}$$

The normal stress is replaced with Eq. (4.27) to develop the explicit form of the force F_s expression given in Eq. (4.33).

$$\boxed{F_S = \frac{\int_{x_t}^{x_s} \left(c' - \gamma_w h_w \tan\phi'\right) \cdot dx + \int_{x_t}^{x_s} \tan\phi' \frac{\gamma h \cdot \left(k_v + 1 - \lambda f_i^{*} k_h\right) + \left(\frac{c' - \gamma_w h_w \tan\phi'}{F_S}\right) \cdot \left(\lambda f_i^{*} - \tan\alpha\right) + q + \lambda E f_i'}{1 - \frac{\lambda f_i^{*} \tan\phi'}{F_S} + \tan\alpha \cdot \left(\frac{\tan\phi'}{F_S} + \lambda f_i^{*}\right)} \cdot dx}{Wk_h + \int_{x_t}^{x_s} \frac{\gamma h \cdot \left(k_v + 1 - \lambda f_i^{*} k_h\right) + \left(\frac{c' - \gamma_w h_w \tan\phi'}{F_S}\right) \cdot \left(\lambda f_i^{*} - \tan\alpha\right) + q + \lambda E f_i'}{\cot\alpha \cdot \left(1 - \frac{\lambda f_i^{*} \tan\phi'}{F_S}\right) + \frac{\tan\phi'}{F_S} + \lambda f_i^{*}} \cdot dx}} \tag{4.33}$$

In Eq. (4.33), F_s appears on both sides and cannot be singled out. Therefore, an iterative approach should be adopted to obtain a result. In the manuscript, a quasi-Newton root finding method is proposed later in Section 4.1.5, hence Eq. (4.33) is arranged into the form given in Eq. (4.35).

$$\text{Let } F_S = \frac{I_1 + I_2}{Wk_h + I_3} \tag{4.34}$$

where I_1, I_2, and I_3: integral terms in Eq. (4.33) (i.e. the arrangement of the terms in Eq. (4.33) and (4.34) follow the same order).

To satisfy horizontal force equilibrium, both sides of Eq. (4.34) should yield the same result. Therefore, a governing equation can be defined for horizontal force equilibrium as follows:

$$\boxed{f_H(F_S, \lambda) = \frac{I_1 + I_2}{F_S} - I_3 - Wk_h = 0} \tag{4.35}$$

where $f_H(F_S, \lambda)$: governing equation for horizontal force equilibrium.

Lastly, moment equilibrium is satisfied with respect to a common rotational center, illustrated as point *R* in Figure 4.1a. To satisfy this condition, the moments generated by the external, inertial and base reaction forces are equated to zero in Eq. (4.36). In this calculation, the internal forces, *E* and *X*, are ignored, considering that the forces on the opposite sides of an interface would cancel out and generate zero net moment. However, it is worth mentioning that an internal moment equilibrium equation can be used to determine the location of the line of thrust at any interface.

$$\sum M = \left\{ \begin{aligned} & -Q\cdot\left(x_R - x_Q\right) - W\cdot\left[\left(1+k_v\right)\cdot\left(x_R - x_C\right) - k_h\cdot\left(y_R - y_C\right)\right] \\ & +\int_{x_t}^{x_s} s\cdot\left[\sin\alpha\cdot\left(x_R - x\right) - \cos\alpha\cdot\left(y_R - y_f\right)\right]\cdot dx \\ & +\int_{x_t}^{x_s} \sigma_n\cdot\left[\cos\alpha\cdot\left(x_R - x\right) + \sin\alpha\cdot\left(y_R - y_f\right)\right]\cdot dx \end{aligned} \right\} = 0 \qquad (4.36)$$

The expression in Eq. (4.36) is arranged by substituting the shear stress, $s(x)$, with Eq. (4.25). The resulting expression in Eq. (4.37) is essentially similar to the "moment F_S" of GLE, given in Eq. (2.15). However, there are some differences based on the arrangement of the terms.

$$F_S = \frac{\displaystyle\int_{x_t}^{x_s} \left\{\left[c' - \gamma_w h_w \tan\phi'\right]\cdot\left[\tan\alpha\cdot\left(x_R - x\right) - \left(y_R - y\right)\right]\right\}\cdot dx}{\left\langle \begin{aligned} & -\int_{x_t}^{x_s} \sigma_n\cdot\left\{\cos\alpha\cdot\left[\left(x_R - x\right) - \frac{\tan\phi'}{F_S}\cdot\left(y_R - y\right)\right] + \sin\alpha\cdot\left[\left(y_R - y\right) + \frac{\tan\phi'}{F_S}\cdot\left(x_R - x\right)\right]\right\} dx \\ & +Q\cdot\left(x_R - x_Q\right) + W\cdot\left[\left(1+k_v\right)\cdot\left(x_R - x_C\right) - k_h\cdot\left(y_R - y_C\right)\right] \end{aligned} \right\rangle} \qquad (4.37)$$

Normal stress is replaced with Eq. (4.27) to obtain the explicit form of the moment F_S equation, given in Eq. (4.38).

$$F_S = \frac{\displaystyle\int_{x_t}^{x_s} \left\{ \left[c' - \gamma_w h_w \tan\phi' \right] \cdot \left[\tan\alpha \cdot (x_R - x) - (y_R - y) \right] \right\} \cdot dx}{\left\langle \begin{array}{l} -\displaystyle\int_{x_t}^{x_s} \left\{ (x_R - x) - \frac{\tan\phi'}{F_S} \cdot (y_R - y) + \tan\alpha \cdot \left[(y_R - y) + \frac{\tan\phi'}{F_S} \cdot (x_R - x) \right] \right\} \\ \qquad \times \left\{ \dfrac{\gamma h \cdot \left(k_v + 1 - \lambda f_i^* k_h \right) + \left(\dfrac{c' - \gamma_w h_w \tan\phi'}{F_S} \right) \cdot \left(\lambda f_i^* - \tan\alpha \right) + q + \lambda E f_i'}{1 - \dfrac{\lambda f_i^* \tan\phi'}{F_S} + \tan\alpha \cdot \left(\dfrac{\tan\phi'}{F_S} + \lambda f_i^* \right)} \right\} \cdot dx \\ + \; Q \cdot (x_R - x_Q) + W \cdot \left[(1 + k_v) \cdot (x_R - x_C) - k_h \cdot (y_R - y_C) \right] \end{array} \right\rangle} \tag{4.38}$$

Similar to the procedure adopted previously, Eq. (4.38) is arranged to form the governing equation given in Eq. (4.40).

Let $F_S = \dfrac{I_4}{-I_5 + Q \cdot (x_R - x_Q) + W \cdot \left[(1 + k_v) \cdot (x_R - x_C) - k_h \cdot (y_R - y_C) \right]}$ (4.39)

$$\boxed{f_M(F_S, \lambda) = \frac{I_4}{F_S} + I_5 - Q \cdot (x_R - x_Q) - W \cdot \left[(1 + k_v) \cdot (x_R - x_C) - k_h \cdot (y_R - y_C) \right] = 0} \tag{4.40}$$

where I_4 and I_5: integral terms in Eq. (4.38), and f_M (F_S, λ): governing equation for moment equilibrium.

The resulting formulation is similar to that of GLE, presented in Chapter 2. There are two governing equations (i.e. Eqs. (4.35) and (4.40)) and two unknowns (i.e. F_S and λ). Using Eqs. (4.35) and/or (4.40), it is possible to obtain solutions based on the assumptions of Bishop, Janbu, Lowe and Karafiath, Corps of Engineers, Morgenstern-Price, and consequently Spencer. However, Fellenius' method ignores vertical force equilibrium, instead follows a different assumption to calculate base normal stresses (i.e. refer to Section 2.1.2.1). Therefore, the equations are modified to obtain a solution for Fellenius' method as follows:

Special Case: Fellenius' force assumption

Considering the infinitesimal element given in Figure 4.1b, the forces are resolved along the slip surface. From force equilibrium along the base normal direction, dN and σ_n can be obtained as follows:

$$\frac{dN}{dx} = \sigma_n = \gamma h \cdot \left[(k_v + 1) \cdot \cos\alpha - k_h \sin\alpha \right] + q \cos\alpha \tag{4.41}$$

Fellenius' method ignores internal forces completely and calculates F_S based on moment equilibrium. Therefore Eq. (4.38) can be modified by substituting Eq. (4.41) for σ_n, and replacing λ with zero. After arranging, F_S can be singled out as given in Eq. (4.42).

$$\left(F_{S,M}\right)_F = \frac{\int_{x_t}^{x_s} \left\{ \left[c' - \gamma_w h_w \tan\phi' \right] \cdot \left[\tan\alpha \cdot (x_R - x) - (y_R - y) \right] \right\} \cdot dx + \int_{x_t}^{x_s} \left\{ \begin{array}{l} \tan\phi' \cos^2\alpha \cdot \left[\gamma h \cdot (k_v + 1 - k_h \tan\alpha) + q \right] \\ \times \left[\tan\alpha \cdot (x_R - x) - (y_R - y) \right] \end{array} \right\} \cdot dx}{-\int_{x_t}^{x_s} \left\{ \begin{array}{l} \cos^2\alpha \cdot \left[\gamma h \cdot (k_v + 1 - k_h \tan\alpha) + q \right] \\ \times \left[x_R - x + \tan\alpha \cdot (y_R - y) \right] \end{array} \right\} \cdot dx + Q \cdot (x_R - x_Q) + W \cdot \left[(1 + k_v) \cdot (x_R - x_C) - k_h \cdot (y_R - y_C) \right]} \tag{4.42}$$

where $(F_{S,M})_F$: moment F_S based on Fellenius' normal force assumption.

Additionally, in this study, Fellenius' normal force assumption is used to calculate a F_S based on horizontal force equilibrium. It should be noted that this not a common approach in the literature, rather an experimental trial to evaluate the agreement of the results with rigorous LEMs. To obtain the force F_S based on this assumption, Eq. (4.41) is simply substituted into Eq. (4.33) and λ is replaced with zero. The resulting expression is given in Eq. (4.43).

$$\left(F_{S,H}\right)_F = \frac{\int_{x_t}^{x_s} (c' - \gamma_w h_w \tan\phi') \cdot dx + \int_{x_t}^{x_s} \tan\phi' \cos^2\alpha \cdot \left[\gamma h \cdot (k_v + 1 - k_h \tan\alpha) + q \right] \cdot dx}{W k_h + \int_{x_t}^{x_s} \sin^2\alpha \cdot \left\{ \gamma h \cdot \left[(k_v + 1) \cdot \cot\alpha - k_h \right] + q \cot\alpha \right\} \cdot dx} \tag{4.43}$$

where $(F_{S,H})_F$: horizontal force F_S based on Fellenius' normal force assumption.

4.1.3. Solution Approaches for the Governing Equations

In the following sub-sections, two solution approaches are proposed to compute the governing equations. First, an analytical approach is adopted to derive closed-form solutions. Then, numerical integration approaches are discussed with their available implementations in the literature.

4.1.3.1. Closed-Form Solution with Analytical Integration

Using the derivation given in this sub-section, it is possible to compute exact solutions for the governing equations, hence avoid free-body discretization and the associated precision losses altogether. The derivation initiates with Eqs. (4.35) and (4.40), which can be adapted to find results for several LEMs by manipulating the internal force function, f_i, and λ coefficient. Among those, λ can be treated as a constant, while f_i is a method specific dependent variable that can be a trigonometric function, a polynomial in any order or even a specific user-defined function. Therefore, the analytical derivation initiates with an assumption regarding the generalized form of f_i. It is sufficient to assume a constant internal force function for the approaches proposed by Fellenius, Bishop, Janbu, Corps of Engineers (i.e. *case* (*i*)) and Spencer, hence the following formulation adopts the relations given in Eqs. (4.44) and (4.45).

$$f_i = const.. \in \mathbb{R}\,, \qquad f_i' = \frac{df_i}{dx} = 0 \tag{4.44}$$

$$f_i^* = f_i \tag{4.45}$$

In the governing equation related to force equilibrium, Eq. (4.35), there are three integral terms, which are explicitly given in Eqs. (4.46)–(4.48) for the sake of clarity.

$$I_1 = \int_{x_t}^{x_s} \left(c' - \gamma_w h_w \tan\phi'\right)\cdot dx \tag{4.46}$$

$$I_2 = \int_{x_t}^{x_S} \tan\phi' \frac{\gamma h\cdot\left(k_v + 1 - \lambda f_i^* k_h\right) + \left(\dfrac{c' - \gamma_w h_w \tan\phi'}{F_S}\right)\cdot\left(\lambda f_i^* - \tan\alpha\right) + q + \lambda E f_i'}{1 - \dfrac{\lambda f_i^* \tan\phi'}{F_S} + \tan\alpha\cdot\left(\dfrac{\tan\phi'}{F_S} + \lambda f_i^*\right)}\cdot dx \tag{4.47}$$

$$I_3 = \int_{x_t}^{x_s} \frac{\gamma h \cdot \left(k_v + 1 - \lambda f_i^* k_h\right) + \left(\frac{c' - \gamma_w h_w \tan\phi'}{F_S}\right) \cdot \left(\lambda f_i^* - \tan\alpha\right) + q + \lambda E f_i'}{\cot\alpha \cdot \left(1 - \frac{\lambda f_i^* \tan\phi'}{F_S}\right) + \frac{\tan\phi'}{F_S} + \lambda f_i^*} \cdot dx \tag{4.48}$$

The dependent variables in the equations are replaced with the function definitions given in Eqs. (4.1)–(4.13). After applying the internal force assumption, given in Eqs. (4.44) and (4.45), the integrals can be arranged into the polynomial forms given in Eqs. (4.49)–(4.51). The coefficients in the equations can be calculated using the expressions given in Eq. (4.52).

$$I_1 = \int_{x_t}^{x_s} \left(A_1 x^2 + B_1 x + C_1\right) \cdot dx \tag{4.49}$$

$$I_2 = \int_{x_t}^{x_s} \frac{A_2 x^3 + B_2 x^2 + C_2 x + D_2}{E_2 x + F_2} \cdot dx \tag{4.50}$$

$$I_3 = \int_{x_t}^{x_s} \frac{A_3 x^3 + B_3 x^2 + C_3 x + D_3}{G_3 / \left(E_3 x + F_3\right) + H_3} \cdot dx \tag{4.51}$$

$$\boxed{\begin{gathered}
A_1 = -a_{hw}\gamma_w \tan\phi',\ B_1 = -b_{hw}\gamma_w \tan\phi',\ C_1 = c' - d_{hw}\gamma_w \tan\phi' \\
\xi = \gamma \cdot \left(k_v + 1 - \lambda f_i k_h\right),\ \eta = b_f - \lambda f_i \\
A_2 = -\frac{2a_f A_1}{F_S},\ B_2 = a_h \xi + a_q - \frac{\eta A_1 + 2a_f B_1}{F_S} \\
C_2 = b_h \xi + b_q - \frac{\eta B_1 + 2a_f C_1}{F_S},\ D_2 = d_h \xi + d_q - \frac{\eta C_1}{F_S} \\
E_2 = 2a_f \cdot \left(\frac{1}{F_S} + \frac{\lambda f_i}{\tan\phi'}\right),\ F_2 = \frac{\eta}{F_S} + \frac{1 + b_f \lambda f_i}{\tan\phi'} \\
A_3 = A_2,\ B_3 = B_2,\ D_3 = D_2,\ E_3 = 2a_f,\ F_3 = b_f \\
G_3 = 1 - \frac{\lambda f_i \tan\phi'}{F_S},\ H_3 = \frac{\tan\phi'}{F_S} + \lambda f_i
\end{gathered}} \tag{4.52}$$

Through a series polynomial arrangement and substitution, the closed-form solutions of the definite integrals are obtained as given in Eqs. (4.53)–(4.55). Note that the coefficients in the equations are not subscripted for the sake of simplicity. However, for each integral, the corresponding polynomial coefficients in Eq. (4.52) should be applied in the calculations.

$$I_1 = \left(\frac{Ax^3}{3} + \frac{Bx^2}{2} + Cx \right) \Bigg|_{x_t}^{x_s} \tag{4.53}$$

$$I_2 = \left[\begin{array}{l} \dfrac{\left(DE^3 - CE^2F + BEF^2 - AF^3\right) \cdot \ln\left(\left|Ex + F\right|\right)}{E^4} \\ + \dfrac{A}{3E}x^3 + \dfrac{BE - AF}{2E^2}x^2 + \dfrac{CE^2 - BEF + AF^2}{E^3}x \end{array} \right] \Bigg|_{x_t}^{x_s} \tag{4.54}$$

$$I_3 = \left\{ \left[\begin{array}{l} \text{-}12G \cdot \left(\begin{array}{l} DE^3H^3 - CE^2FH^3 - CE^2GH^2 \\ + BEF^2H^3 + 2BEFGH^2 \\ + BEG^2H - AF^3H^3 - 3AF^2GH^2 \\ - 3AFG^2H - AG^3 \end{array} \right) \cdot \ln\left(\left|EHx + FH + G\right|\right) \\ + 3AE^4H^4x^4 + 4E^3H^3 \cdot \left(BEH - AG\right) \cdot x^3 \\ + 6E^2H^2 \cdot \left(CE^2H^2 - BEGH + AFGH + AG^2\right) \cdot x^2 \\ + 12EH \cdot \left(\begin{array}{l} DE^3H^3 \text{-} CE^2GH^2 \text{+} BEFGH^2 \\ \text{+} BEG^2H \text{-} AF^2GH^2 \text{-} 2AFG^2H \text{-} AG^3 \end{array} \right) \cdot x \end{array} \right] \cdot \frac{1}{12E^4H^5} \right\} \Bigg|_{x_t}^{x_s} \tag{4.55}$$

The solution for I_1 is quite straightforward, however, I_2 and I_3 require additional considerations. When the slip surface is defined by a linear segment (i.e. $a_f = 0$), the coefficients A_2, A_3, E_2, and E_3 become zero. When these values are substituted, 0/0 form indeterminacy is encountered in Eqs. (4.54) and (4.55). Furthermore, the equations are ill-conditioned for a_f values approaching zero since E_2 and E_3 appear in the denominators as high-order exponential terms. This issue is already addressed in SQS formulation with the threshold value applied to a_f in Eq. (3.10). To overcome indeterminacy, closed-form solutions of I_2 and I_3 are explicitly derived for linear order surface functions and abbreviated as $I_{2,lin}$ and $I_{3,lin}$. In short, for linear surfaces, Eqs. (4.54) and (4.55) are replaced with Eqs. (4.56) and (4.57), respectively.

$$A_2 = E_2 = 0 \rightarrow I_{2,lin} = \int_{x_t}^{x_s} \frac{Bx^2 + Cx + D}{F} \cdot dx = \left[\frac{1}{F} \cdot \left(\frac{Bx^3}{3} + \frac{Cx^2}{2} + Dx \right) \right] \Bigg|_{x_t}^{x_s} \tag{4.56}$$

$$A_3 = E_3 = 0 \rightarrow I_{3,lin} = \int_{x_t}^{x_s} \frac{Bx^2 + Cx + D}{G/F + H} \cdot dx = \left[\frac{1}{G/F + H} \cdot \left(\frac{Bx^3}{3} + \frac{Cx^2}{2} + Dx \right) \right] \Bigg|_{x_t}^{x_s} \tag{4.57}$$

In the governing equation related to moment equilibrium, Eq. (4.40), there are two integral terms, I_4 and I_5 in Eqs. (4.58) and (4.59), respectively.

$$I_4 = \int_{x_t}^{x_s} \left\{ \left[c' - \gamma_w h_w \tan\phi' \right] \cdot \left[\tan\alpha \cdot (x_R - x) - (y_R - y) \right] \right\} \cdot dx \tag{4.58}$$

$$I_5 = \int_{x_t}^{x_s} \begin{array}{l} \left\{ (x_R - x) - \dfrac{\tan\phi'}{F_S} \cdot (y_R - y) + \tan\alpha \cdot \left[(y_R - y) + \dfrac{\tan\phi'}{F_S} \cdot (x_R - x) \right] \right\} \\ \times \left\{ \dfrac{\gamma h \cdot \left(k_v + 1 - \lambda f_i^* k_h\right) + \left(\dfrac{c' - \gamma_w h_w \tan\phi'}{F_S} \right) \cdot \left(\lambda f_i^* - \tan\alpha \right) + q + \lambda E f_i'}{1 - \dfrac{\lambda f_i^* \tan\phi'}{F_S} + \tan\alpha \cdot \left(\dfrac{\tan\phi'}{F_S} + \lambda f_i^* \right)} \right\} \end{array} \cdot dx \tag{4.59}$$

Similar to the previous steps, the dependent variables are substituted with Eqs. (4.1)–(4.13), (4.44) and (4.45). Then, the integrals are arranged into the polynomial forms given in Eqs. (4.60) and (4.61), where the coefficients are calculated using the expressions in Eq. (4.62).

$$I_4 = \int_{x_t}^{x_s} \left(A_4 x^4 + B_4 x^3 + C_4 x^2 + D_4 x + E_4 \right) \cdot dx \tag{4.60}$$

$$I_5 = \int_{x_t}^{x_s} \frac{A_5 x^6 + B_5 x^5 + C_5 x^4 + D_5 x^3 + E_5 x^2 + F_5 x + G_5}{H_5 x + M_5} \cdot dx \tag{4.61}$$

$$\boxed{\begin{gathered}
\omega = d_f + b_f x_R - y_R,\ A_4 = -a_f A_1,\ B_4 = a_f \cdot (2 A_1 x_R - B_1) \\
C_4 = \omega A_1 + a_f \cdot (2 x_R B_1 - C_1),\ D_4 = \omega B_1 + 2 a_f x_R C_1,\ E_4 = \omega C_1 \\
\kappa_3 = -2 a_f^{\,2},\ \kappa_2 = -a_f \cdot \left(3 b_f + \frac{\tan\phi'}{F_S} \right),\ \kappa_1 = 2 a_f \cdot \left(\frac{x_R \tan\phi'}{F_S} + y_R - d_f \right) - b_f^{\,2} - 1 \\
\kappa_0 = x_R + \left(d_f - y_R \right) \cdot \frac{\tan\phi'}{F_S} + b_f \cdot \left(\frac{x_R \tan\phi'}{F_S} + y_R - d_f \right) \\
\mu_3 = \frac{-2 a_f A_1}{F_S},\ \mu_2 = a_h \xi + a_q - \frac{\eta A_1 + 2 a_f B_1}{F_S},\ \mu_1 = b_h \xi + b_q - \frac{\eta B_1 + 2 a_f C_1}{F_S}, \\
\mu_0 = d_h \xi + d_q - \frac{\eta C_1}{F_S},\ A_5 = \kappa_3 \mu_3,\ B_5 = \kappa_3 \mu_2 + \kappa_2 \mu_3,\ C_5 = \kappa_3 \mu_1 + \kappa_2 \mu_2 + \kappa_1 \mu_3 \\
D_5 = \kappa_3 \mu_0 + \kappa_2 \mu_1 + \kappa_1 \mu_2 + \kappa_0 \mu_3,\ E_5 = \kappa_2 \mu_0 + \kappa_1 \mu_1 + \kappa_0 \mu_2,\ F_5 = \kappa_1 \mu_0 + \kappa_0 \mu_1 \\
G_5 = \kappa_0 \mu_0,\ H_5 = 2 a_f \cdot \left(\frac{\tan\phi'}{F_S} + \lambda f_i \right),\ M_5 = 1 - \lambda f_i \cdot \frac{\tan\phi'}{F_S} + b_f \cdot \left(\lambda f_i + \frac{\tan\phi'}{F_S} \right)
\end{gathered}} \tag{4.62}$$

Similarly, the integrals are analytically solved to obtain the closed-form solutions given in Eqs. (4.63) and (4.64). For each integral, the corresponding polynomial coefficients in Eq. (4.62), are applied.

$$I_4 = \left(\frac{Ax^5}{5} + \frac{Bx^4}{4} + \frac{Cx^3}{3} + \frac{Dx^2}{2} + Ex \right) \Bigg|_{x_t}^{x_s} \tag{4.63}$$

$$I_5 = \left\{ \begin{bmatrix} 60 \cdot \begin{pmatrix} AM^6 - BHM^5 + CH^2M^4 - DH^3M^3 \\ + EH^4M^2 - FH^5M + GH^6 \end{pmatrix} \cdot \ln\left(\left| Hx + M \right| \right) \\ + 10AH^6x^6 - 12H^5 \cdot \left(AM - BH \right) \cdot x^5 \\ + 15H^4 \cdot \left(AM^2 - BHM + CH^2 \right) \cdot x^4 \\ - 20H^3 \cdot \left(AM^3 - BHM^2 + CH^2M - DH^3 \right) \cdot x^3 \\ + 30H^2 \cdot \left(AM^4 - BHM^3 + CH^2M^2 - DH^3M + EH^4 \right) \cdot x^2 \\ - 60H \cdot \left(AM^5 - BHM^4 + CH^2M^3 - DH^3M^2 + EH^4M - FH^5 \right) \cdot x \end{bmatrix} \cdot \frac{1}{60H^7} \right\} \Bigg|_{x_t}^{x_s} \tag{4.64}$$

In this case, I_5 is indeterminate for linear surface functions, considering that A_5 and H_5 are zero when a_f is zero. Accordingly, the closed-form solution of I_5 is explicitly derived for linear surface functions and abbreviated as $I_{5,lin}$ in Eq. (4.65).

$$\begin{aligned} A_2 = B_5 = C_5 = E_5 = 0 \rightarrow I_{5,lin} &= \int_{x_t}^{x_s} \frac{Dx^3 + Ex^2 + Fx + G}{M} \cdot dx \\ &= \left[\frac{1}{M} \cdot \left(\frac{Dx^4}{4} + \frac{Ex^3}{3} + \frac{Fx^2}{2} + Gx \right) \right] \Bigg|_{x_t}^{x_s} \end{aligned} \tag{4.65}$$

<u>*Special Case: Fellenius' force assumption*</u>

For Fellenius' method, the nature of the governing equations given in Eqs. (4.42) and (4.43) are significantly different from other methods. Therefore, a separate derivation is required to obtain an analytical solution. However, the procedure is more or less similar. The main difference in Fellenius' method is that the F_S values can be directly obtained from the closed-form solutions. These derivations and the resulting F_S equations are given in Appendix B.

4.1.3.2. Approximation with Numerical Integration

The definite integrals in the governing equations can also be evaluated using numerical integration methods. In this study, the accuracy of the well-known approaches like *Riemann sum*, *trapezoidal rule*, *Simpson's 1/3 rule* and *Gauss quadrature* approximation are investigated. It is worth mentioning that, when the slip surface is defined by linear segments (i.e. conventional slices), midpoint Riemann sum approximation reduces the accuracy of ILEM to that of GLE exactly. On the other hand, higher order approximation rules can prove to be more efficient. In fact, Gauss quadrature approximation was previously implemented by Fırat [69, 70] and Low et al. [71] based on similar ideas. The studies of Fırat adopt procedures of slices to analyze circular surfaces, yet the proposed formulation treats the sliding masses like single free-bodies. To be more specific, the surfaces are evaluated with single-step Gauss quadrature approximations over whole intervals, resulting in significantly improved convergence rates. Differently, Low performed experiments with general slip surfaces; however, utilized linear slice representation for both types of surfaces. Consequently, the capabilities of the method were not fully exploited, producing arguably limited improvements on computational efficiency and result accuracy compared to the quadratic surface representation adopted in this study.

4.1.4. Extension of ILEM to Complex Problems

The formulations given in the previous sections assume constant soil parameters and continuous single-function representation for all surfaces (i.e. groundwater table, slip and ground surfaces), as well as the distributed surcharge loading. For more complex cases, the governing equations can be evaluated using the summation of integrals for discrete segments, as defined in Eq. (4.66).

$$I = \sum_{i=1}^{n} \left[I \right]_i \Big|_{[x_i, x_{i+1}]} \tag{4.66}$$

where n: number of segments, $[I]_i$: any definite integral defined for the i^{th} segment, evaluated for the interval $[x_i, x_{i+1}]$.

To demonstrate, a comprehensive example is given in Figure 4.2. The example slip surface is composed of 4 splines, which are further divided into sub-intervals at geometric or parametric discontinuities (i.e. layer transitions, slope toe and crest locations, intersections with the groundwater level and any point where the surcharge load is discontinuous).

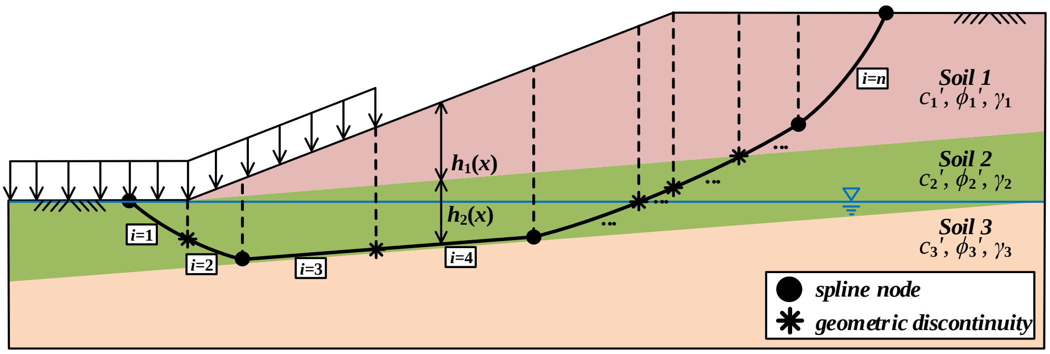

Figure 4.2: Illustration of ILEM application

It is possible to account for variable soil shear strength parameters using this process; however, profiles with variable soil unit weight require further considerations. In such cases, computing the total weight, W, and the location of its center of gravity, $C(x_c, y_c)$, is straightforward. On the other hand, evaluating the normal stress based on Eq. (4.27) or (4.41) can get rather complicated. A simple “get around” to this problem is to manipulate the function that represents the height of soil, $h(x)$. It is possible to define the height of soil within each layer, $h_j(x)$, in terms of quadratic expressions. Then, an equivalent soil height can be computed using Eq. (4.67) and adopted instead of Eq. (4.5) in the calculations. Using this approach, center of gravity calculations, more specifically Eq. (4.10), should be modified slightly. The rest of the formulation can be implemented as is.

$$h(x) = \frac{1}{\gamma_l} \cdot \sum_{j=1}^{l} \gamma_j h_j(x) \tag{4.67}$$

(i.e. implemented with γ_l)

where l: number of soil layers above the slip surface.

4.1.5. *Interpretation of Common LEMs and F_S Evaluation with Broyden's Method*

The derivation of the governing equations in ILEM formulation is essentially similar to GLE, with the exception of differential equation representation. Therefore, interpretation of other LEMs follows the pattern previously discussed in Section 2.1.2. However, in this section, these approaches are personalized for ILEM. The governing equations and unknown variables for each LEM are summarized, and concise discussions are given in Table 4.1. It is should be noted that the following sections refer to these methods with the abbreviations given in this table.

Table 4.1: ILEM interpretation of common LEMs

Abbreviation: Method	Equation(s)	Unknown(s)	Explanation
FM: Fellenius' method	$(F_{S,M})_F = const.$	–	Conventional Fellenius' method; direct solution is possible from moment equilibrium.
	$(F_{S,H})_F = const.$	–	Experimental Fellenius' method; direct solution is possible from horizontal force equilibrium.
BS: Bishop's simplified method	$f_M\ (F_S, 0) = 0$	F_S	Set λ=0; solve the equation for F_S.
JS: Janbu's simplified method	$f_H\ (F_S, 0) = 0$	F_S	Set λ=0; solve the equation for F_S.
LK: Lowe and Karafiath's method	$f_H\ (F_S, 1) = 0$	F_S	Set λ=1 and apply internal force assumption in Eq. (2.17); solve the equation for F_S.
CE: Corps of Engineers method	$f_H\ (F_S, 1) = 0$	F_S	Set λ=1 and apply internal force assumption in Eq. (2.18) or (2.19); solve the equation for F_S.
SM: Spencer's method	$f_H\ (F_S, \lambda) = 0$ $f_M\ (F_S, \lambda) = 0$	F_S, λ	Apply internal force assumption in Eq. (2.20); solve the 2×2 system of equations for F_S and λ.
MP: Morgenstern-Price method	$f_H\ (F_S, \lambda) = 0$ $f_M\ (F_S, \lambda) = 0$	F_S, λ	Apply any reasonable internal force assumption; solve the 2×2 system of equations for F_S and λ.

$(F_{S,M})_F$: Eq. (4.42) – $(F_{S,H})_F$: Eq. (4.43) – f_H: Eq. (4.35) – f_M: Eq. (4.40)

Using Fellenius' force assumption, it is possible to single out the F_S in Eqs. (4.42) and (4.43), hence a direct solution is possible for both, conventional and experimental FM, which are based on moment and horizontal force equilibrium, respectively. However, other assumptions need indirect approaches using the governing equations. Defined in

Eq. (4.68), the most complex case is associated with the rigorous methods, where 2×2 systems of nonlinear equations are solved to determine the F_S and λ values. Among the many possible techniques, the present study proposes Broyden's multivariate quasi-Newton root finding method [64] for the problem.

$$\mathbf{x} = \left(F_S, \lambda\right), \ \mathbf{f}\,(\mathbf{x}) = \left(f_H, f_M\right) = 0 \qquad (4.68)$$

where **x**: unknown vector and **f**: vector-valued function.

The procedure, formulated below for two-variable problems, is adopted in ILEM to obtain solutions for rigorous methods like SM and MP. Single-variable version of the same procedure is implemented for the simplified methods like BS, JS, LK, and CE variants.

***Step 1*:** Prescribe the error tolerance, ε_{tol}, and make initial guesses for F_S and λ. The quality of the initial guesses greatly affects the convergence of gradient-based methods, hence reasonable inputs are essential.

It is suitable to use the solution of FM to estimate an initial F_S value in the same order of magnitude as the final result. Observations throughout the study informally suggest that the experimental force equilibrium approach is reliable, even for odd slip surface geometries. For such surfaces, the conventional FM often finds unrealistic solutions. Therefore, Eq. (4.69) is suggested for the initial F_S value.

$$\left(F_S\right)_0 = \left(F_{S,H}\right)_F \qquad (4.69)$$

where $(F_S)_0$: initial F_S guess for Broyden's method and $(F_{S,H})_F$: force F_S based on experimental Fellenius' method (i.e. refer to Eq. (4.33) and Appendix B).

For λ coefficient, it is not possible to obtain an initial guess using the simplified methods. Suitably, Zhu et al. [72] proposed an empirical correlation based on average slip surface inclination. Note that the correlation, given in Eq. (4.70) is computed in a manner similar to the interslice force function of Corps of Engineers method, given in Eq (2.18).

$$\lambda_0 = 0.7 \cdot \frac{f(x_s) - f(x_t)}{x_s - x_t} \tag{4.70}$$

where λ_0: initial λ guess for Broyden's method.

Step 2**:** Evaluate the initial vector-valued function, $\mathbf{f}_0$, and the Jacobian matrix, $\mathbf{J}_0$, defined in Eq. (4.71), respectively. It is possible to evaluate the partial derivatives in $\mathbf{J}_0$ using finite difference method.

$$\mathbf{J}_0 = \begin{bmatrix} \dfrac{\partial f_H}{\partial F_S} & \dfrac{\partial f_H}{\partial \lambda} \\ \dfrac{\partial f_M}{\partial F_S} & \dfrac{\partial f_M}{\partial \lambda} \end{bmatrix} \tag{4.71}$$

Step 3**:** Update the unknown vector, $\mathbf{x}$, using Eq. (4.72) and increase the iteration number by one.

$$\mathbf{x}_{t+1} = \mathbf{x}_t - \mathbf{J}_t^{-1}\mathbf{f}_t \tag{4.72}$$

$$t = t + 1$$

where t: denotes the iteration number.

Step 4**:** Compute the vector-valued function, $\mathbf{f}_t$, and differential vectors, $\Delta\mathbf{x}_t$ and $\Delta\mathbf{f}_t$ using Eq. (4.73).

$$\Delta\mathbf{x}_t = \mathbf{x}_t - \mathbf{x}_{t-1},\ \Delta\mathbf{f}_t = \mathbf{f}_t - \mathbf{f}_{t-1} \tag{4.73}$$

Step 5**:** Compute absolute error related to Broyden's method, ε_b, using Eq. (4.74). Terminate if ε_b is smaller than the tolerance, ε_{tol}.

$$\varepsilon_b = \left\|\Delta\mathbf{x}\right\|_\infty \tag{4.74}$$

Step 6**:** Update the inverse Jacobian matrix using Eq. (4.75) and return to Step 3. The method adopts a rank-one update instead of computing the Jacobian matrix in every iteration. In addition, Broyden further refined the formulation with *Sherman-Morrison Formula* to update the inverse of the Jacobian matrix directly.

$$\mathbf{J}_t^{-1} = \mathbf{J}_{t-1}^{-1} + \frac{\Delta\mathbf{x}_t - \mathbf{J}_{t-1}^{-1}\Delta\mathbf{f}_t}{\Delta\mathbf{x}_t^{\mathbf{T}}\mathbf{J}_{t-1}^{-1}\Delta\mathbf{f}_t}\Delta\mathbf{x}_t^{\mathbf{T}}\mathbf{J}_{t-1}^{-1} \tag{4.75}$$

4.2. Numerical Experiments

In this section, the closed-form formulation of ILEM is validated and the computational the efficiency ILEM variants based on numerical integration methods are evaluated through extensive experimentation. Utilizing the critical slip surfaces located in Chapter 3, a benchmark set is constructed in Section 4.2.1. Then in Section 4.2.2, the closed-form version of ILEM, denoted as ILEM-CF, is implemented to find results based on common limit equilibrium assumptions. After validating the applicability of the proposed formulation, the results are further used as a basis of comparison for the subsequent sections. In Section 4.2.3, ILEM formulation is implemented with numerical integration methods, in search of improvements on computational efficiency. Based on these results, an efficient ILEM variant is compared with GLE formulation and proposed as an alternative limit equilibrium formulation in Section 4.2.4.

4.2.1. Benchmark Problems

The benchmark slope stability analysis problems adopted in this section are essentially the same as Chapter 3, except that a surface optimization routine is not incorporated in the experiments. Since the current objective is to evaluate the stability analysis modules, introducing a stochastic element (i.e. optimization algorithm) would unnecessarily influence the outcomes by instigating bias to the model. In order to avoid this issue, the slip surfaces are pre-defined for the analyses as illustrated in Figure 4.3. The surfaces are exactly the same as those obtained with SQS in Section 3.2. For each example, the axis of moment equilibrium, R, and spline transition points are indicated; and the detailed surface information is provided in Appendix A.

For each slip surface, the indicated rotational axis is the center of the best-fit arc determined through a regression analysis with the following criteria: (i) the arc must pass through the slip toe and scarp, (ii) the soil weight inside the arc must be equal to the weight of the sliding mass. The indicated rotational centers are only utilized for

FM and BS, which are conventionally not applicable to analyze general slip surfaces, yet similar approaches are adopted in the commercial analysis software. *However, it should be emphasized that the location of the rotational axis significantly affects the results in simplified moment equilibrium methods, hence such an approach is questionable for practical applications*. On the other hand, the results of rigorous LEMs are not sensitive to the position of the rotational axis; therefore, any reasonable point can be selected. For rigorous LEMs, the gravitational centers of the sliding masses are conveniently considered as the reference points for moment equilibrium.

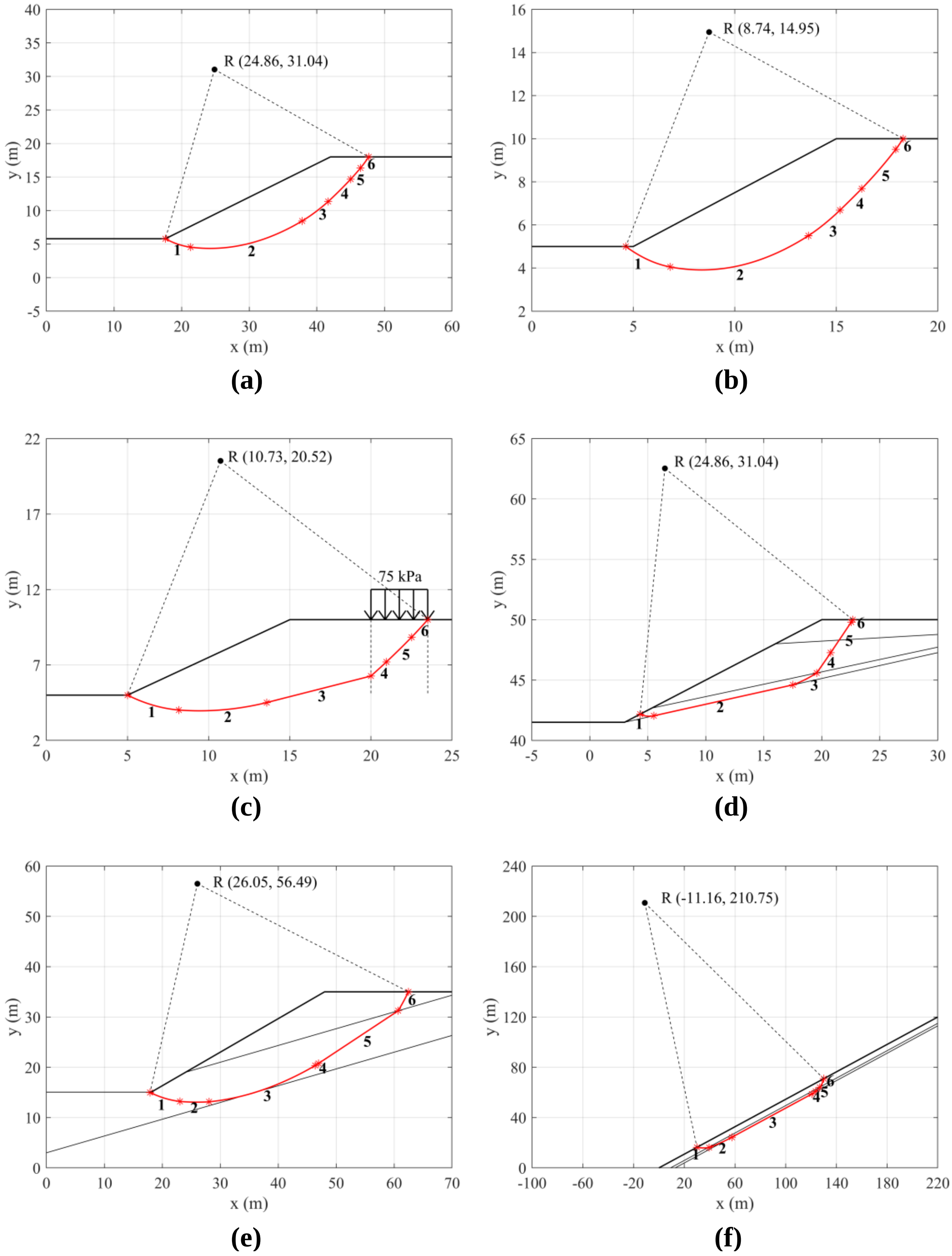

Figure 4.3: Slip surfaces and rotational centers
(a) *Example 1* **(b)** *Example 2* (*i*) **(c)** *Example 2* (*ii*)
(d) *Example 3* **(e)** *Example 4* **(f)** *Example 5* (*i*)

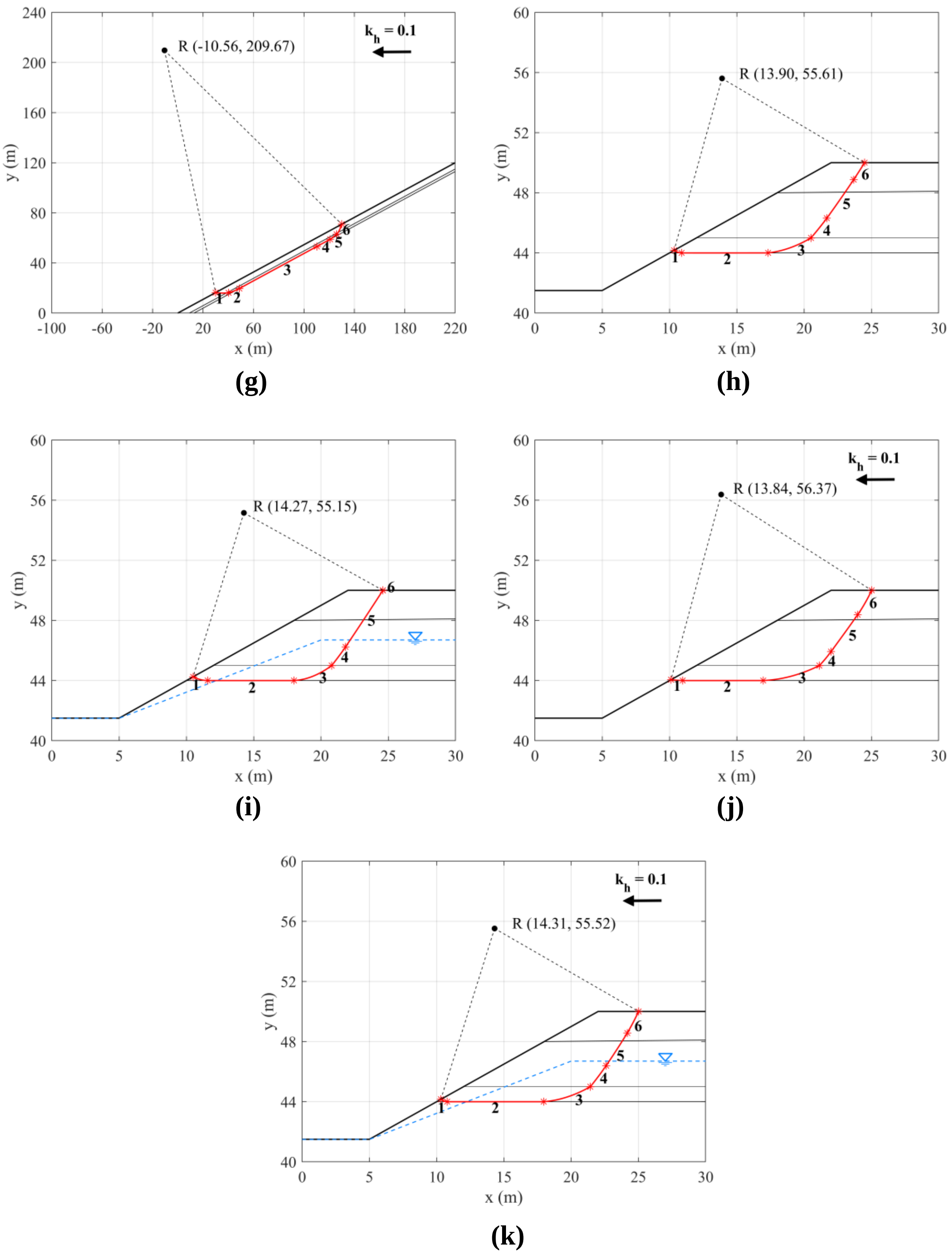

Figure 4.3 (cont'd): Slip surfaces and rotational centers
(g) *Example 5* (*ii*) **(h)** *Example 6* (*i*) **(i)** *Example 6* (*ii*)
(j) *Example 6* (*iii*) **(k)** *Example 6* (*iv*)

4.2.2. Closed-Form Solution Approach for Common LEMs

In this section, the benchmark problem set is utilized to validate the reliability of the proposed analysis framework. Furthermore, the closed-form equations and the resulting formulation ILEM-CF is verified as a precise unified method for common limit equilibrium assumptions. The experiments adopt ILEM-CF for FM, BS, JS, CE-*Case* (*i*) and SM approaches, and approximate the true F_S values for LK, CE-*Case* (*ii*) and MP using excessive discretization and numerical evaluation. Therefore, the results reported in this section are exact within the limits of the error tolerance, ε_{tol}, which is prescribed as 10^{-15} for Broyden's quasi-Newton technique. It should be noted that FM is utilized to find F_S values based on both, moment and horizontal force equilibrium. Lastly, MP is adopted with half-sine internal force function.

The results are reported in Table 4.2 for all limit equilibrium assumptions and benchmark problems. The table denotes ILEM-CF solutions and the approximated true values with the subscripts "*CF*" and "*AT*", respectively. It is noticeable that the results given for SM are in agreement with the ones previously reported with GLE in Table 3.21. In fact, the F_S values of ILEM-CF are slightly improved versions of the ones previously obtained using 70 slices. Since SM encloses the entire analytical derivation, the outcomes also validate the closed-form ILEM formulation for the simplified methods that can be reduced from SM.

The comparison between different approaches can also prove to be beneficial to verify the reliability of ILEM. For instance, the results of SM and MP, which only differ in the applied internal force functions, are strongly correlated. The average deviation in F_S is about 0.7%, suggesting that the rigorous formulation is not highly sensitive to the selection of the internal force function, as previously argued by Morgenstern and Price [3]. To evaluate the results of the simplified approaches, relative differences values are calculated with respect to SM and MP and denoted as RD_1 and RD_2, respectively. Based on these measures BS accurately estimates F_S with mean RD values below 1%. This is already an expected outcome for circular failure analyses. In this case, the procedure adopted to assign the center of rotation may have resulted in a practical way of achieving similar accuracy for general slip surfaces. However, the reliability of this approach requires careful assessment with complete analysis frameworks. Regarding the force equilibrium methods, JS always underestimates F_S as expected [2]. With the application of internal force function in LK and CE, the results approach to those of rigorous methods. However, *Case* (*ii*) assumption of CE fails to produce reliable results based on the mean *RD* values that exceed 4.5%.

It is interesting to note that the results of the conventional FM are reasonably close to those of SM and MP. However, the trials during the study point out that its application within a general slip surface optimization framework often yields unrealistic outcomes. On the other hand, the experimental FM is observed to be more consistent to produce F_S values, at least in the same order of magnitude as the other methods. Therefore, the experimental FM based on force equilibrium is proposed as a simple yet efficient method to provide initial guesses for the iterative analyses. With this embedment, divergence issues are seldom encountered and the capabilities of Broyden's method ensure sufficient accuracy within 3 to 5 iterations.

Table 4.2: ILEM solutions for common LEMs

Abbreviation:	**FM**	**FM**	**BS**	**JS**	**LK**	**CE**	**CE**	**SM**	**MP**
Description:	**Fellenius (i.e. moment)**	**Fellenius (i.e. force)**	**Bishop simplified**	**Janbu simplified**	**Lowe & Karafiath**	**Corps of Engineers Case (i)**	**Corps of Engineers Case (ii)**	**Spencer**	**Morgenstern-Price (i.e. half-sine)**
	$(F_S)_{CF}$	$(F_S)_{CF}$	$(F_S)_{CF}$	$(F_S)_{CF}$	$(F_S)_{AT}$	$(F_S)_{CF}$	$(F_S)_{AT}$	$(F_S)_{CF}$	$(F_S)_{AT}$
Example 1	1.8703	1.9836	1.9637	1.8314	2.0037	2.0348	2.1033	1.9770	1.9657
Example 2 (*i*)	1.2490	1.3179	1.3024	1.2115	1.3399	1.3843	1.4627	1.3218	1.3139
Example 2 (*ii*)	0.9503	1.0926	0.9863	0.8960	1.0309	0.9911	0.9994	0.9975	0.9777
Example 3	1.0794	1.0982	1.0886	1.0851	1.1039	1.1024	1.1028	1.0877	1.0866
Example 4	0.3983	0.3941	0.4053	0.3951	0.4088	0.4284	0.4612	0.4110	0.4078
Example 5 (*i*)	0.9785	0.9829	0.9992	0.9888	0.9794	1.0157	1.0157	1.0095	0.9978
Example 5 (*ii*)	0.8085	0.8077	0.8235	0.8139	0.8065	0.8382	0.8382	0.8396	0.8248
Example 6 (*i*)	1.3080	1.4280	1.3261	1.3029	1.4172	1.3892	1.4136	1.3301	1.3289
Example 6 (*ii*)	1.1823	1.3120	1.1932	1.1823	1.3056	1.2748	1.3002	1.1967	1.1954
Example 6 (*iii*)	1.0303	1.0315	1.0473	1.0118	1.0389	1.0405	1.0542	1.0418	1.0421
Example 6 (*iv*)	0.9198	0.9131	0.9354	0.9078	0.9286	0.9371	0.9507	0.9315	0.9299
***Mean RD_1* (%)**	**2.86**	**3.78**	**0.84**	**3.98**	**2.84**	**2.40**	**4.53**	–	**0.67**
***Mean RD_2* (%)**	**2.22**	**3.73**	**0.40**	**3.35**	**2.87**	**2.93**	**5.19**	**0.68**	–

$(F_S)_{CF}$: true value of F_S evaluated with closed-form solution, $(F_S)_{AT}$: approximated true value of F_S with numerical integration,
RD_1 and RD_2: relative difference compared to Morgenstern-Price method with constant and half-sine internal force function, respectively.

4.2.3. The Efficiency of Numerical Integration Methods

Aiming to develop a computationally efficient ILEM variant, the benchmark examples are further analyzed with approximation methods, instead of using the closed-form formulation. Accordingly, common numerical integration techniques like *Riemann sum*, *trapezoidal rule*, *Simpson's 1/3 rule*, and *Gauss quadrature* are incorporated into the formulation of ILEM. A summary of these methods are given in Table 4.3, where the number of quadrature nodes "n_Q", their positions, and weights are indicated for an arbitrary function, $f(x)$, within the normalized interval of [-1, 1]. Based on these definitions, the below-given equation can be used to approximate the value of a definite integral.

$$\int_{-1}^{1} f(x)dx \approx \frac{1}{2} \cdot \sum_{i=1}^{n_Q} f(x_i) \cdot w_i \tag{4.76}$$

Table 4.3: Summary of numerical integration methods

Method	n_Q	Nodes on [-1, +1]	Weights
Midpoint Riemann sum	1	$x = 0$	$w = 2$
Trapezoidal rule	2	$x_1 = -1,\ x_2 = +1$	$w_1 = 1,\ w_2 = 1$
Simpson's 1/3 rule	3	$x_1 = -1,\ x_2 = 0,\ x_3 = +1$	$w_1 = 1/3,\ w_2 = 4/3,\ w_3 = 1/3$
Gauss quadrature	2	$x_1 = -1/\sqrt{3},\ x_2 = +1/\sqrt{3}$	$w_1 = 1,\ w_2 = 1$
Gauss quadrature	3	$x_1 = -\sqrt{3/5},\ x_2 = 0,\ x_3 = +\sqrt{3/5}$	$w_1 = 5/9,\ w_2 = 8/9,\ w_3 = 5/9$

where n_Q: number of quadrature nodes within each interval.

The efficiency of GLE formulation is also evaluated in comparison to these methods. In order to avoid any bias due to possible differences in the computational implementation of these formulations, ILEM analysis procedure is interpreted to yield results for GLE. When the slip the surface is discretized into linear segments, adoption of midpoint Riemann sum reduces ILEM formulation to GLE, based on the derivation given in Section 4.1.2.

For the analyses, SM is adopted. Approximation intervals are determined by discretizing the slip surfaces into segments with the procedures given in Section 4.1.4.

Then, they are further refined into equally spaced sub-intervals to increase the precision. The number of sub-intervals, multiplied by n_Q gives the number of governing function evaluations for F_S, denoted with *NFE*. Note that the minimum *NFE* required for F_S evaluation varies for different integration methods, and the calculations ignore the iterations within Broyden's root-finding procedure.

The results of the analyses are illustrated with the convergence graphs given in Figure 4.4. In these graphs, x-axes indicate *NFE* and y-axes represent the absolute error of F_S values (i.e. not relative, the values are absolute deviations from true F_S values) with respect to those obtained with the closed-form equations. The convergence graphs demonstrate that the precision of GLE is comparably lower than other methods, except for the trapezoidal rule, which is computationally more demanding. Simpson's 1/3 rule and 2-node Gauss quadrature are relatively more efficient. However, these methods may require a degree of refinement for "rotational" slip surfaces, as illustrated in Figures 4.4a and 4.4b. In general, surfaces with planar segments are easier to analyze as the order and complexity of the integrand functions reduce for linear functions. On the other hand, 3-node Gauss quadrature approximation is invariably precise for SM without further surface refinement.

It is notable in some cases that the approximation of the method does not improve until a certain point. This is more visible for the convergence graphs given in Figures 4.4f and 4.4g, which are associated with the infinite slope problem, *Example 5*. The slip surfaces in these problems include wide planar segments. Considering a linear surface, the integrands in I_1 through I_4 (i.e. refer to Eqs. (4.49)–(4.51) and (4.60)) reduce to 2nd order polynomials and the integrand in I_5 in Eq. (4.61) reduces to 3rd order, all of which are approximated exactly using 2 and 3-node Gauss quadrature rules. Therefore, the linear segments are refined unnecessarily in these experiments. Regardless, 3-node Gauss quadrature approximation yields impartial results with those of ILEM-CF without any refinement, and thus selected as a computationally efficient addition to the formulation of ILEM.

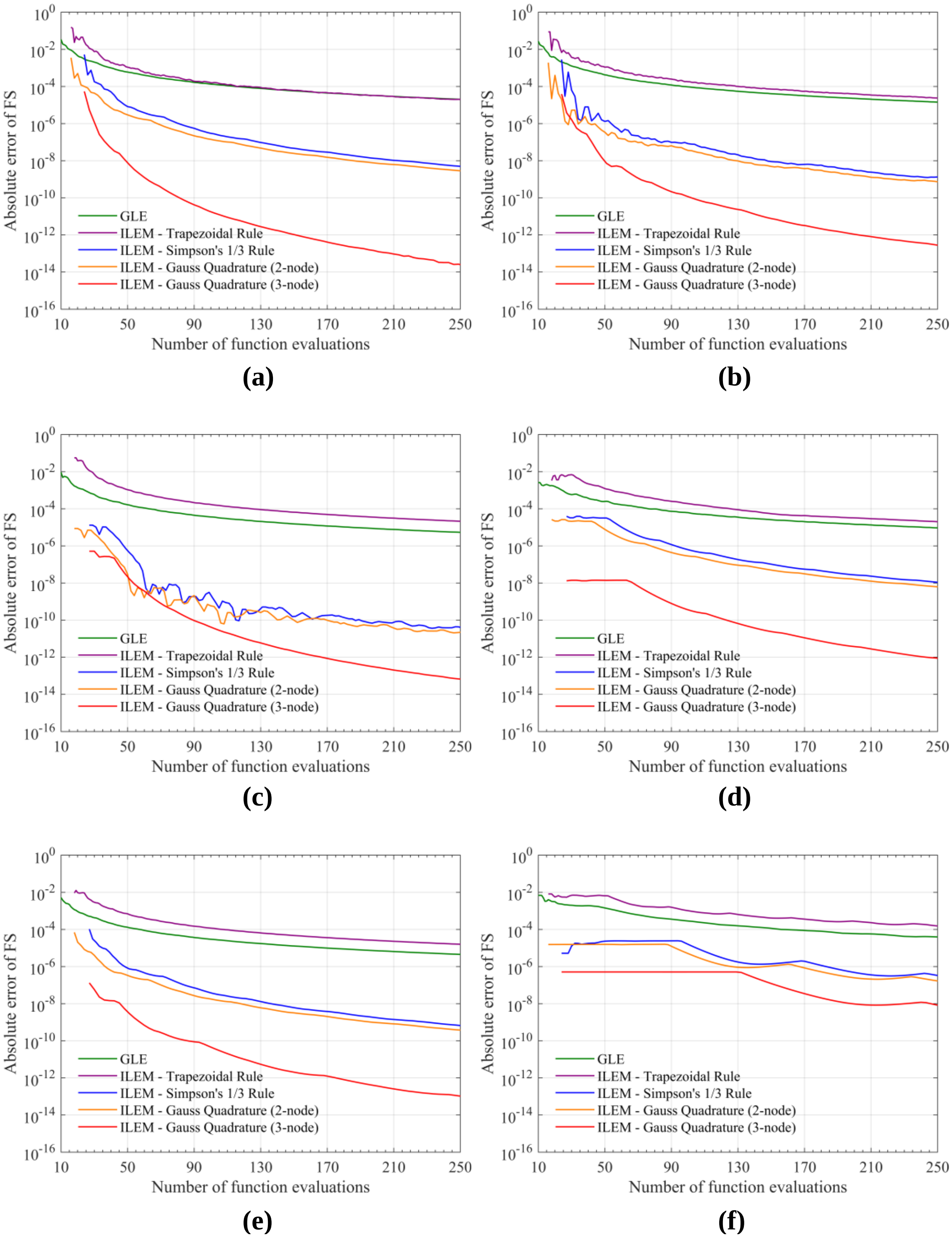

Figure 4.4: Convergence of numerical integration methods
(a) *Example 1* **(b)** *Example 2* (*i*) **(c)** *Example 2* (*ii*)
(d) *Example 3* **(e)** *Example 4* **(f)** *Example 5* (*i*)

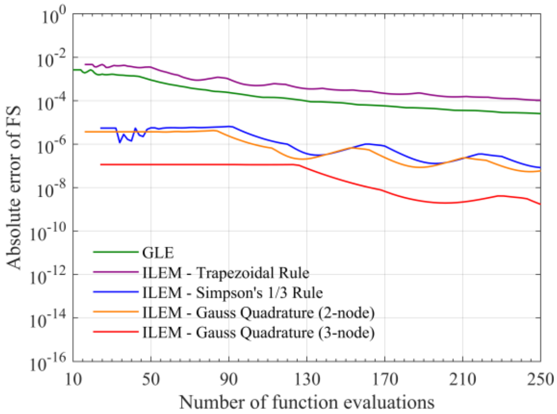

(g)

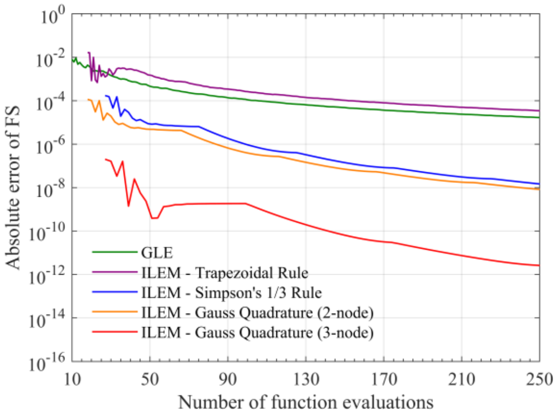

(h)

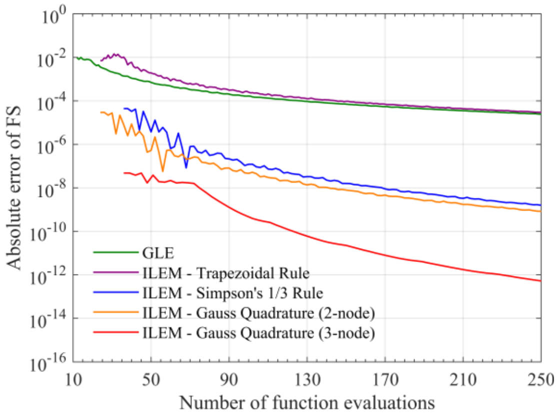

(i)

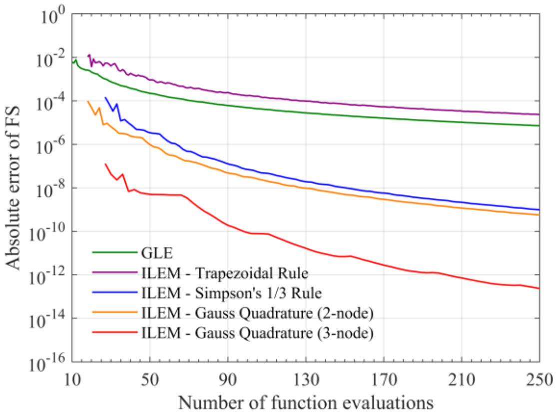

(j)

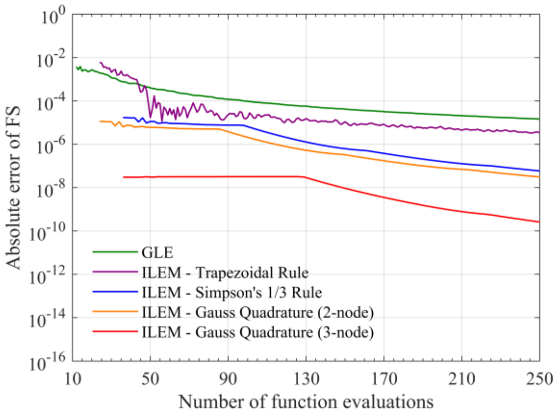

(k)

Figure 4.4 (cont'd): Convergence of numerical integration methods **(g)** *Example 5* (*ii*) **(h)** *Example 6* (*i*) **(i)** *Example 6* (*ii*) **(j)** *Example 6* (*iii*) **(k)** *Example 6* (*iv*)

4.2.4. Comparison of ILEM with GLE

The experiments for SM in the previous section promote a computationally efficient ILEM variant based on 3-node Gauss quadrature approximation, denoted as ILEM-GQ3 from now on. In this section, the reliability of this configuration is validated for other limit equilibrium assumptions through a comparison with GLE and true F_S values reported in Table 4.2. Using ILEM-GQ3, the slip surfaces are analyzed without any refinement, hence the number of function evaluations, *NFE*, is the minimum required for each example. Accordingly, the numbers of slices used for GLE are adjusted to equivalent values for fair comparison.

Considering the above configurations, an extract of the results obtained with SM are given in Table 4.4. For each benchmark problem, the outcomes of GLE and ILEM-GQ3 are summarized based on the approximated F_S and λ values; and reported together with the values obtained using ILEM-CF. Furthermore, absolute errors of approximated F_S values are also given for both formulations. The results further illustrate the capability of ILEM-GQ3, which reports precise values for F_S in five significant figures. Although the results of GLE stay within practically acceptable error margins, such reliability is not possible at the same computational cost.

Table 4.4: Comparison of ILEM and GLE – Spencer's method

		GLE			ILEM-GQ3			ILEM	
	NFE	F_S	λ	ε_{F_S}	F_S	λ	ε_{F_S}	$(F_S)_{CF}$	λ
Example 1	24	1.9799	0.3026	3.E-03	1.9769	0.3023	**5.E-05**	1.9770	0.3025
Example 2 (*i*)	24	1.3239	0.2506	2.E-03	1.3218	0.2495	**4.E-05**	1.3218	0.2496
Example 2 (*ii*)	27	0.9983	0.2875	7.E-04	0.9975	0.2874	**5.E-07**	0.9975	0.2874
Example 3	27	1.0884	0.0753	7.E-04	1.0877	0.0702	**1.E-08**	1.0877	0.0702
Example 4	27	0.4115	0.2441	5.E-04	0.4110	0.2428	**1.E-07**	0.4110	0.2428
Example 5 (*i*)	24	1.0118	0.4541	2.E-03	1.0095	0.4527	**7.E-06**	1.0095	0.4527
Example 5 (*ii*)	24	0.8412	0.5688	2.E-03	0.8396	0.5676	**1.E-06**	0.8396	0.5676
Example 6 (*i*)	27	1.3321	0.1440	2.E-03	1.3300	0.1377	**2.E-07**	1.3301	0.1377
Example 6 (*ii*)	36	1.1981	0.0726	1.E-03	1.1967	0.0692	**5.E-08**	1.1967	0.0691
Example 6 (*iii*)	27	1.0428	0.4182	1.E-03	1.0418	0.4136	**1.E-07**	1.0418	0.4136
Example 6 (*iv*)	36	0.9322	0.3336	8.E-04	0.9315	0.3317	**3.E-08**	0.9315	0.3317

where *GQ3*: 3-node Gauss quadrature, *CF*: closed-form solution, *NFE*: number of function evaluations.

Considering the simplified methods such as FM, BS, JS, LK and CE, the outcomes, given in Tables 4.5–4.11, are similar to those of SM, which further validates the enhanced efficiency of ILEM-GQ3 over GLE. Except for a few instances, the proposed method reports precise F_S values. On the other hand, the experiments with MP raise some questions and inspire possible improvements. As mentioned previously, MP is adopted with half-sine internal force function, which significantly affects the complexity of the governing equations. As a result, the precision of both GLE and ILEM-GQ3 are comparably reduced, as illustrated in Table 4.12. GLE formulation is prone to significant error with relatively lower numbers of slices, especially in *Examples 1* and *2* (*i*). ILEM-GQ3 can find more acceptable values for F_S; however, λ coefficients, and consequently the estimated force distributions still deviate from the approximated true cases. Addressing this issue, either a higher-order approximation method or a surface refinement procedure may be adopted for MP. Considering the latter alternative, the problems are analyzed using 48 function evaluations. As a result, the solutions of both methods reach more satisfactory levels. Although ILEM-GQ3 is visibly the better alternative, further improvements may be achieved by developing a more efficient surface refinement procedure in the future studies.

Table 4.5: Comparison of ILEM and GLE – conventional Fellenius' method

		GLE*		**ILEM-GQ3**		**ILEM**
	NFE	F_S	ε_{Fs}	F_S	ε_{Fs}	$(F_S)_{CF}$
Example 1	24	1.8722	2.E-03	1.8703	**1.E-05**	1.8703
Example 2 (*i*)	24	1.2497	7.E-04	1.2488	**1.E-04**	1.2490
Example 2 (*ii*)	27	0.9507	4.E-04	0.9503	**7.E-07**	0.9503
Example 3	27	1.0801	7.E-04	1.0794	**3.E-06**	1.0794
Example 4	27	0.3985	2.E-04	0.3983	**5.E-07**	0.3983
Example 5 (*i*)	24	0.9813	3.E-03	0.9785	**5.E-07**	0.9785
Example 5 (*ii*)	24	0.8104	2.E-03	0.8085	**1.E-07**	0.8085
Example 6 (*i*)	27	1.3090	1.E-03	1.3080	**3.E-06**	1.3080
Example 6 (*ii*)	36	1.1839	2.E-03	1.1823	**3.E-06**	1.1823
Example 6 (*iii*)	27	1.0309	6.E-04	1.0303	**1.E-06**	1.0303
Example 6 (*iv*)	36	0.9207	9.E-04	0.9198	**8.E-06**	0.9198

*GLE normally does not accommodate Fellenius' method, here it is regarded as a solution approach.

Table 4.6: Comparison of ILEM and GLE – experimental Fellenius' method

		GLE*		ILEM-GQ3		ILEM
	NFE	F_S	ε_{Fs}	F_S	ε_{Fs}	$(F_S)_{CF}$
Example 1	24	1.9867	3.E-03	1.9836	**1.E-06**	1.9836
Example 2 (*i*)	24	1.3194	2.E-03	1.3179	**3.E-06**	1.3179
Example 2 (*ii*)	27	1.0934	7.E-04	1.0926	**1.E-06**	1.0926
Example 3	27	1.0989	6.E-04	1.0982	**4.E-06**	1.0982
Example 4	27	0.3945	3.E-04	0.3941	**1.E-06**	0.3941
Example 5 (*i*)	24	0.9854	3.E-03	0.9829	**9.E-06**	0.9829
Example 5 (*ii*)	24	0.8096	2.E-03	0.8077	**2.E-06**	0.8077
Example 6 (*i*)	27	1.4291	1.E-03	1.4280	**7.E-06**	1.4280
Example 6 (*ii*)	36	1.3126	6.E-04	1.3120	**4.E-06**	1.3120
Example 6 (*iii*)	27	1.0324	9.E-04	1.0315	**4.E-06**	1.0315
Example 6 (*iv*)	36	0.9140	1.E-03	0.9131	**2.E-05**	0.9131

*GLE normally does not accommodate Fellenius' method, here it is regarded as a solution approach.

Table 4.7: Comparison of ILEM and GLE – Bishop's simplified method

		GLE		ILEM-GQ3		ILEM-CF
	NFE	F_S	ε_{Fs}	F_S	ε_{Fs}	$(F_S)_{CF}$
Example 1	24	1.9662	2.E-03	1.9637	**2.E-05**	1.9637
Example 2 (*i*)	24	1.3038	1.E-03	1.3024	**1.E-05**	1.3024
Example 2 (*ii*)	27	0.9867	4.E-04	0.9863	**2.E-07**	0.9863
Example 3	27	1.0894	8.E-04	1.0886	**8.E-08**	1.0886
Example 4	27	0.4057	4.E-04	0.4053	**5.E-08**	0.4053
Example 5 (*i*)	24	1.0003	1.E-03	0.9992	**6.E-06**	0.9992
Example 5 (*ii*)	24	0.8247	1.E-03	0.8235	**1.E-06**	0.8235
Example 6 (*i*)	27	1.3274	1.E-03	1.3261	**1.E-07**	1.3261
Example 6 (*ii*)	36	1.1945	1.E-03	1.1932	**2.E-08**	1.1932
Example 6 (*iii*)	27	1.0482	9.E-04	1.0473	**1.E-07**	1.0473
Example 6 (*iv*)	36	0.9364	1.E-03	0.9354	**2.E-09**	0.9354

Table 4.8: Comparison of ILEM and GLE – Janbu's simplified method

		GLE		ILEM-GQ3		ILEM-CF
	NFE	F_S	ε_{Fs}	F_S	ε_{Fs}	$(F_S)_{CF}$
Example 1	24	1.8334	2.E-03	1.8314	**2.E-06**	1.8314
Example 2 (*i*)	24	1.2123	9.E-04	1.2115	**6.E-07**	1.2115
Example 2 (*ii*)	27	0.8963	3.E-04	0.8960	**4.E-08**	0.8960
Example 3	27	1.0856	5.E-04	1.0851	**6.E-08**	1.0851
Example 4	27	0.3953	3.E-04	0.3951	**2.E-08**	0.3951
Example 5 (*i*)	24	0.9898	9.E-04	0.9888	**6.E-06**	0.9888
Example 5 (*ii*)	24	0.8150	1.E-03	0.8139	**1.E-06**	0.8139
Example 6 (*i*)	27	1.3034	6.E-04	1.3029	**4.E-07**	1.3029
Example 6 (*ii*)	36	1.1830	7.E-04	1.1823	**2.E-07**	1.1823
Example 6 (*iii*)	27	1.0120	3.E-04	1.0118	**5.E-08**	1.0118
Example 6 (*iv*)	36	0.9085	7.E-04	0.9078	**1.E-05**	0.9078

Table 4.9: Comparison of ILEM and GLE – Lowe and Karafiath's method

		GLE		ILEM-GQ3		ILEM
	NFE	F_S	ε_{Fs}	F_S	ε_{Fs}	$(F_S)_{AT}$
Example 1	24	2.0071	3.E-03	2.0035	**2.E-04**	2.0037
Example 2 (*i*)	24	1.3420	2.E-03	1.3398	**1.E-04**	1.3399
Example 2 (*ii*)	27	1.0318	9.E-04	1.0309	**4.E-07**	1.0309
Example 3	27	1.1050	1.E-03	1.1039	**1.E-08**	1.1039
Example 4	27	0.4094	6.E-04	0.4088	**2.E-06**	0.4088
Example 5 (*i*)	24	0.9829	3.E-03	0.9794	**1.E-06**	0.9794
Example 5 (*ii*)	24	0.8086	2.E-03	0.8065	**2.E-07**	0.8065
Example 6 (*i*)	27	1.4185	1.E-03	1.4172	**1.E-06**	1.4172
Example 6 (*ii*)	36	1.3064	8.E-04	1.3056	**5.E-07**	1.3056
Example 6 (*iii*)	27	1.0401	1.E-03	1.0389	**1.E-06**	1.0389
Example 6 (*iv*)	36	0.9299	1.E-03	0.9286	**7.E-10**	0.9286

Table 4.10: Comparison of ILEM and GLE – Corps of Engineers method Case (i)

		GLE		ILEM-GQ3		ILEM
	NFE	F_S	ε_{Fs}	F_S	ε_{Fs}	$(F_S)_{CF}$
Example 1	24	2.0381	3.E-03	2.0349	**7.E-05**	2.0348
Example 2 (*i*)	24	1.3855	1.E-03	1.3843	**3.E-05**	1.3843
Example 2 (*ii*)	27	0.9916	5.E-04	0.9911	**6.E-07**	0.9911
Example 3	27	1.1028	4.E-04	1.1024	**1.E-06**	1.1024
Example 4	27	0.4288	4.E-04	0.4284	**1.E-06**	0.4284
Example 5 (*i*)	24	1.0177	2.E-03	1.0157	**7.E-06**	1.0157
Example 5 (*ii*)	24	0.8397	1.E-03	0.8382	**1.E-06**	0.8382
Example 6 (*i*)	27	1.3897	5.E-04	1.3892	**5.E-07**	1.3892
Example 6 (*ii*)	36	1.2754	6.E-04	1.2748	**5.E-07**	1.2748
Example 6 (*iii*)	27	1.0410	4.E-04	1.0405	**3.E-07**	1.0405
Example 6 (*iv*)	36	0.9377	5.E-04	0.9371	**9.E-08**	0.9371

Table 4.11: Comparison of ILEM and GLE – Corps of Engineers method Case (ii)

		GLE		ILEM-GQ3		ILEM
	NFE	F_S	ε_{Fs}	F_S	ε_{Fs}	$(F_S)_{AT}$
Example 1	24	2.1064	3.E-03	2.1034	**1.E-04**	2.1033
Example 2 (*i*)	24	1.4642	1.E-03	1.4628	**6.E-05**	1.4627
Example 2 (*ii*)	27	1.0001	6.E-04	0.9994	**5.E-06**	0.9994
Example 3	27	1.1032	4.E-04	1.1028	**2.E-06**	1.1028
Example 4	27	0.4619	6.E-04	0.4612	**9.E-06**	0.4612
Example 5 (*i*)	24	1.0177	2.E-03	1.0157	**7.E-06**	1.0157
Example 5 (*ii*)	24	0.8397	1.E-03	0.8382	**1.E-06**	0.8382
Example 6 (*i*)	27	1.4140	3.E-04	1.4136	**9.E-07**	1.4136
Example 6 (*ii*)	36	1.3010	8.E-04	1.3002	**9.E-07**	1.3002
Example 6 (*iii*)	27	1.0546	3.E-04	1.0542	**5.E-07**	1.0542
Example 6 (*iv*)	36	0.9511	4.E-04	0.9507	**2.E-07**	0.9507

Table 4.12: Comparison of ILEM and GLE – Morgenstern-Price method

$f_i(x)=\sin\left[\pi\left(\frac{x-x_t}{x_s-x_t}\right)\right]$		GLE			ILEM-GQ3			ILEM	
	NFE	F_S	λ	ε_{Fs}	F_S	λ	ε_{Fs}	$(F_S)_{AT}$	$(\lambda)_{AT}$
Example 1	24	1.9760	0.4031	1.E-02	1.9648	0.4180	**9.E-04**	1.9657	0.3722
Example 2 (*i*)	24	1.3215	0.3258	8.E-03	1.3098	0.3286	**4.E-03**	1.3139	0.3053
Example 2 (*ii*)	27	0.9818	0.3843	4.E-03	0.9785	0.3899	**8.E-04**	0.9777	0.3922
Example 3	27	1.0880	0.0886	1.E-03	1.0871	0.0751	**4.E-04**	1.0866	0.0675
Example 4	27	0.4094	0.3013	2.E-03	0.4077	0.2629	**1.E-04**	0.4078	0.2540
Example 5 (*i*)	24	1.0002	0.6331	2.E-03	0.9971	0.5930	**7.E-04**	0.9978	0.5823
Example 5 (*ii*)	24	0.8264	0.8665	2.E-03	0.8239	0.8146	**9.E-04**	0.8248	0.7936
Example 6 (*i*)	27	1.3344	0.1690	5.E-03	1.3330	0.1731	**4.E-03**	1.3289	0.1468
Example 6 (*ii*)	36	1.1979	0.0809	3.E-03	1.1969	0.0797	**2.E-03**	1.1954	0.0712
Example 6 (*iii*)	27	1.0468	0.4873	5.E-03	1.0464	0.5005	**4.E-03**	1.0421	0.4219
Example 6 (*iv*)	36	0.9322	0.3641	**2.E-03**	0.9321	0.3719	**2.E-03**	0.9299	0.3265
Example 1	48	1.9695	0.3839	4.E-03	1.9655	0.3776	**1.E-04**	1.9657	0.3722
Example 2 (*i*)	48	1.3168	0.3156	3.E-03	1.3136	0.3073	**3.E-04**	1.3139	0.3053
Example 2 (*ii*)	48	0.9798	0.3877	2.E-03	0.9780	0.3904	**3.E-04**	0.9777	0.3922
Example 3	48	1.0870	0.0736	4.E-04	1.0867	0.0688	**9.E-05**	1.0866	0.0675
Example 4	48	0.4084	0.2747	6.E-04	0.4078	0.2648	**3.E-05**	0.4078	0.2540
Example 5 (*i*)	48	0.9994	0.6549	2.E-03	0.9974	0.5903	**4.E-04**	0.9978	0.5823
Example 5 (*ii*)	48	0.8257	0.8564	9.E-04	0.8244	0.8071	**5.E-04**	0.8248	0.7936
Example 6 (*i*)	48	1.3311	0.1539	2.E-03	1.3297	0.1488	**8.E-04**	1.3289	0.1468
Example 6 (*ii*)	48	1.1970	0.0773	2.E-03	1.1957	0.0723	**3.E-04**	1.1954	0.0712
Example 6 (*iii*)	48	1.0456	0.4729	4.E-03	1.0425	0.4273	**4.E-04**	1.0421	0.4219
Example 6 (*iv*)	48	0.9314	0.3523	2.E-03	0.9305	0.3386	**7.E-04**	0.9299	0.3265

4.3. Discussion of Results

The experiments in this chapter serve disparate objectives, yet support each other to validate the collective performance of the proposed unified limit equilibrium method, ILEM. The first part of the experiments mostly serves as a verification of the formulation and derivation of the closed-form governing equations within. The results based on SM indicate that ILEM-CF yields similar, more specifically slight improved F_S values compared to those obtained using GLE. Based on these outcomes, the proposed formulation can eliminate free-body discretization and the corresponding errors of approximation completely. The error margin of this variant is equal to the prescribed tolerance value, which is an enhancement on reliability over other formulations in the literature. Furthermore, the results validate ILEM as a unified formulation for common limit equilibrium assumptions.

Despite these positive features, closed-form equations are considerably lengthy and tedious to evaluate. Therefore, their application within a complete analysis framework may translate to be computationally upscale. Addressing this issue, an efficient ILEM variant is developed based on 3-node Gauss quadrature method, denoted as ILEM-GQ3. Compared to GLE, ILEM-GQ3 exhibits significant improvement on result precision, yielding reliable approximations without free-body discretization or surface refinement for most LEMs. Using SM, FM, BS, JS, LK, and CE, single evaluations over entire surface intervals can yield exact solutions for 5 significant figures, except for rare occurrences. On the other hand, GLE is prone to considerable error without extensive slicing, especially when a relatively complex internal force function is incorporated. This issue is clearly visible for MP, which is applied with half-sine function in the experiments. Although affected by this implementation, ILEM-GQ3 estimates relatively better and practically acceptable solutions. Furthermore, surface refinement can improve the results at a reasonable computational demand. With these enhancements and unique characteristics, ILEM is proposed as a refined alternative to the available unified limit equilibrium formulations.

CHAPTER 5

SUMMARY AND CONCLUDING REMARKS

Engineering problem solving often exploits analytical and numerical methods within extended models of mechanics. Consequently, developing reliable solution approaches is only possible with a clear understanding of the applied mathematical concepts. With this on mind, the present study relies on the assessment of available limit equilibrium formulations and incorporated analysis procedures, in order to develop enhanced alternatives. In light of these assessments, a collective of novel procedures is proposed within the unified formulation of Integrated Limit Equilibrium Method (ILEM), which illustrates that basic mathematical techniques can be manipulated to effectively solve slope stability analysis problems.

ILEM incorporates two distinct methods to generate and analyze general slip surfaces. For surface generation, a modified spline interpolation procedure is developed through considerations of kinematical admissibility and surface flexibility. The procedure, named Scaled Quadratic Spline method (SQS), utilizes piecewise continuous quadratic order functions to represent the slip surfaces and includes a unique scaling operation to stimulate linear segments and abrupt transitions. With these implementations, SQS provides the flexibility to represent composite failure surfaces accurately without requiring excessive numbers of geometric parameters, which is an improvement over the available methods. The performance of SQS is validated through comparative benchmark testing and the method is proposed as an enhanced surface generation method with significant improvements on computational efficiency and result accuracy with respect to other approaches.

The second component of ILEM is the refined stability analysis module. Using quadratic order functions for surface representation, it was possible to develop a unified formulation of common LEMs based on differential equations. The formulation is extended to derive closed-form governing equations, which can be adapted to evaluate precise F_S values for many of the common LEMs. Despite bearing the characteristics of procedures of slices, ILEM treats slip surfaces as single free-bodies, evaluating the F_S with single-step computations over whole intervals. As a result, ILEM eliminates free-body discretization and the related approximation errors of conventional LEMs completely. Furthermore, the formulation allows the implementation of high-order numerical approximation techniques, which can yield precise approximations with marginal numbers of function evaluations. The experiments demonstrate that 3-node Gauss quadrature approximation is a suitable approach, producing considerable improvement on computational efficiency over slice approximation. Based on these findings, ILEM is proposed as an improved alternative to the available slope stability analysis procedures.

In order to realize its full potential, the future studies should focus on several aspects to further develop ILEM. First, an extensive study is required to incorporate or develop an improved surface optimization routine. The convergence rate of SQS is promising and the resulting optimization problems are relatively low-dimensional. Therefore, a hybrid stochastic-deterministic optimization method may be a suitable option to improve the efficiency. With this enhancement, ILEM may facilitate the applicability of the computationally demanding probabilistic analysis models. Similarly, an extension of ILEM to three-dimensional analysis problems could make significant contributions as these problems are considerably more difficult and substantially demanding for practical applications.

REFERENCES

[1] Abramson LW, Lee TS, Sharma S, Boyce GM. *Slope Stability and Stabilization Methods*. New York: Wiley; 2002.

[2] Duncan JM, Wright SG, Brandon TL. *Soil Strength and Slope Stability*. Hoboken, NJ: Wiley; 2014.

[3] Morgenstern NR, Price VE. The analysis of the stability of general slip surfaces. *Géotechnique* 1968;**15**:79–93. doi:10.1680/geot.1965.15.1.79

[4] Taylor DW. *Fundamentals of Soil Mechanics*. New York: Wiley; 1948.

[5] Taylor DW. Stability of Earth Slopes. *Journal of Boston Society of Civil Engineers* 1937;**24**:197–246.

[6] Frohlich OK. The factor of safety with respect to sliding of amass of soil along the arc of a logarithmic spiral. In: *Proceedings of the Third International Conference on Soil Mechanics and Foundation Engineering, 1953, Switzerland*. Zurich: Organizing Committee; 1953:230–3.

[7] Fellenius W. *Staten Jarnjvagars Geoteknniska Commission*. Stockholm: 1922.

[8] Petterson KE. The early history of circular sliding surfaces. *Géotechnique* 1955;**5**:275–96. doi:10.1680/geot.1955.5.4.275

[9] Fellenius W. *Erdstatische Berechnungen mit Reibung and Kohaesion*. Berlin: Ernst & Sohn; 1927.

[10] Bishop AW. The use of slip circle in the stability analysis of earth slopes. *Géotechnique* 1955;**5**:7–17. doi:10.1680/geot.1955.5.1.7

[11] Janbu N. Application of composite slip surface for stability analysis. In: *Proceedings of the European Conference on Stability of Earth Slopes, 1954, Sweden*. Stockholm: 1954;**3**:43–9.

[12] Lowe J, Karafiath L. Stability of earth dams upon drawdown. In: *Proceedings of the First PanAmerican Conference on Soil Mechanics and Foundation Engineering, 1960, Mexico City*. 1960;**2**:537-52.

[13] U.S. Army Corps of Engineers. *Engineering and Design: Stability of Earth and Rock–Fill Dams, Engineer Manual EM 1110–2–1902*. Washington, DC: Department of the Army, Office of the Chief of Engineers; 1970.

[14] Spencer E. A method of analysis of the stability of embankments assuming parallel inter-slice forces. *Géotechnique* 1967;**17**:11–26. doi:10.1680/geot.1967.17.1.11

[15] Sarma SK. Stability analysis of embankments and slopes. *Géotechnique* 1973;**23**:423–33. doi:10.1680/geot.1973.23.3.423

[16] Fredlund DG, Krahn J, Pufahl DE. The relationship between limit equilibrium slope stability methods. In: *Proceedings of the 10th International Conference on Soil Mechanics and Foundation Engineering, 1981, Stockholm*. Rotterdam: A.A. Balkerna; 1981:409-16.

[17] Goh ATC. Search for critical slip circle using genetic algorithms. *Civil Engineering and Environmental Systems* 2000;**17**:181–211. doi:10.1080/02630250008970282

[18] Mccombie P, Wilkinson P. The use of the simple genetic algorithm in finding the critical factor of safety in slope stability analysis. *Computers and Geotechnics* 2002;**29**:699–714. doi:10.1016/s0266-352x(02)00027-7

[19] Das SK. Slope stability analysis using genetic algorithm. *The Electronic Journal of Geotechnical Engineering*;2005;**10**A.

[20] Zolfaghari AR, Heath AC, McCombie PF. Simple genetic algorithm search for critical non-circular failure surface in slope stability analysis. *Computers and Geotechnics* 2005;**32**:139–52. doi:10.1016/j.compgeo.2005.02.001

[21] Sun J, Li J, Liu Q. Search for critical slip surface in slope stability analysis by spline-based GA method. *Journal of Geotechnical and Geoenvironmental Engineering* 2008;**134**:252–6. doi:10.1061/(ASCE)1090-0241(2008)134:2(252)

[22] Sengupta A, Upadhyay A. Locating the critical failure surface in a slope stability analysis by genetic algorithm. *Applied Soft Computing* 2009;**9**:387–92. doi:10.1016/j.asoc.2008.04.015

[23] Li YC, Chen YM, Zhan TLT, Ling DS, Cleall PJ. An efficient approach for locating the critical slip surface in slope stability analyses using a real-coded genetic algorithm. *Canadian Geotechnical Journal* 2010;**47**:806–20. doi:10.1139/T09-124

[24] Zhu J, Chen C. Search for circular and noncircular critical slip surfaces in slope stability analysis by hybrid genetic algorithm. *Journal of Central South University* 2014;**21**:387–97. doi:10.1007/s11771-014-1952-1

[25] Jurado-Piña R, Jimenez R. A genetic algorithm for slope stability analyses with concave slip surfaces using custom operators. *Engineering Optimization* 2014;**47**:453–72. doi:10.1080/0305215x.2014.895339

[26] Song C, Chu X, Li L, Wang J. An improved differential evolution algorithm for the slope stability analysis. In: *Proceedings of 2011 International Conference on Electric Technology and Civil Engineering (ICETCE), 2011, Lushan*. IEEE; 2011:72–5. doi:10.1109/ICETCE.2011.5774334

[27] Yalcin Y, Pekcan O, Altun M. Analysis of slopes using elitist differential evolution algorithm. In: *Proceedings of the 6th International Conference on Engineering Optimization (EngOpt), 2018, Lisboa*. Springer; 2019:815–26. doi:10.1007/978-3-319-97773-7_71

[28] Cheng Y, Li L, Chi S. Particle swarm optimization algorithm for the location of the critical non-circular failure surface in two-dimensional slope stability analysis. *Computers and Geotechnics* 2007;**34:**92–103. doi:10.1016/j.compgeo.2006.10.012

[29] Cheng YM, Li L, Chi SC. Performance studies on six heuristic global optimization methods in the location of critical slip surface. *Computers and Geotechnics* 2007;**34**:462–84. doi:10.1016/j.compgeo.2007.01.004

[30] Khajehzadeh M, Taha MR, El-Ahafie A, Eslami M. Locating the general failure surface of earth slope using particle swarm optimisation. *Civil Engineering and Environmental Systems* 2012;**29:** 41–57. doi:10.1080/10286608.2012.663356

[31] Gandomi AH, Kashani AR, Mousavi M, Jalalvandi M. Slope stability analyzing using recent swarm intelligence techniques. *International Journal for Numerical and Analytical Methods in Geomechanics* 2015;**39**:295–309. doi:10.1002/nag.2308

[32] Malkawi AIH, Hassan WF, Sarma SK. Global search method for locating general slip surface using monte carlo techniques. *Journal of Geotechnical and Geoenvironmental Engineering* 2001;**127**:688–98. doi:10.1061/(ASCE)1090-0241(2001)127:8(688)

[33] Cheng Y, Li L, Lansivaara T. An improved harmony search minimization algorithm using different slip surface generation methods for slope stability analysis. *Engineering Optimization* 2008;**40**:95–115. doi:10.1080/03052150701618153

[34] Rocscience Inc. Slide 2D. Version 7. Limit equilibrium slope stability analysis. www.rocscience.com. Toronto, Canada 2016.

[35] Fredlund DG, Zhang ZM, Lam L. Effect of the axis of moment equilibrium in slope stability analysis. *Canadian Geotechnical Journal* 1992;**29**:456–65. doi:10.1139/t92-050

[36] Transportation Research Board. *Landslides: Investigation and Mitigation. TRB Special Report 247*. Washington, DC: National Academy Press; 1996.

[37] Cheng YM, Lau CK. Slope Stability *Analysis and Stabilization: New Methods and Insight*. Boca Raton: CRC Press; 2014.

[38] Zhu DY, Lee CF, Qian QH, Chen GR. A concise algorithm for computing the factor of safety using the Morgenstern-Price method. *Canadian Geotechnical Journal* 2005;**42:**272–8. doi:10.1139/t04-072.

[39] Cheng YM. Location of critical failure surface and some further studies on slope stability analysis. *Computers and Geotechnics* 2003;**30**:255–67. doi:10.1016/S0266-352X(03)00012-0

[40] Sarma SK, Tan D. Determination of critical slip surface in slope analysis. *Géotechnique* 2006;**56**:539–55. doi:10.1680/geot.2006.56.8.539

[41] Bolton HPJ, Heymann G, Groenwold AA. Global search for critical failure surface in slope stability analysis. *Engineering Optimization* 2003;**35:**51–65. doi:10.1080/0305215031000064749

[42] Li L, Chi SC, Lin G. The genetic algorithm incorporating harmony procedure and its application to the search for the non-circular critical slip surface for soil slopes. *Journal of Hydraulic Engineering* 2005;**36**:913–18.

[43] Ching RKH, Fredlund DG. Some difficulties associated with the limit equilibrium method of slices. *Canadian Geotechnical Journal* 1983;**20**:661–72. doi:10.1139/t83-074

[44] Espinoza RD, Bourdeau PL. Unified formulation for analysis of slopes with general slip surface. *Journal of Geotechnical Engineering* 1994;**120;**1185–204. doi:(ASCE)0733-9410(1994)120:7(1185)

[45] Cheng YM, Zhu LJ. Unified formulation for two dimensional slope stability analysis and limitations in factor of safety determination. *Soils and Foundations* 2005;**44;**121–8. doi:10.3208/sandf.44.6_121

[46] Arai K, Tagyo K. Determination of noncircular slip surface giving the minimum factor of safety in slope stability analysis. *Soils and Foundations* 1985;**25**:43–51. doi:10.3208/sandf1972.25.43

[47] Baker R. Determination of the critical slip surface in slope stability computations. *International Journal for Numerical and Analytical Methods in Geomechanics* 1980;**4**:333–59. doi:10.1002/nag.1610040405

[48] Yamagami T, Jiang J. A search for the critical slip surface in three- dimensional slope stability analysis. *Soils and Foundations* 1997;**37**:1–16. doi:10.3208/sandf.37.3_1

[49] Celestino T, Duncan J. Simplified search for non-circular slip surface. In: *Proceedings of the 10th international conference on soil mechanics and foundation engineering, 1981, Stockholm*. Rotterdam: A.A. Balkema; 1981:391–4.

[50] Li K, White W. Rapid evaluation of the critical slip surface in slope stability problems. *International Journal for Numerical and Analytical Methods in Geomechanics* 1987;**11**:449–73. doi:10.1002/nag.1610110503

[51] Chen Z, Shao C. Evaluation of minimum factor of safety in slope stability analysis. *Canadian Geotechnical Journal* 1983:**25**;735–48. doi:10.1139/t88-084

[52] Nguyen V. Determination of critical slope failure surface. *Journal of Geotechnical Engineering* 1985:**111**;238–50.

[53] Yamagami T, Ueta Y. Search for noncircular slip surfaces by the Morgenstern-Price method. In: *Proceedings of 6th International Conference on Numerical Methods in Geomechanics, 1988, Innsbruck*. Rotterdam: A.A. Balkema; 1988:1335-40.

[54] DeNatale JS. Rapid identification of critical slip surface: structure. *Journal of Geotechnical Engineering* 1991:**117**;1568-89.

[55] Greco VR. Efficient Monte Carlo technique for locating critical slip surface. *Journal of Geotechnical Engineering* 1996:**122;**517–25. doi:10.1061/(ASCE)0733-9410(1996)122:7(517)

[56] Malkawi AIH, Hassan WF, Sarma SK. An efficient search method for finding the critical circular slip surface using the Monte Carlo technique. *Canadian Geotechnical Journal* 2001:**38;**1081–9. doi:10.1139/cgj-38-5-1081

[57] Kahatadeniya KS, Nanakorn P, Neaupane KM. Determination of the critical failure surface for slope stability analysis using ant colony optimization. *Engineering Geology* 2009;**108**:133–41. doi:10.1016/j.enggeo.2009.06.010

[58] Gao W. Premium-penalty ant colony optimization and its application in slope stability analysis. *Applied Soft Computing* 2016;**43**:480–8. doi:10.1016/j.asoc.2016.03.001

[59] Khajehzadeh M, Taha MR, El-Shafie A, Eslami M. Search for critical failure surface in slope stability analysis by gravitational search algorithm. *International Journal of the Physical Sciences* 2011;**6**:5012–21. doi:10.5897/IJPS11.694

[60] Khajehzadeh M, Taha MR, El-Shafie A, Eslami M. A modified gravitational search algorithm for slope stability analysis. *Engineering Applications of Artificial Intelligence* 2012;**25**:1589–97. doi:10.1016/j.engappai.2012.01.011

[61] Kang F, Li J, Ma Z. An artificial bee colony algorithm for locating the critical slip surface in slope stability analysis. *Engineering Optimization* 2013;**45**:207–23. doi:10.1080/0305215X.2012.665451

[62] Kashani AR, Gandomi AH, Mousavi M. Imperialistic Competitive Algorithm: A metaheuristic algorithm for locating the critical slip surface in 2-dimensional soil slopes. *Geoscience Frontiers* 2016;**7**:83–9. doi:10.1016/j.gsf.2014.11.005

[63] Storn R, Price K. Differential evolution – a simple and efficient heuristic for global optimization over continuous spaces. *Journal of Global Optimization* 1997:**11**;341–59. doi:10.1023/A:1008202821328

[64] Broyden CG. A Class of methods for solving nonlinear simultaneous equations. *Mathematics of Computation* 1965;**19**:577–93. doi:10.1090/S0025-5718-1965-0198670-6.

[65] Salimi H. Stochastic Fractal Search: A powerful metaheuristic algorithm. *Knowledge-Based Systems* 2015;**75**:1–18. doi:10.1016/j.knosys.2014.07.025

[66] de Melo VV, Banzhaf W. Drone Squadron Optimization: a novel self-adaptive algorithm for global numerical optimization. *Neural Computing and Applications* 2017. doi:10.1007/s00521-017-2881-3

[67] Fredlund DG, Krahn J. Comparison of slope stability methods of analysis. *Canadian Geotechnical Journal* 1977;**14**:429–39. doi:10.1139/t77-045

[68] Wilcoxon F. Individual comparisons by ranking methods. *Biometrics Bulletin* 1945;**1**:80-3. doi:10.2307/3001968

[69] Fırat S. *Critical assessment of existing slope stability formulae and application to slope stabilisation*. PhD [dissertation]. Pontypridd: University of Glamorgan; 1998.

[70] Fırat S. Stability analysis of pile-slope system. *Scientific Research and Essays* 2009;**4**:842–52.

[71] Low BK, Gilbert RB, Wright SG. Slope reliability analysis using generalized method of slices. *Journal of Geotechnical and Geoenvironmental Engineering* 1998;**124**:350–62. doi:10.1061/(ASCE)1090-0241(1998)124:4(350)

[72] Zhu DY, Lee CF, Qian QH, Zou ZS, Sun F. A new procedure for computing the factor of safety using the Morgenstern-Price method. *Canadian Geotechnical Journal* 2001;**38**:882–8. doi:10.1139/cgj-38-4-882

APPENDIX A

RESULT VERIFICATION WITH SLIDE SOFTWARE

Table A.1: Detailed information of critical slip surfaces

Spline number, j →		*1*	*2*	*3*	*4*	*5*	*6*
	$(a_f)_j$	0.0550	0.0221	0.0382	0.0209	0.0406	0.1271
	$(b_f)_j$	-2.4779	-1.0691	-2.2868	-0.8052	-2.5693	-10.5903
Example 1	$(d_f)_j$	32.3746	17.3037	40.2642	8.6797	47.9817	234.0784
	x_j	17.6000	21.3174	37.8326	41.6766	45.0098	46.4531
	x_{j+1}	21.3174	37.8326	41.6766	45.0098	46.4531	47.6616
	$(a_f)_j$	0.1167	0.0574	0.0899	0.0265	0.0754	0.2493
	$(b_f)_j$	-1.7694	-0.9607	-1.8270	0.0985	-1.4908	-7.6672
Example 2 (i)	$(d_f)_j$	10.6912	7.9336	13.7072	-0.9198	11.9956	66.8359
	x_j	4.6305	6.8199	13.6260	15.1794	16.2536	17.9315
	x_{j+1}	6.8199	13.6260	15.1794	16.2536	17.9315	18.2919
	$(a_f)_j$	0.0703	0.0319	0	0.0241	0.0304	0.0517
	$(b_f)_j$	-1.2373	-0.6018	0.2738	-0.0058	-0.2648	-1.2137
Example 2 (ii)	$(d_f)_j$	9.4301	6.7984	0.7905	-3.2537	-0.5849	9.9539
	x_j	5.0000	8.1594	13.5748	20.0000	20.9524	22.5041
	x_{j+1}	8.1594	13.5748	20.0000	20.9524	22.5041	23.5000
	$(a_f)_j$	0.2724	0	0.0653	0.0274	0.0032	0.7405
	$(b_f)_j$	-2.7983	0.2136	-1.9396	0.2836	1.2915	-31.8911
Example 3	$(d_f)_j$	49.1834	40.8591	58.5441	29.5388	19.0602	392.4195
	x_j	4.3406	5.5276	17.5051	19.5585	20.7661	22.5346
	x_{j+1}	5.5276	17.5051	19.5585	20.7661	22.5346	22.6650
	$(a_f)_j$	0.0426	0.0167	0.0151	0.0087	0	0.1191
	$(b_f)_j$	-2.0914	-0.8688	-0.7334	-0.0849	0.7620	-12.5447
Example 4	$(d_f)_j$	38.7752	24.3719	21.7905	5.4979	-15.0186	354.0470
	x_j	17.8903	23.0412	28.0718	46.3783	46.9527	60.6931
	x_{j+1}	23.0412	28.0718	46.3783	46.9527	60.6931	62.4719
	$(a_f)_j$	0.0175	0.0049	0	0.0260	0.0193	0.3762
	$(b_f)_j$	-1.2385	-0.0214	0.5454	-5.6382	-3.9173	-94.4047
Example 5 (i)	$(d_f)_j$	37.7336	9.3219	-6.9988	360.2456	250.0783	5985.6826
	x_j	30.0000	39.5976	57.5702	120.6233	123.5912	126.9294
	x_{j+1}	39.5976	57.5702	120.6233	123.5912	126.9294	129.9977
	$(a_f)_j$	0.0138	0.0168	0	0	0.0210	0.2647
	$(b_f)_j$	-0.9832	-1.0981	0.5454	0.5453	-4.4090	-65.7686
Example 5 (ii)	$(d_f)_j$	33.4300	33.2829	-6.9998	-6.9954	284.4761	4148.1064
	x_j	30.0000	40.1453	48.8225	110.2222	120.7534	125.9343
	x_{j+1}	40.1453	48.8225	110.2222	120.7534	125.9343	129.9998
	$(a_f)_j$	0.4535	0.0001	0.0680	0.0609	0.0223	0.0570
	$(b_f)_j$	-9.9261	-0.0031	-2.2580	-1.4569	0.2754	-1.3552
Example 6 (i)	$(d_f)_j$	98.3159	44.0207	62.7196	49.2821	29.8502	49.0052
	x_j	10.3355	10.8994	17.3211	20.5072	21.6855	23.6786
	x_{j+1}	10.8994	17.3211	20.5072	21.6855	23.6786	24.4883
	$(a_f)_j$	0.2074	0	0.1093	0.0816	0.0098	566.6792
	$(b_f)_j$	-4.8090	0	-3.8839	-2.2717	0.9037	-27871.8870
Example 6 (ii)	$(d_f)_j$	71.8709	44.0000	78.4837	56.9762	21.8666	342766.8388
	x_j	10.4968	11.5911	17.9926	20.7931	21.8217	24.5937
	x_{j+1}	11.5911	17.9926	20.7931	21.8217	24.5937	24.5938
	$(a_f)_j$	0.0295	0.0001	0.0482	0.1528	0.0115	0.2758
	$(b_f)_j$	-0.6829	-0.0021	-1.5977	-5.5144	0.7102	-11.9568
Example 6 (iii)	$(d_f)_j$	47.9438	44.0137	57.2282	93.2993	24.7463	176.4843
	x_j	10.1075	10.9832	16.9629	21.1356	21.9986	23.9800
	x_{j+1}	10.9832	16.9629	21.1356	21.9986	23.9800	25.0178
	$(a_f)_j$	0.5127	0	0.0632	0.0825	0.0492	0.2373
	$(b_f)_j$	-11.1461	-0.0002	-2.2003	-2.4366	-0.9178	-9.9721
Example 6 (iv)	$(d_f)_j$	104.5798	44.0013	63.1377	59.3507	42.0326	150.9610
	x_j	10.3115	10.7740	17.9552	21.4272	22.6005	24.1693
	x_{j+1}	10.7740	17.9552	21.4272	22.6005	24.1693	25.0120

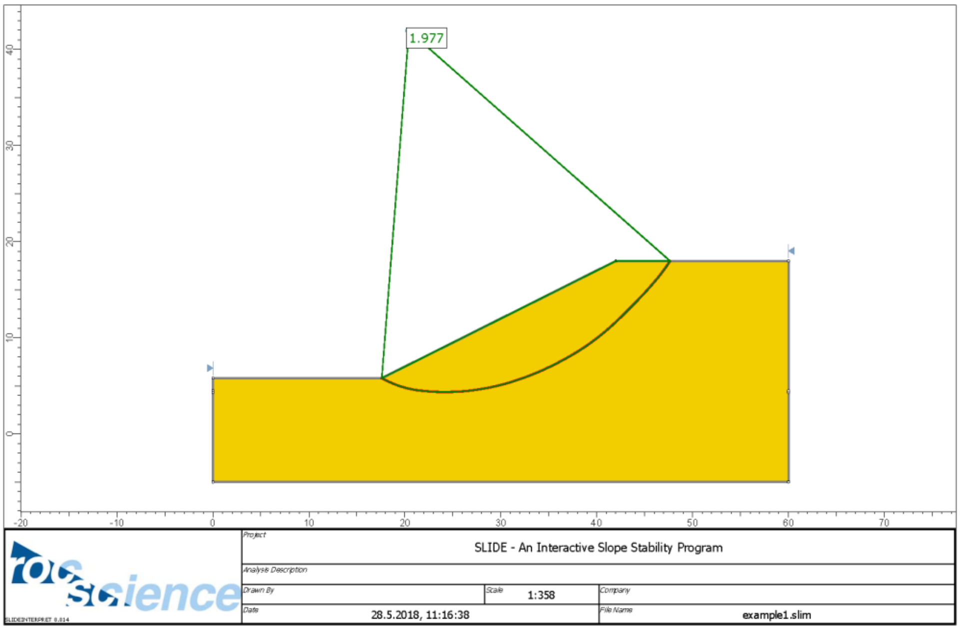

Figure A.1: *Example 1* – result verification using *Slide*

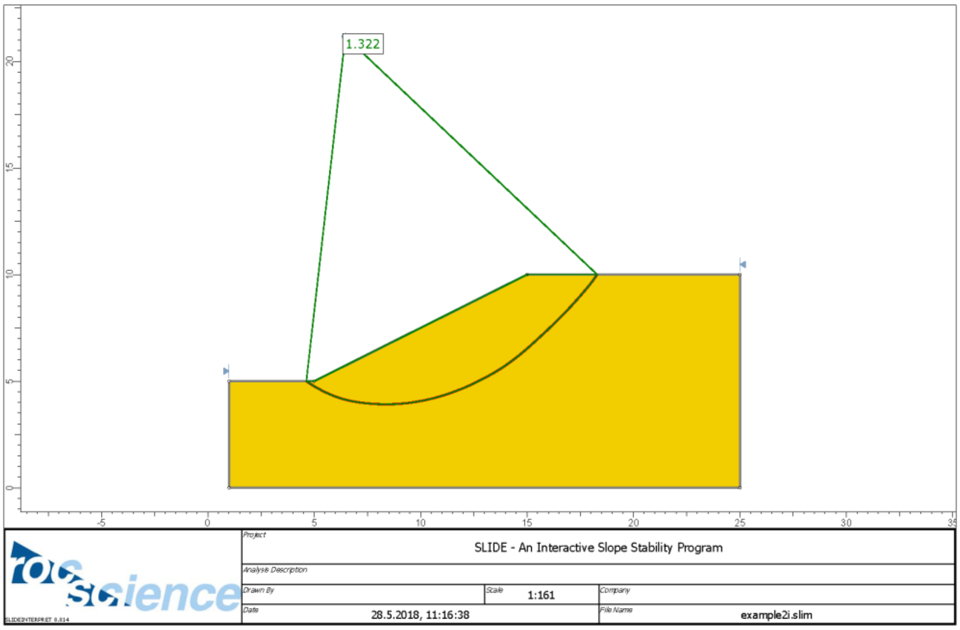

Figure A.2: *Example 2 Case* (*i*) – result verification using *Slide*

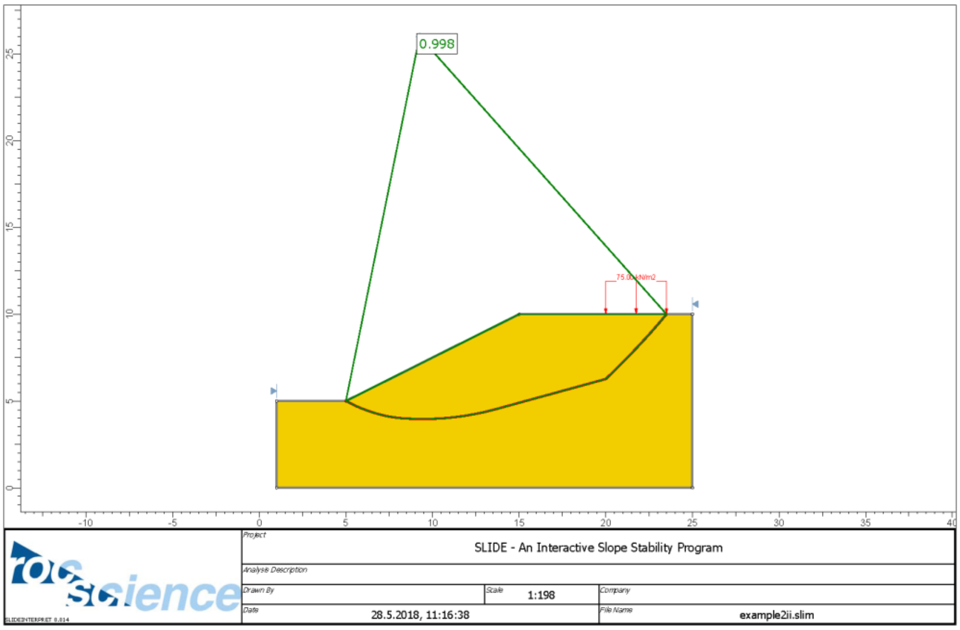

Figure A.3: *Example 2 Case* (*ii*) – result verification using *Slide*

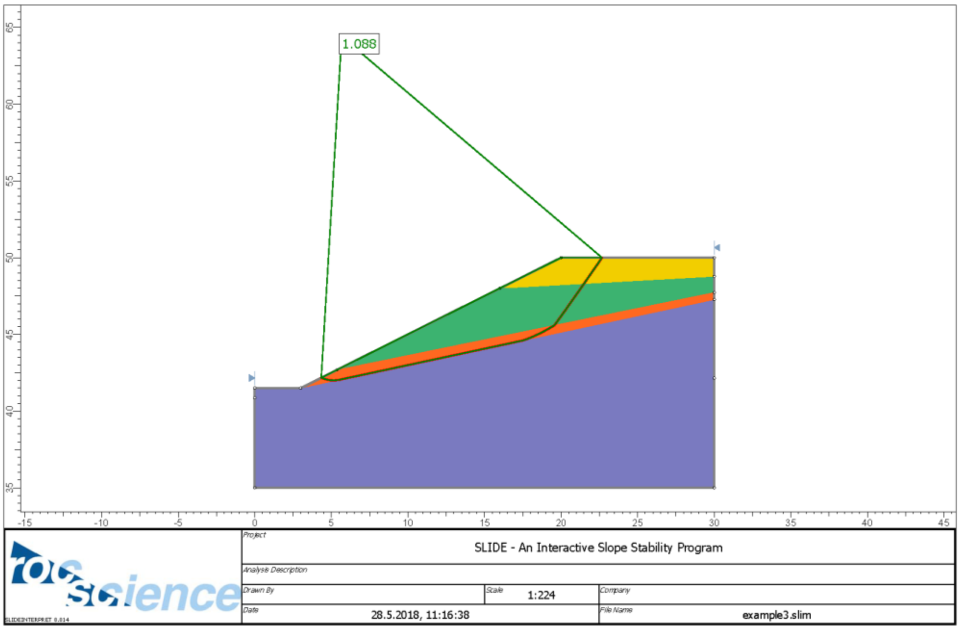

Figure A.4: *Example 3* – result verification using *Slide*

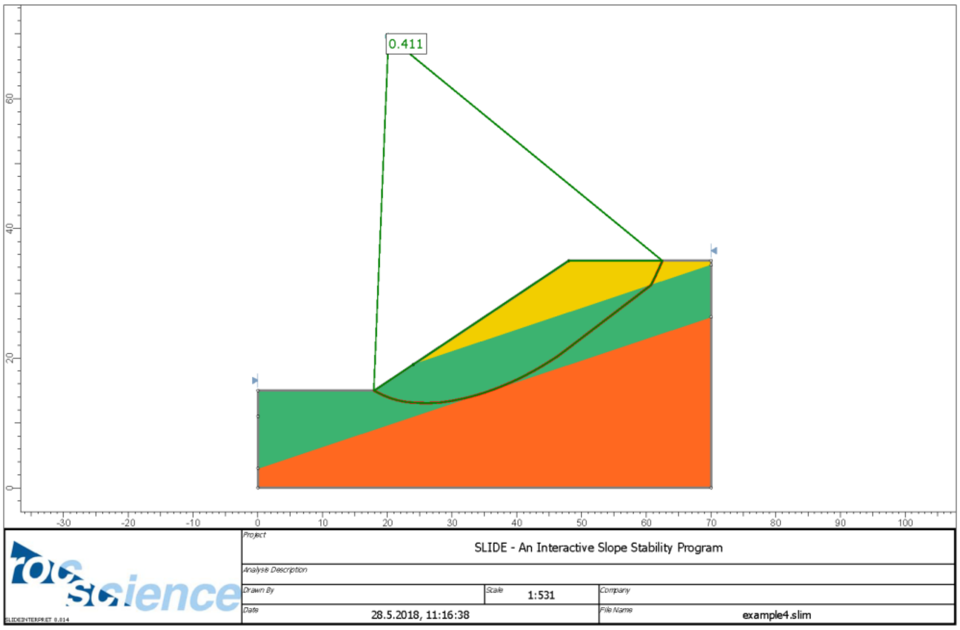

Figure A.5: *Example 4* – result verification using *Slide*

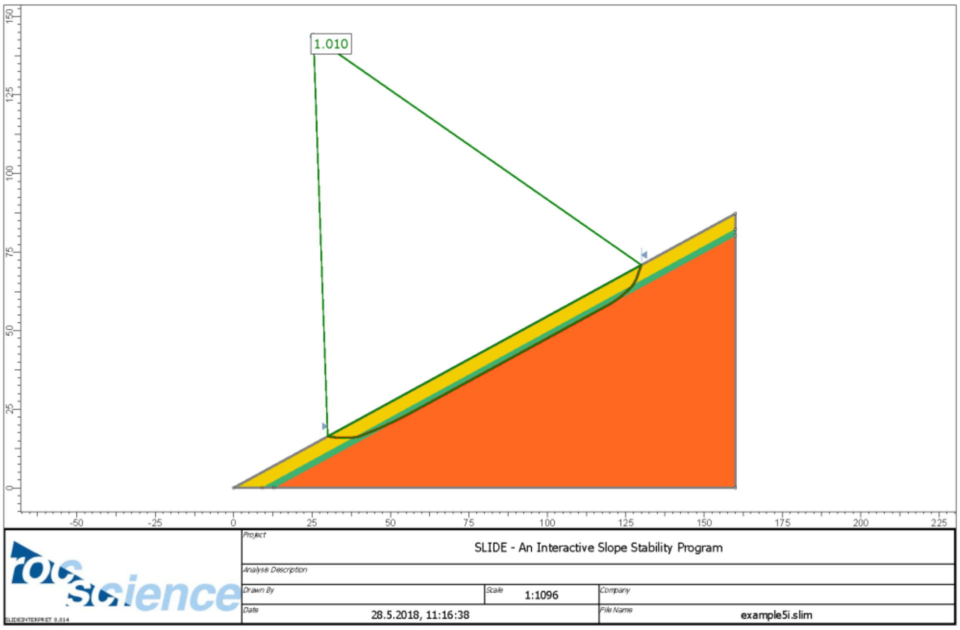

Figure A.6: *Example 5 Case* (*i*) – result verification using *Slide*

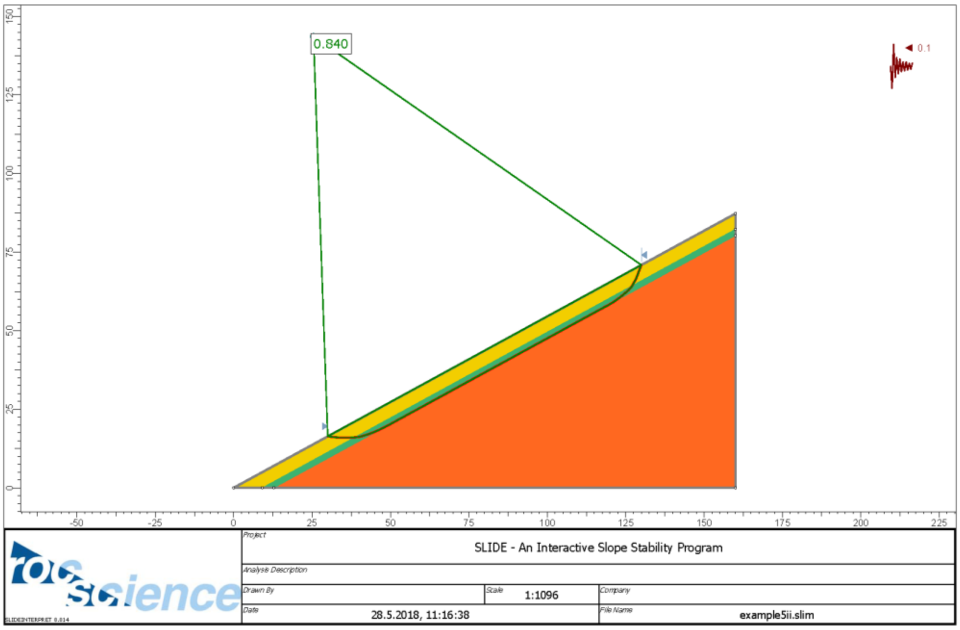

Figure A.7: *Example 5 Case* (*ii*) – result verification using *Slide*

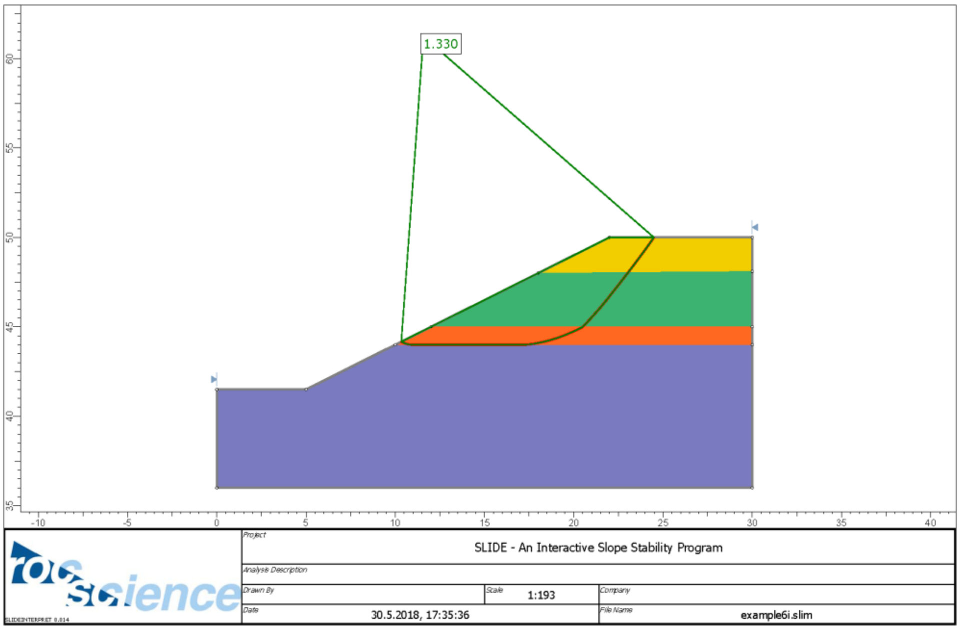

Figure A.8: *Example 6 Case* (*i*) – result verification using *Slide*

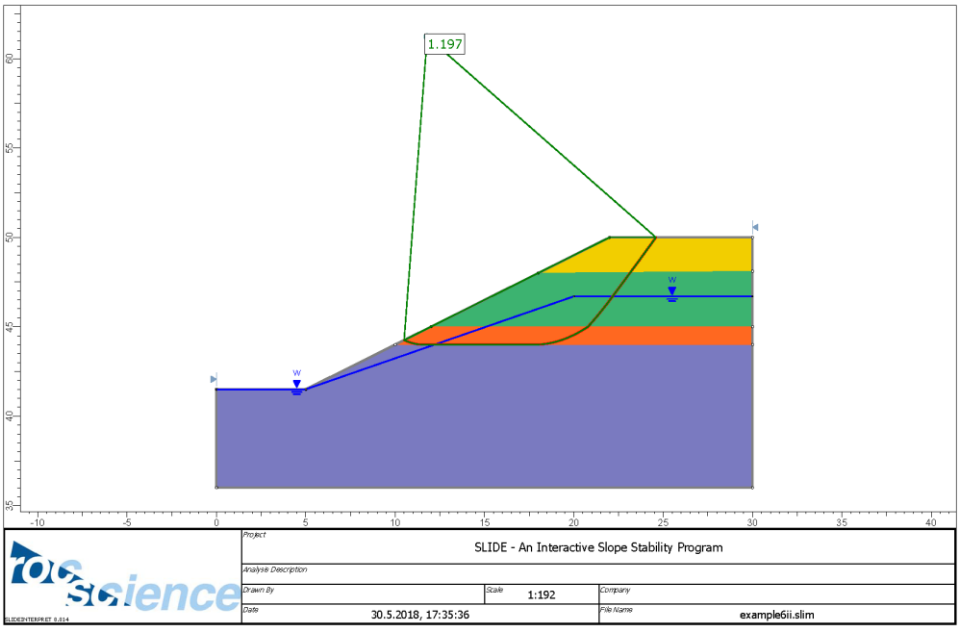

Figure A.9: *Example 6 Case* (*ii*) – result verification using *Slide*

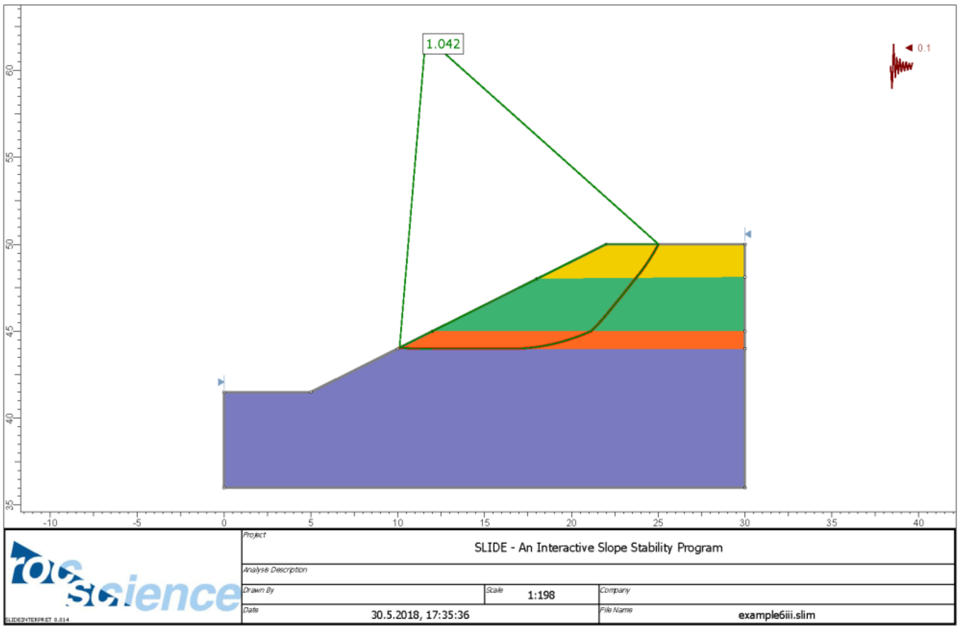

Figure A.10: *Example 6 Case* (*iii*) – result verification using *Slide*

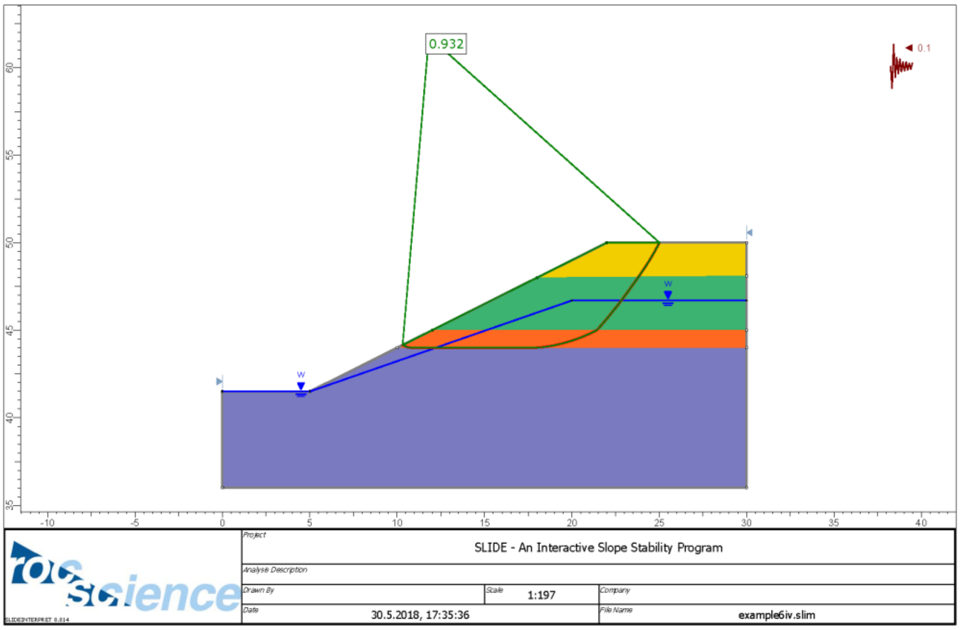

Figure A.11: *Example 6 Case* (*iv*) – result verification using *Slide*

APPENDIX B

CLOSED-FORM EQUATIONS OF FELLENIUS' METHOD

For the horizontal force factor of safety, $(F_{S,H})_F$, the dependent variables in Eq. (4.33) are replaced with the function definitions given in Eqs. (4.1)–(4.13). Then, the resulting expression is arranged as given in Eq. (B.1). I_1 is the same as before and calculated using Eq. (4.53). The other integral terms, I_6 and I_7, are defined in Eqs. (B.2) and (B.3). The coefficients in the integrals can be computed using the expression given in Eq. (B.4).

$$\left(F_{S,H}\right)_F = \frac{I_1 + I_6}{Wk_h + I_7} \tag{B.1}$$

$$I_6 = \int_{x_t}^{x_s} \tan\phi' \cdot \frac{A_6 x^3 + B_6 x^2 + C_6 x + D_6}{G_6 x^2 + H_6 x + M_6} \cdot dx \tag{B.2}$$

$$I_7 = \int_{x_t}^{x_s} \frac{A_7 x^4 + B_7 x^3 + C_7{}^2 x + D_7 x + E_7}{G_7 x^2 + H_7 x + M_7} \cdot dx \tag{B.3}$$

$$\boxed{\begin{gathered}
A_6 = -2a_f a_h \gamma k_h\,,\; B_6 = a_q + a_h \gamma \cdot \left(1 + k_v - b_f k_h\right) - 2a_f b_h k_h \gamma \\
C_6 = b_q + b_h \gamma \cdot \left(1 + k_v - b_f k_h\right) - 2a_f d_h k_h \gamma\,,\; D_6 = d_q + d_h \gamma \cdot \left(1 + k_v - b_f k_h\right) \\
G_6 = 4a_f{}^2,\; H_6 = 4a_f b_f\,,\; M_6 = b_f{}^2 + 1 \\
A_7 = -4a_f{}^2 a_h k_h \gamma,\; B_7 = 2a_f \cdot \left[a_h \gamma \cdot \left(1 + k_v\right) + a_q\right] - 4a_f k_h \gamma \cdot \left(a_h b_f + a_f b_h\right) \\
C_7 = \begin{Bmatrix} b_f \cdot \left[a_h \gamma \cdot \left(1 + k_v\right) + a_q\right] + 2a_f \cdot \left[b_h \gamma \cdot \left(1 + k_v\right) + b_q\right] \\ - k_h \gamma \cdot \left(a_h b_f{}^2 + 4a_f b_f b_h + 4a_f{}^2 d_h\right) \end{Bmatrix} \\
D_7 = \begin{Bmatrix} b_f \cdot \left[b_h \gamma \cdot \left(1 + k_v\right) + b_q\right] + 2a_f \cdot \left[d_h \gamma \cdot \left(1 + k_v\right) + d_q\right] \\ - b_f k_h \gamma \cdot \left(b_f b_h + 4a_f d_h\right) \end{Bmatrix} \\
E_7 = b_f \cdot \left[d_h \gamma \cdot \left(1 + k_v\right) + d_q\right] - b_f{}^2 d_h k_h \gamma\,,\; G_7 = G_6,\; H_7 = H_6,\; M_7 = M_6
\end{gathered}} \tag{B.4}$$

Through analytical integration, closed-form of the integrals can be obtained as given in Eqs. (B.5) and (B.6).

$$I_6 = \tan\phi' \cdot \left\{ \frac{\left[\begin{array}{l} \left(-AGM + AH^2 - BGH + CG^2\right) \cdot \ln\left(\left|Gx^2 + Hx + M\right|\right) \\ + AG^2x^2 - 2G \cdot \left(AH - BG\right) \cdot x \end{array} \right]}{2G^3} + \frac{\left[\left(\begin{array}{l} 3AGHM - 2BG^2M - AH^3 \\ + BGH^2 - CG^2H + 2DG^3 \end{array} \right) \cdot \tan^{-1}\left(\frac{2Gx + H}{\sqrt{4GM - H^2}} \right) \right]}{G^3 \cdot \sqrt{4GM - H^2}} \right\} \Bigg|_{x_t}^{x_s} \tag{B.5}$$

$$I_7 = \left\{ \frac{\left[\begin{array}{l} 3 \cdot \left(2AGHM - BG^2M - AH^3 + BGH^2 - CG^2H + DG^3\right) \cdot \ln\left(\left|Gx^2 + Hx + M\right|\right) \\ + 2AG^3x^3 - 3G^2 \cdot \left(AH - BG\right) \cdot x^2 - 6G \cdot \left(AGM - AH^2 + BGH - CG^2\right) \cdot x \end{array} \right]}{6G^4} + \frac{\left[\left(\begin{array}{l} 2AG^2M^2 - 4AGH^2M + 3BG^2HM - 2CG^3M \\ + 2EG^4 + AH^4 - BGH^3 + CG^2H^2 - DG^3H \end{array} \right) \cdot \tan^{-1}\left(\frac{2Gx + H}{\sqrt{4GM - H^2}} \right) \right]}{G^4 \cdot \sqrt{4GM - H^2}} \right\} \Bigg|_{x_t}^{x_s} \tag{B.6}$$

For both integrals, linear segments result in 0/0 indeterminacy. Therefore, the closed-form solutions of I_6 and I_7 are explicitly derived for linear order surface functions and abbreviated as $I_{6,lin}$ and $I_{7,lin}$ in Eqs. (B.7) and (B.8), respectively.

$$A_6 = G_6 = H_6 = 0 \rightarrow I_{6,lin} = \int_{x_t}^{x_s} \tan\phi' \cdot \frac{Bx^2 + Cx + D}{M} \cdot dx = \left[\frac{\tan\phi'}{M} \cdot \left(\frac{Bx^3}{3} + \frac{Cx^2}{2} + Dx \right) \right] \Bigg|_{x_t}^{x_s} \tag{B.7}$$

$$A_7 = B_7 = G_7 = H_7 = 0 \rightarrow I_{7,lin} = \int_{x_t}^{x_s} \frac{C^2x + Dx + E}{M} \cdot dx = \left[\frac{1}{M} \cdot \left(\frac{Cx^3}{3} + \frac{Dx^2}{2} + Ex \right) \right] \Bigg|_{x_t}^{x_s} \tag{B.8}$$

Similarly for the moment factor of safety, $(F_{S,M})_F$, the dependent variables in Eq. (4.42) are replaced with the function definitions given in Eqs. (4.1)–(4.13), and then arranged into Eq. (B.9). In this case, I_4 is the same expression as in Eq. (4.63). The other integral terms, I_8 and I_9, are defined in Eqs. (B.10) and (B.11). The coefficients in these expressions are given in Eq. (B.12). Then, the closed-form solutions of these integrals are given in Eqs. (B.13) and (B.14).

$$\left(F_{S,M}\right)_F = \frac{I_4 + I_8}{-I_9 + Q\cdot\left(x_R - x_Q\right) + W\cdot\left[\left(1+k_v\right)\cdot\left(x_R - x_C\right) - k_h\cdot\left(y_R - y_C\right)\right]} \tag{B.9}$$

$$I_8 = \int_{x_t}^{x_s} \tan\phi'\cdot\frac{A_8x^5 + B_8x^4 + C_8x^3 + D_8x^2 + E_8x + F_8}{G_8x^2 + H_8x + M_8}\cdot dx \tag{B.10}$$

$$I_9 = \int_{x_t}^{x_s} \frac{A_9x^6 + B_9x^5 + C_9x^4 + D_9x^3 + E_9x^2 + F_9x + P_9}{G_9x^2 + H_9x + M_9}\cdot dx \tag{B.11}$$

$$\boxed{\begin{gathered}
o_2 = -a_f,\ o_1 = 2a_f x_R,\ o_0 = d_f - y_R + b_f x_R \\
\rho_3 = -2a_f a_h k_h \gamma,\ \rho_2 = a_q + a_h\gamma\cdot\left(1+k_v - b_f k_h\right) - 2a_f b_h k_h \gamma \\
\rho_1 = b_q + b_h\gamma\cdot\left(1+k_v - b_f k_h\right) - 2a_f d_h k_h \gamma,\ \rho_0 = d_q + d_h\gamma\cdot\left(1+k_v - b_f k_h\right) \\
A_8 = o_2\rho_3,\ B_8 = o_1\rho_3 + o_2\rho_2,\ C_8 = o_0\rho_3 + o_1\rho_2 + o_2\rho_1 \\
D_8 = o_0\rho_2 + o_1\rho_1 + o_2\rho_0,\ E_8 = o_0\rho_1 + o_1\rho_0,\ F_8 = o_0\rho_0 \\
G_8 = G_6,\ H_8 = H_6,\ M_8 = M_6 \\
\delta_3 = -2a_f^{\ 2},\ \delta_2 = -3a_f b_f,\ \delta_1 = -1 + 2a_f\cdot\left(y_R - d_f\right) - b_f^{\ 2} \\
\delta_0 = x_R + b_f\cdot\left(y_R - d_f\right) \\
A_9 = \delta_3\rho_3,\ B_9 = \delta_3\rho_2 + \delta_2\rho_3,\ C_9 = \delta_3\rho_1 + \delta_2\rho_2 + \delta_1\rho_3 \\
D_9 = \delta_3\rho_0 + \delta_2\rho_1 + \delta_1\rho_2 + \delta_0\rho_3,\ E_9 = \delta_2\rho_0 + \delta_1\rho_1 + \delta_0\rho_2 \\
F_9 = \delta_1\rho_0 + \delta_0\rho_1,\ P_9 = \delta_0\rho_0 \\
G_9 = G_6,\ H_9 = H_6,\ M_9 = M_6
\end{gathered}} \tag{B.12}$$

$$I_8 = \tan\phi'\cdot\left\{\frac{\left[\begin{aligned} &6\cdot\begin{pmatrix} AG^2M^2 - 3AGH^2M + 2BG^2HM - CG^3M \\ + EG^4 + AH^4 - BGH^3 + CG^2H^2 - DG^3H \end{pmatrix}\cdot\ln\left(\left|Gx^2 + Hx + M\right|\right) \\ &+3AG^4x^4 - 4G^3\cdot(AH - BG)\cdot x^3 \\ &-6G^2\cdot(AGM - AH^2 + BGH - CG^2)\cdot x^2 \\ &+12G\cdot(2AGHM - BG^2M - AH^3 + BGH^2 - CG^2H + DG^3)\cdot x \end{aligned}\right]}{12G^5} - \frac{\left[\begin{pmatrix} 5AG^2HM^2 - 2BG^3M^2 - 5AGH^3M \\ + 4BG^2H^2M - 3CG^3HM + 2DG^4M \\ + EG^4H + AH^5 - BGH^4 + CG^2H^3 \\ - DG^3H^2 - 2FG^5 \end{pmatrix}\cdot\tan^{-1}\left(\frac{2Gx + H}{\sqrt{4GM - H^2}}\right)\right]}{G^5\cdot\sqrt{4GM - H^2}}\right\}\Bigg|_{x_t}^{x_s} \tag{B.13}$$

$$I_9 = \left\{ -\frac{\left[\begin{aligned} & 30 \cdot \begin{pmatrix} 3AG^2HM^2 - BG^3M^2 - 4AGH^3M \\ + 3BG^2H^2M - 2CG^3HM + DG^4M \\ + EG^4H + AH^5 - BGH^4 \\ + CG^2H^3 - DG^3H^2 - FG^5 \end{pmatrix} \cdot \ln\left(\left|Gx^2 + Hx + M\right|\right) \\ & - 12AG^5x^5 + 15G^4 \cdot (AH - BG) \cdot x^4 \\ & + 20G^3 \cdot \left(AGM - AH^2 + BGH - CG^2\right) \cdot x^3 \\ & - 30G^2 \cdot \begin{pmatrix} 2AGHM - BG^2M - AH^3 \\ + BGH^2 - CG^2H + DG^3 \end{pmatrix} \cdot x^2 \\ & - 60G \cdot \begin{pmatrix} AG^2M^2 - 3AGH^2M + 2BG^2HM \\ - CG^3M + EG^4 + AH^4 - BGH^3 \\ + CG^2H^2 - DG^3H \end{pmatrix} \cdot x \end{aligned}\right]}{60G^6} + \frac{\left[\begin{pmatrix} 2G^6P - 2AG^3M^3 + 9AG^2H^2M^2 - 5BG^3HM^2 \\ + 2CG^4M^2 - 2EG^5M - 6AGH^4M + 5BG^2H^3M \\ - 4CG^3H^2M + 3DG^4HM + EG^4H^2 + AH^6 \\ - BGH^5 + CG^2H^4 - DG^3H^3 - FG^5H \end{pmatrix} \cdot \tan^{-1}\left(\frac{2Gx + H}{\sqrt{4GM - H^2}}\right)\right]}{G^6 \cdot \sqrt{4GM - H^2}} \right\} \Bigg|_{x_t}^{x_s} \quad \text{(B.14)}$$

Both I_8 and I_9 are indeterminate for linear surfaces. Therefore, the closed-form solutions of these integrals are derived for linear order surface functions separately and given in Eqs (B.15) and (B.16).

$$A_8 = B_8 = G_8 = H_8 = 0 \rightarrow I_{8,lin} = \int_{x_t}^{x_s} \tan\phi' \cdot \frac{Cx^3 + Dx^2 + Ex + F}{M} \cdot dx = \left[\frac{\tan\phi'}{M} \cdot \left(\frac{Cx^4}{4} + \frac{Dx^3}{3} + \frac{Ex^2}{2} + Fx\right)\right]\Bigg|_{x_t}^{x_s} \quad \text{(B.15)}$$

$$A_9 = B_9 = C_9 = G_9 = H_9 = 0 \rightarrow I_{9,lin} = \int_{x_t}^{x_s} \frac{Dx^3 + Ex^2 + Fx + P}{M} \cdot dx = \left[\frac{1}{M} \cdot \left(\frac{Dx^4}{4} + \frac{Ex^3}{3} + \frac{Fx^2}{2} + Px\right)\right]\Bigg|_{x_t}^{x_s} \quad \text{(B.16)}$$